Nano Energy 52 (2018) 441–473

Contents lists available at ScienceDirect

Nano Energy

journal homepage: www.elsevier.com/locate/nanoen

Review

Recent advancements in supercapacitor technology

Waseem Raza[a], Faizan Ali[b], Nadeem Raza[c], Yiwei Luo[a], Ki-Hyun Kim[f,*], Jianhua Yang[a], Sandeep Kumar[e,*], Andleeb Mehmood[a], Eilhann E. Kwon[d,*]

[a] State Key Laboratory of Fine Chemicals, School of Chemical Engineering Dalian University of Technology, Dalian 116024, PR China
[b] Key Laboratory of Materials Modification by Laser, Ion, and Electron Beams (Ministry of Education), School of Materials Science and Engineering, Dalian University of Technology, Dalian 116024, PR China
[c] Govt. Emerson College Affiliated with Bahauddin Zakaryia University, Multan, Pakistan
[d] Department of Environment and Energy, Sejong University, Seoul 05006, Republic of Korea
[e] Department of Bio and Nano Technology, Guru Jambheshwar University of Science and Technology, Hisar, Haryana 125001, India
[f] Department of Civil & Environmental Engineering, Hanyang University, 222 Wangsimni-Ro, Seoul 04763, Republic of Korea

ARTICLE INFO

Keywords:
Supercapacitors
Conducting polymers
Composites
Metal oxides
Electrolytes

ABSTRACT

Supercapacitors (SCs) are attracting considerable research interest as high-performance energy storage devices that can contribute to the rapid growth of low-power electronics (e.g., wearable, portable electronic devices) and high-power military applications (e.g., guided missile techniques and highly sensitive naval warheads). The performance of SCs can be assessed in terms of the electrochemical properties determined through a combination between the electrode and the electrolyte materials. Likewise, the charge storage capacities of SCs can be affected significantly by selection of such materials (e.g., via surface redox mechanisms). Enormous efforts have thus been put to make them more competitive with existing options for energy storage such as rechargeable batteries. This article reviews recent advances in SC technology with respect to charge storage mechanisms, electrode materials, electrolytes (e.g., particularly paper/fiber-like 3D porous structures), and their practical applications. The challenges and opportunities associated with the commercialization of SCs are also discussed.

1. Introduction

Since the Industrial Revolution, the social and economic prosperity of the nation has depended on the massive consumption of fossil resources (coal, gas, and oil) as a readily accessible carbon source [1,2]. The total world energy demand from fossil fuels was estimated to be 13.731 billion tons of oil equivalent (BTOE) as of 2012 and is expected to approach 18.30 BTOE in 2035 [3]. The depletion and uneven distribution of natural resources has already caused economic problems (e.g., price fluctuations and unbalanced supply chains), resulting in issues in various domains such as energy generation and storage, industrial operations, and transportation [1,4–7]. Moreover, the massive worldwide consumption of fossil fuels has caused carbon accumulation in the natural cycle [8–10]. CO_2 from anthropogenic activities is the major contributor to the greenhouse gases causing significant environmental changes [11–14]. A strategic guideline (*i.e.,* adaptation and mitigation) to resolve the global-scale imbalance in carbon inventory was thus proposed by the United Nations (UN) in 2007 [15]. In line with those efforts, many studies have already considered how to restrict the consumption of fossil resources [16–21]. As part of those mitigation strategies, the development of renewable energy sources (such as solar energy, tidal energy, geothermal energy, wind energy, and biofuels) has also been pursued extensively [22–29]. Public awareness on global climate change has also led to various types of political legislation (e.g., the renewable fuel standard and renewable portfolio standard) intended to motivate the expansion and commercialization of renewable energy options [30,31].

Except for biofuels, most renewable energies are supplied as electricity (electric power). As such, there has been great demand for a reliable technical platform for electrochemical storage, including batteries, fuel cells, and electrochemical supercapacitors (SCs) [32,33]. In particular, SCs have drawn more attention than batteries because of their fast storage capability (i.e., low discharge time: SC: 1–10 s vs. lithium ion battery: 10–60 min) and enhanced cyclic stability (SC > 30,000 h vs. battery > 500 h) [34]. Beyond low energy density, recent advancements in SCs in terms of electrode materials and electrolytes hold significant potential to fill the gap between batteries and fuel cells and existing electrolytic-capacitor technology. Fig. 1(a) illustrates the number of publications (papers, books, patents, and authentic reports) on Google Scholar (accessed on April 2018) for the keyword of *supercapacitor*.

* Corresponding authors.
E-mail addresses: kkim61@hanyang.ac.kr (K.-H. Kim), ksandeep36@yahoo.com (S. Kumar), ekwon74@sejong.ac.kr (E.E. Kwon).

https://doi.org/10.1016/j.nanoen.2018.08.013
Received 25 June 2018; Received in revised form 12 July 2018; Accepted 7 August 2018
Available online 10 August 2018
2211-2855/

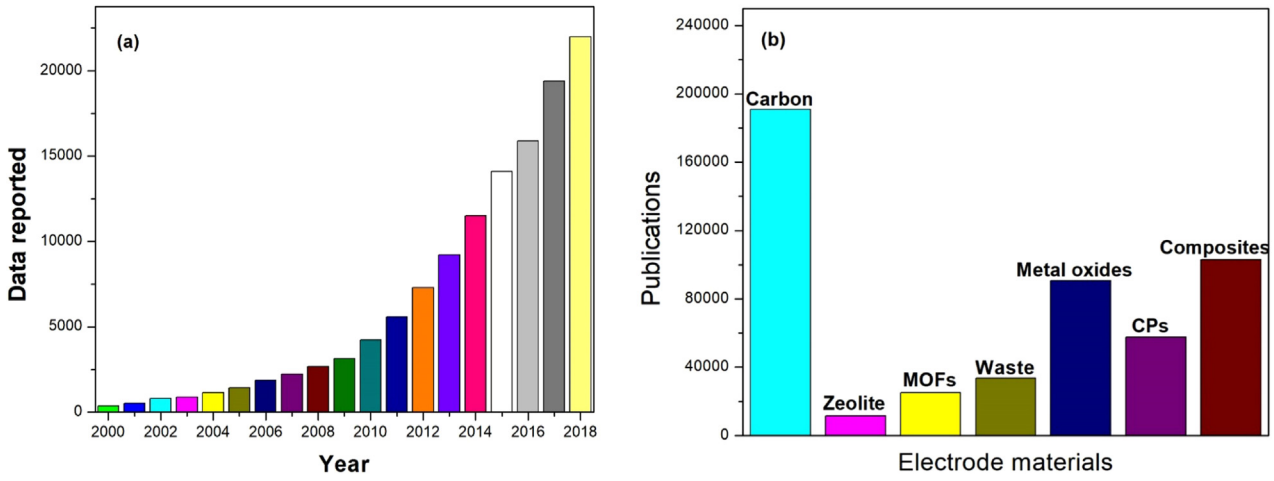

Fig. 1. Statistical survey on the research activities toward supercapacitor: a) presents the number of publications including articles, books, and other authentic open literature (2000–2018 (predicted)) from a search using *supercapacitor* as a keyword in Google Scholar. In b), the results are provided on the basis of publications about the supercapacitor materials cited in this review.

An SC is a pulse current system used to meet high current and specific power (10,000 W Kg^{-1}) requirements for durations of less than 1 min. Consequently, SCs can be used alone or in combination with another energy storage option (i.e., batteries) to offer improved power efficiency and enhanced cycle life for applications such as hybrid vehicles, cranes, trains, and elevators [35–37]. In 1957, the first patent for a prototype SC was reported and issued [38]. Until the 1990s, the demand for SC technology was low outside the field of hybrid electric vehicles [39]. Now, extensive development in SC technology aims to increase the electrical performance of electrode materials [40]. In drive systems that use power from a voltage source, diverse types of SCs are already being used to fulfil the power demand for starting and recovering braking energy [41,42]. Therefore, SCs are a viable option for many energy storage applications, including as back-up power supplies to provide protection against power disruptions [39,43,44].

The performance of SCs is significantly affected by many factors, such as the electrochemical properties of the electrode materials, the choice of electrolyte, and the potential window of the electrodes [45]. Enormous research efforts have hence been directed to the development of advanced materials for SC electrodes with appropriate structural designs to facilitate effective electron transport and ionic diffusion [46]. Fig. 1(b) shows the annual development of new electrode materials to improve the performance of SCs. This review focuses on the charge storage mechanisms of SCs, providing a brief summary of the latest advances in electrode materials (carbon-based materials, metal oxides, and conducting polymers), electrolyte choices, work done to fabricate new potential electrodes from waste, and a comparison of selected SCs. Furthermore, we briefly discuss the technical challenges for developing SCs with high enough energy density to compete with existing rechargeable batteries.

2. Supercapacitors: emerging energy stores

In line with recent technical advances in electric-powered devices in terms of cycle life, charge time, and specific power, SCs have become promising candidates in diverse fields that require high energy throughput (hybrid electric vehicles) and stable energy throughput (sensitive automation, computer chips, and portable electronic devices) [47]. SCs can already be used in power systems that require high-power throughput, but not necessarily at the maximum level of energy storage capacity. SCs cannot store the maximum level of energy, which restricts their use in energy backup devices.

SCs bridge the gap (cell voltage, specific power, and operating cost) between batteries and conventional dielectric capacitors; the latter are known to be perfect for quick storage/release power systems [48], offering power delivery and uptake of 196 kW kg^{-1} (10–100 times the energy density of electrolytic capacitors) in just a few seconds [44,49,50]. This is indeed beneficial for systems designed for energy recovery, i.*e.*, powerful braking in a transport system. However, SCs can possess much higher energy density (0.5–0.6 kJ L^{-1}) than conventional dielectric capacitors (0.01 W h L^{-1}) [51]. The attractive characteristics of SCs (higher power densities and quick charge and discharge processes) also impart reliable power throughputs. As seen in Fig. 2, the trade-off between energy and power density for energy storage in various devices can be well described graphically by the Ragone plot [52]. Despite the usefulness of the Ragone plot for estimating energy storage performance, however, it does not include other critical factors (e.g., cost estimation, cycle life, and safety). Therefore, it is important to consider those components also to best understand energy storage technology.

The main distinctions between batteries and SCs in storage mechanism, power limitations, energy storage, charge rate, and charge life limitations are illustrated in Fig. 3. For example, for batteries, the charge rate is kinetically limited, but for SCs it is high as the discharge rate. The cycle life of SCs (1 million h to 30,000 h) is extraordinarily higher than that of batteries (~ 500 h), and SCs offer remarkably low recharge times (SC: 1–10 s vs. battery: 10–60 min) [53]. Some key characteristics (specific energy, cycle life, charge/discharge time, and mechanism of charge storage) of capacitors, SCs, and batteries are

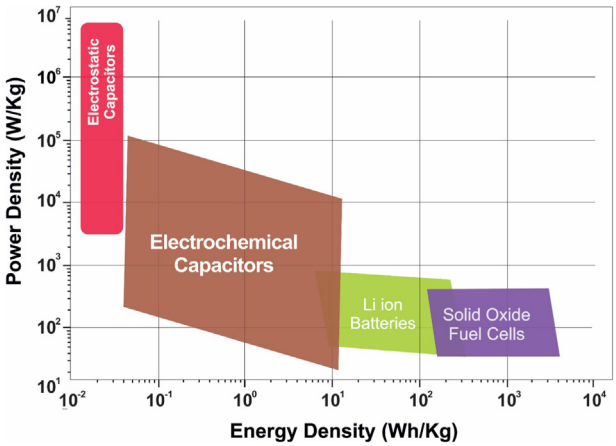

Fig. 2. Ragone plots for representative energy storage devices such as batteries, fuel cells, and supercapacitors [52].

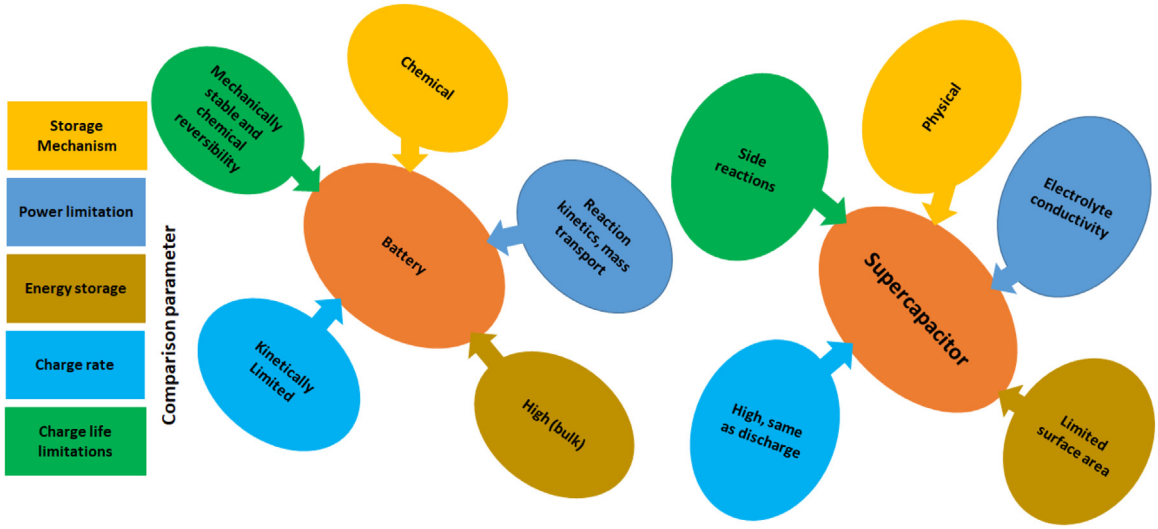

Fig. 3. Comparison between batteries and SCs through different operational parameters [84].

Table 1
Comparison of the basic performance metrics between different electrochemical energy storage systems.

Order	Characteristics	Capacitor	Supercapacitor	Battery	Ref.
1	Specific energy (Wh kg^{-1})	< 0.1	Up to 1091	Up to 1606	[49,337]
2	Specific power (W kg^{-1})	> 10,000	Up to 19,6000	< 1000	[49]
3	Discharge time	10^{-6} –10^{-3} S	s to min	0.03–3 h	[338]
4	Charge time	10^{-6} –10^{-3} S	s to min	1–5 h	[338]
5	Coulombic efficiency (%)	About 100	Up to 99 [339]	70–85	[338]
6	Cycle life	Almost infinite	> 500,000	About 1000	
7	Charge storage determinants	Electrode area and dielectric	Microstructure of electrode and electrolyte	Thermodynamics and active mass	[338]

summarized and compared in Table 1. This comparison shows that SCs can withstand half-millions of cycles because of their storage mechanisms, which do not involve reversible chemical reactions. Among the many variables used to assess the performance characteristics of energy storage devices, the operating temperature range is an important point of interest. The thermal stability of SCs can be tuned by wise choices for the materials and electrolytes used during the electrochemical process. SCs can operate at temperatures between − 40 and 100 °C [54], whereas batteries can be operated only between − 20 and 60 °C [34,50].

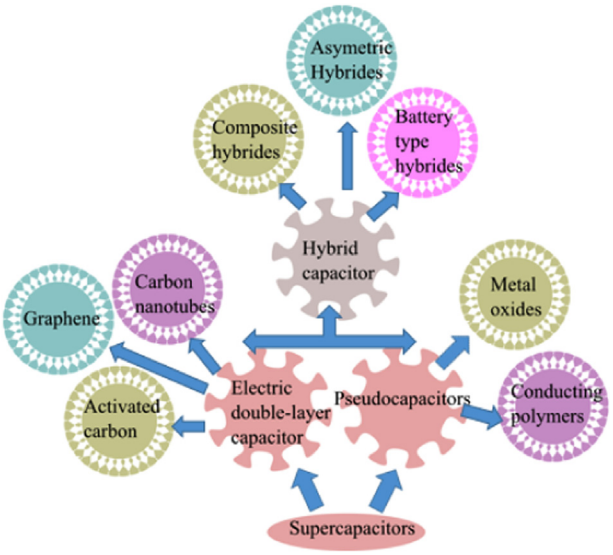

Fig. 4. Types of supercapacitors [336].

Although all those parameters are important for SC study, device capacitance is the main electrical feature used to evaluate SC performance. Several efforts have been made to enhance device capacitance, such as (a) developing nanoporous materials or hierarchal micro- to nano-structures with a large effective surface area [55,56] (e.g., homogeneous deposition of MnO_2 nanorods on GO (graphene oxide) to prevent aggregations, obtain a high effective MnO_2 surface area for charge transfer, and shorten the ionic diffusion path in the charging/discharging process) [57]; (b) improving the wetting electrode surface exposed to the electrolyte [58] (*e.g.*, GO possesses many oxygen-based functional groups that improve the total capacitance through additional Faradaic reaction effects and increase the wettability of porous carbons with electrolytes); (c) adjusting the mass transport mechanisms (e.g., the adjusted mass for a single layer of MWCNTs with a graphene electrode is approximately 2.65 ± 0.02 mg cm^{-2}) [59]; and (d) using innovative and active materials that allow high mass transportation (e.g., a graphene–nickel cobaltite nanocomposite/activated carbon (AC) with a mass loading of 10 mg cm^{-2} achieved 618 F g^{-1}) [60]. A mass-loading increase in pseudocapacitive materials results in higher resistance, limited access of electrolyte ions to the bulk of the active material, and lower specific capacitance [61–63]. Several types of SCs are already used commercially, and they can be categorized (hybrid, pseudo, etc.) by their charging mechanisms or the materials used in the electrodes, as shown in Fig. 4.

3. Energy storage mechanisms in supercapacitors

The mechanism of energy storage for SCs can be explained using three types of capacitive behaviors: (1) electrochemical double layer capacitors (EDLC) use the pure electric charge that accumulates at the electrode interface, (2) pseudo-capacitance (PC) develops from quick

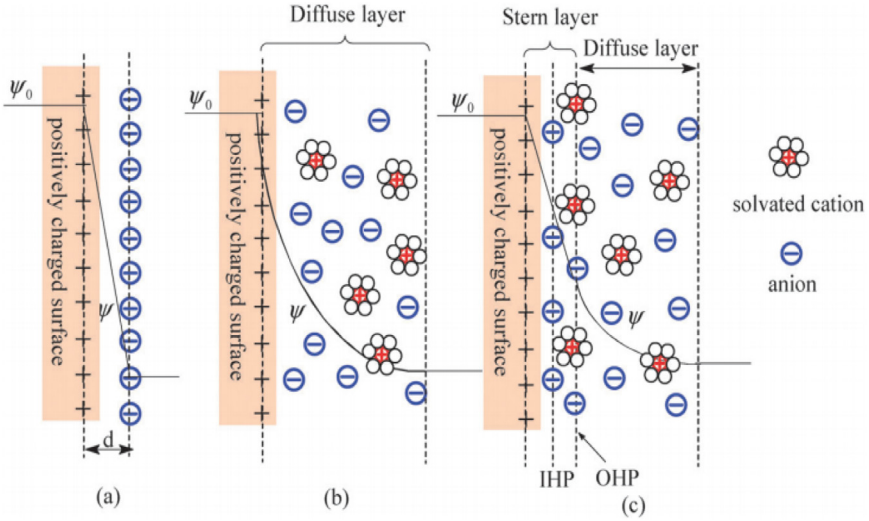

Fig. 5. Models for the electrical double layer at a positively charged surface: **(a)** the Helmholtz model, **(b)** the Gouy–Chapman model, and **(c)** the Stern model [64].

and reversible surface redox processes, and (3) hybrid capacitors take advantage of both mechanisms.

3.1. Electrochemical double layer capacitors

EDLCs exhibit higher energy density higher than conventional capacitors due to their maximum effective surface space and very small charge separation distances. EDLCs contain an electrolyte (such as KOH, H_2SO_4, or Na_2CO_3) between the electrodes instead of the dielectric medium used in conventional capacitors. Several physical parameters impose limitations on the performance of conventional capacitors, primarily inadequate charge storage space and the geometry of the two charging plates [64]. As schematically explained in Fig. 5(a), the concept for EDLCs was initially proposed and shaped in the 19th century by Helmholtz during investigations of opposite charges on colloidal particle interfaces. According to the proposed model, opposite charges are layered at the electrode/electrolyte interface and parted by an atomic distance, similar to two-plate, conventional capacitors. The Helmholtz model was modified by Gouy and Chapman into the diffusive layer model (Fig. 5(b)) [65,66]. The capacitance of 2 separated arrays of charges should increase reciprocally with their distance. Generally, it is assumed that EDLCs follow the same capacitive behavior as parallel plate capacitors [67]. Therefore, a large magnitude of capacitance would rise with point charges as they become closer to the electrode surface. Furthermore, Stern proposed a combined model between the Helmholtz and Gouy-Chapman models to acknowledge two regions of particle distribution—an inner region called the Stern layer (compact layer) and a diffusive layer (Fig. 5(c)). Within the Stern layer, ions (usually hydrated) are an effective adsorbate for the conductor. Moreover, the compact layer contains specific adsorbate ions (as anions in many cases, regardless of the electrode charge nature) and non-specific adsorbate counter-ions. The two types of adsorbed ions are distinguished as the inner and outer Helmholtz planes. The diffusive layer region can be explained according to the Gouy–Chapman model: the kinetic energy of the counter-ions results in a diffuse double layer affected by the thickness. The capacitance for an EDLC (C_{dl}) is a combination of the Stern layer capacitance (C_H) and the diffusive region capacitance (C_{diff}). Mathematically, C_{dl} can be written as:

$$\frac{1}{Cdl} = \frac{1}{H} + \frac{1}{Cdiff} \tag{1}$$

The electrical conduction of an EDLC at the planner electrode surfaces is controlled by the electrical field across the electrode and electrolyte and also the chemical affinities between them. Because an electrode exhibits a high specific area with a porous structure, EDLC behavior is highly contingent on porosity. Thus, the transportation of particles in the confined system is critically governed by factors such as the affinity of the tortuous mass transfer path, the area constraints within the pores, the electrical phenomenon related to the solution, and the pore surface wettability by the solution. Fig. 6 schematically demonstrates the mechanism for EDLCs using porous carbon conducting materials. The specific capacitance for EDLCs can be calculated as:

$$C = \frac{er\epsilon o \times A}{d} \tag{2}$$

In Eq. (2), $\mathcal{E}_r$, $\mathcal{E}_0$, A, and d represent the dielectric constant of the electrolyte, vacuum permittivity, electrode specific surface area available to the ionic species of the electrolyte, and EDL effective thickness (Debye length), respectively. In Eq. (2), the close relationship between the specific capacitance (C) and available area (A) is pertinent.

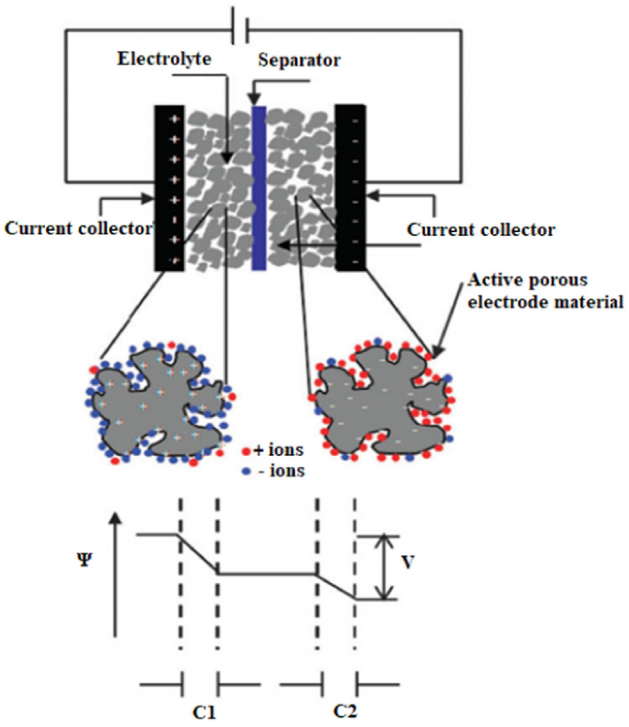

Fig. 6. Schematic for an EDLC made from porous electrode materials [64].

However, in practice, many researchers have pointed out that the expected linear relationships are not technically challenging [68,69]. This discrepancy is explained by the electrode sub-micropores, which do not contribute to the EDL formation. This likely reflects the unapproachability associated with sub-micropores on the surface in terms of steric factors such as ion size. For instance, Raymundo-Pinero et al. [70] reported the influence of micropores on the overall capacitance and found a specific capacitance of up to 357 F/g due to partial desolation of hydrated ions.

Numerous studies have explored the mechanistic relationship between pore size and capacitance [44,71–74]. In sum, they reported inconsistent capacitance in carbon-based electrodes with the pore sizes smaller than 1 nm. They also reported that no linear relationship could be established between the specific surface area and capacitance when using activated carbons and aqueous or organic electrolytes [44]. Furthermore, pores smaller than 0.5 nm were generally not accessible to hydrated ions (1 nm) [75].

A well-defined pore size distribution (i.e., micropores and mesopores with diameters of less than 2 nm and 2–50 nm, respectively) increases capacitance [76]. In this respect, manipulating porosity is important to enhancing the ionic conductivity of electrolytes [77,78]. Comparative studies have assessed the relationship between pore size and different electrolytes using activated carbons [79,80]. Fig. 7 is a graphical comparison of volumetric capacitance (activated carbon at 800 °C) versus the Brunauer-Emmett-Teller (BET) surface area using three different electrolytes. The trend of volumetric capacitance for 1 M H_2SO_4 was similar to that of 6 M KOH. The experimental data indicate that for an aqueous medium, the optimum pore size is about 0.7 nm. Furthermore, the value of volumetric capacitance is constant when pore diameter is larger than 1.1 nm (micropore < 2 nm, mesopore 2–50 nm, macropore > 50 nm). Fig. 7 indicates that the optimal pore for the formation of an effective double layer in organic medium is 0.8 nm. The slightly higher pore size for organic medium compared with aqueous medium can be explained by steric factors such as the ion size in the organic electrolyte.

In general, EDCC (electric double cylinder capacitor) and EWCC (electric wire-in-cylinder capacitor) models can be best explained using mesoporous and microporous carbon electrodes, respectively, as shown

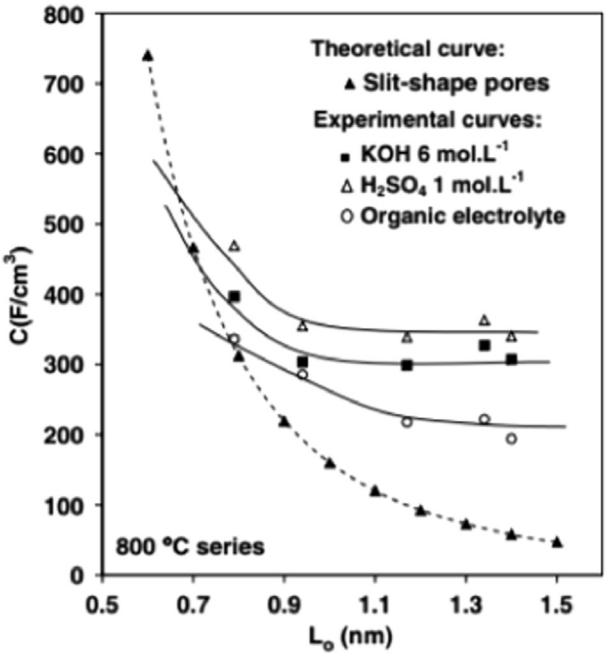

Fig. 7. Relationship between the volumetric capacitance (theoretical and experimental) and the pore size in aqueous or organic medium [70].

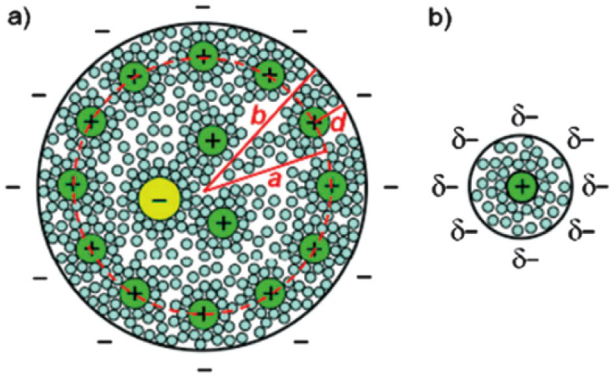

Fig. 8. Schematic layout (top views) for a) a negatively charged meso-pore with solvated cations approaching the pore wall to form an electric double-cylinder capacitor and b) a negatively charged micro-pore with cations lining up along the pore axis to form an electric wire-in-cylinder capacitor [48].

in Fig. 8 [48]. In addition, Eqs. (3) and (4) provide easy estimations for EDCC and EWCC, respectively.

$$C = \frac{\varepsilon_r \varepsilon_o}{bln\left[\frac{b}{b-d}\right]}A \tag{3}$$

$$C = \frac{\varepsilon_r \varepsilon_o}{bln\left[\frac{b}{a_o}\right]}A \tag{4}$$

The parameters involved in Eqs. (3) and (4) are as follows: b denotes the pore radius, d is the ionic distance approaching the carbon electrode surface, and a_0 is the magnitude of electron density around the ionic species (counter-ion effective size) [64]. For the EDCC and EWCC models, researchers successfully obtained a good fit with the mathematical results from Eqs. (3) and (4) for any carbon materials and electrolytes. The observations of inconsistent increments in capacitance for pore sizes less than 1 nm and slightly increased capacitance with pore sizes bigger than 2 nm can be explained using the EWCC and EDCC models. Moreover, the material dielectric constant calculated by fitting the data into Eq. (4) is very near to the vacuum value, which indicates that the desolation of hydrous ions took place prior to their penetration of the micropores. Despite those theoretical and experimental studies, the EDL charge storage mechanisms in nanostructured surfaces has not been fully elucidated. There is thus much demand for in-depth theoretical and experimental studies to accurately assess the charge storage mechanisms inside the micropores for sustainable EDLC development.

3.2. Pseudo-capacitors

The PC mechanism is based on a Faradaic charge process (electron transfer across the electrode interface by the oxidation or reduction of a chemical species) that can be reversible or irreversible. In the reversible process, no new chemical species are produced during the chemical reactions (oxidation/reduction), and new species are produced in the irreversible Faradaic process. Notably, the response of pseudo-capacitive materials is identical to that of double layer capacitors.

PC depends intrinsically on particle sizes and morphologies, e.g., amorphous $RuO_2{\cdot}nH_2O$ ($RuO_2{\cdot}1H_2O$: 1.9 nm = 720 F/g vs. $RuO_2{\cdot}0.2H_2O$: 9.9 nm = 200 F/g) [81] and orthorhombic Nb_2O_5 (T-phase: 35 nm = 400 F/g) [82]. Extrinsic PC is only accessible in nanostructured surfaces. Further inside the bulk, the same material does not show PC because of phase transformations during the ion storage process [83]. Kinetically, electroanalytical experiments offer a way to distinguish PC materials from battery-type materials. For example, PC electrodes are distinguished by redox reactions of transition metal oxides and reversible doping/de-doping in conducting polymers (CPs). To build such electrodes, the most commonly used materials are

carbons, metal oxides, and CPs [84,85]. PC can be many fold (10–100) greater than the capacitance of an EDLC. But the power performance of PC is lower than that of an EDLC because the slower Faradaic mechanism exhibits shrinking and swelling during charging and discharging, which leads to poor cycle life and mechanical stability [86].

For devices using PC, most electric charge is transported to the bulk or surface adjacent to the solid electrode surfaces [87]. Thus, the interactions between the electrolyte and the solid material involve a Faradaic reaction to reflect the mechanism of charge transfer, which depends on voltage. Therefore, PC is voltage dependent. In the development of ultra-capacitors using PC, three types of electrochemical processes are commonly involved: surface adsorption of electrolyte ions, redox reactions involving electrolyte ions, and doping/de-doping of CP materials in the electrode. The first two processes rely mainly on surface mechanisms, so the specific area of the electrode materials greatly affects the performance. The last process, using CP materials in the electrode, relies on a bulk process, so the surface area does not much affect the capacitance. In all cases, the electrode materials must exhibit maximum electronic conductivity for the distribution and collection of the electric current.

3.3. Hybrid capacitors

SCs represent a middle ground between batteries and capacitors which can be categorized into EDLCs and PCs. The main difference lies in charge storage mechanisms; in EDLCs, no chemical reaction occurs on electrodes, while charges buildup at electrode/electrolyte interface. In contrast, PCs exhibit high capacitance (e.g., compared to EDLCs), as they instigate redox reactions to occur near the electrode surface. It is simple to know that energy density of SCs is decided by two factors; electrode capacitance and cell voltage. As an effective method for increasing their capacitance, one may consider developing the nanosized and porous electrode material with the enhanced energy density. Alternative approach is to build asymmetric/ hybrid SCs with two types which can utilize the potential gap (between the two types of electrodes) to increase the total cell voltage; i.e., positive and negative electrodes are made by PC and EDLC material, respectively. There are two types of asymmetric/hybrid SCs. Firstly, capacitor type electrode/ capacitor type electrode SCs (e.g., redox/redox type such as EDLCs/ redox type). The second type is a capacitor type electrode/battery type electrode SCs [88,89].

For former, the fundamental electrodes candidates are carbon materials, conductive polymers (CPs), and transition metal compounds (TMCs). Cong et al. [90] fabricated the graphene/ polyaniline(PANI) based SCs, which showed high capacitance $\sim 763\ F g^{-1}$ at $1\ A g^{-1}$ in 1 M H_2SO_4 as compared to individual components like PANI ($\sim 520\ F g^{-1}$) and graphene ($\sim 180\ F g^{-1}$). A poly(3,4-ethylenedioxythiophene) (PEDOT) electrode was established by Anothumakkool and co-worker [91]. As these authors used PVA- H_2SO_4 gel as the electrolyte, the gel showed high volumetric energy density of $1\ mW h cm^{-3}$ [91]. Recently, the potential of TMCs (e.g., nitrides, metal oxides, carbides, and sulfides) has been studied for SCs. They can offer higher specific capacitances than carbon electrodes. For example, Binitha et al. [92] established electro-spinning method to fabricate porous α-Fe_2O_3 fiber and nano grain structures, which showed electrochemical properties in 1 M LiOH but somewhat distinctive capacitance of $256\ F g^{-1}$ and $102\ F g^{-1}$, respectively. Alternatively, Co based oxides/hydroxides have also attracted incredible attention for use in SCs. For example, porous $Co(OH)_2$ based SCs exhibited high capacitance $609\ F g^{-1}$ [93].

With the rapid growing market of hybrid-electric vehicles and electronic devices, there has been an ever urgent demand for electric energy storage devices with extremely high energy/power densities and good cycle life time. Lithium ion batteries have high energy density such as 150–200 $Wh kg^{-1}$, although they exhibit limited cycle life time (100–500 cycles). Additionally, the charging-rate is also problem related with Li ion batteries, because a fast charging rate can cause the safety issue of Li plating. On the other hand, for charging SCs, it takes only in minutes or seconds. As such, the combination of both high energy of Li ion batteries and fast charging rate of SCs has led to the development of (battery like) hybrid capacitors [94,95].

Recently, boron-doped diamond (BDD) films were fabricated with carbon nanofibers (CNFs) by Yu et al. [96]. The resulting CNF/BDD EDLC product was evaluated as capacitor electrodes using 1 M H_2SO_4 as the electrolyte. CNF/BDD PCs were then prepared by using a reducing species (0.05 M $Fe(CN)_6^{3-/4-}$) in a 1 M Na_2SO_4 aqueous solution. Their electrical performance remained intact after 10,000 charging/discharging cycles, confirming the stability of the materials. The power densities for the PC and EDLC devices were 25.3 and $27.3\ kW kg^{-1}$, respectively, and the energy densities were 44.1 and $22.9\ W h kg^{-1}$, respectively. The CNF/BDD vertically aligned hybrid films were effective enough for near-future use in highly efficient industry-oriented battery-like SCs.

For the development of a battery-like SC, it requires a suitable electrode material which must have a large surface area, while assisting the mobility of electrons and ions. On this note, several strategic developments have been proposed: (1) improving the conductivity of the electrodes [97]; (2) using nano-architectures for electrodes to minimize the diffusional pathways while attaining higher surface areas [98]; (3) developing 3D materials to accelerate ionic diffusion into several directions (*i.e.,* porous structures) [99]; and (4) minimizing the diffusional activation energy of the ionic species. Therefore, to meet such demand, various materials have been tested extensively such as carbon-based materials with sp^2 and sp^3 *atomic orbital* hybridizations, with different allotropic forms (*e.g.*, diamond, fullerenes, graphene, nanotubes, *etc.*), and with various dimensionalities (0D–3D) [100–103]. For most of the ECs explored in these approaches, organic binders such as polytetrafluoroethylene were used as pressed or coated electrode supporters and mixed with the carbon-based materials. Both electronic transportation inside electrodes and the diffusion of ionic species on the electrode surfaces are usually partially hindered, due possibly to the poor properties of the binders (e.g., low conductivity and relatively poor stability). Likewise, the novel synthesis of binder-free carbon electrodes is highly desirable in fabricating battery-like SCs.

Another major concern in constructing battery-like SCs lies in the selection of a suitable electrolyte. In general, EDLCs use inert electrolytes, whereas PS preferably uses electrolytes made of redox species and coated onto conductive substrates with metal oxides and polymers. Another efficient technique for fabricating PC SCs is modifying the electrolytes through the addition of soluble redox species. For this unique approach, the amount of redox species used is a major factor in determining the charge storage capacity which can be easily controlled. However, the contribution of that technique to the overall performance of SCs is as yet incompletely understood.

4. Characterization techniques for energy storage mechanisms

SC performance can be evaluated using parameters such as cell capacitance, series resistance, energy density, time, and operating voltage [45]. Many techniques are being used to evaluate those parameters, and the inconsistencies of the various evaluation methods and practices have created discrepancies and hurdles for the transfer of new SC technology into commercial implementation. Generally, three techniques are used to evaluate SC performance, and their merits and demerits are briefly summarized in Table 2. The main objective of these three techniques is to evaluate the electrochemical characteristics of energy storage devices from different points of view. For example, in cyclic voltammetry (CV), current is measured using the fixed scan rate and potential, whereas galvanostatic charge/discharge (GCD) uses current density and fixed potential, and electrochemical impedance spectroscopy (EIS) uses impedance or capacitance. In SCs, GCD is the most reliable parameter for evaluating electrochemical behavior. In addition to these techniques

Table 2
Technical merits and demerits of the CV, GCD, and EIS techniques.

S. No	Technique	Merits and demerits
1	CV	**Merits** • Degradation process [340] • Specific capacitance [341] • Differentiate between EDLC and PC [341] **Demerits** • Show only kinetic aspects; thermodynamic aspect is neglected
2	GCD	**Merits** • Capacitance [342] • Differentiate between EDL and PC [341] **Demerits** • Show same triangular shape for all double layer capacitive materials
3	EIS	**Merits** • Separately evaluate various resistances in a system [343] • Specific capacitance evaluation [344] • Differentiate between resistive and inductive nature [345] • Nondestructive technique • Relaxation time for recharging [346] • Degradation behavior [347] **Demerits** • Evaluation at small voltage only [348] • Discrete behavior above 10^6 Hz

4.1. Cyclic voltammetry

Cyclic voltammetry (CV) is an operative technique in electrochemistry. It measures the current produced when an applied voltage is in excess to that predicted by the Nernst equation. It has been widely used to illustrate the electrical performance of energy storage devices. The mechanism of CV follows the sweep of linear voltage to the electrodes. In short, a positive voltage sweep charges to a definite voltage (0–0.8 V), and after achieving maximum voltage, the sweep is immediately reversed for discharging. CV is an important technique for evaluating the mechanism of energy storage devices because it can generate a species in a forward scan and then probe its fate in the reverse scan, all within a few seconds. CV is unique technique that works on the principle of three electrodes (working, reference, and counter). The electrochemical performance of electrochemical capacitors can be evaluated using the applied voltage and current response. Eq. (5a) is a mathematical expression for calculating EDLC capacitance [104,105]:

$$C = \frac{Q_{total}}{2\Delta V} \tag{5a}$$

where Q_{total} is the CV curve integral area, which represents the total charge in coulombs, and ΔV is the change in voltage between the terminals of the device.

Eq. 5b expresses specific capacitance:

$$C_S = \frac{C}{m} \tag{5b}$$

Where C is the capacitance for a two-electrode cell evaluated using Eq. (5a), and m is associated with the active material masses of both electrodes.

Recently, Tanwilaisiri et al. [106] evaluated 3D printed supercapacitors by applying a potential window in the range of 0–0.8 V at scan rates of 0.02, 0.06, and 0.10 V s^{-1}. They found that the capacitance (C) decreased from 182 mF to 32 mF as the scan rate increased from 0.02 to 0.10 V s^{-1}. In other words, changing the scan rate highly affected the capacitance of the SC. The decrease in capacitance as the scan rates increase can be attributed to reduced efficiency in the ion diffusion process at higher scan rates. In general, at lower scan rates, ionic diffusion has enough time to penetrate the inner pores of the electrode, resulting in high capacitance. The specific capacitance calculated from Eq. 5b was 193.20 m F g^{-1} for a capacitance of 182 mF; this reduction was explained in terms of increased resistance caused by the penetration of PVA to the carbon pores. Wang et al. [107] also evaluated PC SCs using the CV method. They calculated specific capacitance values for SCs of 441, 399, 347, 265, and 182 F/g^{-1} at the scan rates of 5, 10, 20, 50, and 100 mV s^{-1}, respectively. Moreover, the information provided by CV curves, mainly a series of CV data at different voltage scan rates and evaluated capacitances, makes it possible to identify the type of electrochemical reaction, such as capacitive or faradic, during the charging and discharging processes. In most cases, the voltammogram can be modified by slow multielectron transfers; thus those electrons transfer reactions can easily distinguish specific types of reaction [108].

4.2. Galvanostatic charge/discharge test

Galvanostatic charge/discharge (GCD) is a traditional method to evaluate a series of SC performance parameters, such as capacitance, energy density, power density, ESR, and cycle stability. The GCD process follows the responsive potential relative to time and calculates information associated with an electrochemical phenomenon's occurrence in the SC electrode material. The overall GCD measurement process involves two steps: first, the SC charges via a constant current, and second, it is discharged in a specific time or voltage range. The capacitance can be estimated using Eq. (6):

$$C = \frac{i\Delta V}{\Delta t} \tag{6}$$

where i denotes the discharging current, ΔV is the discharge voltage for a device, and Δt is the discharging time [104,105]. The single-electrode specific capacitance (C_s) can be obtained from Eq. (7):

$$C_s = \frac{i\Delta V}{m\Delta t} \tag{7}$$

where i is again the discharging current, ΔV is the discharge voltage for a device, m denotes the total weight of two electrodes, and Δt can be one of several attributes, such as the discharging time [109,110]. The energy and power densities of an SC can be calculated as follows [109].

$$E = \frac{C\Delta V}{2} \tag{8}$$

$$P = \frac{E}{\Delta t} \tag{9}$$

Where C denotes the specific capacitance and Δt and ΔV are the discharging time and applied voltage, respectively. Moreover, volumetric specific capacitance and areal capacitance are also used to evaluate the performance of the supercapitor. In case of volumetric capacitance (F/cm^3), gravimetric specific capacitance is multiplied with the density of the electrode (density of active material) [111]. Likewise, the areal capacitance (F/cm^2) can be calculated by dividing capacitance of the electrode with area of the working electrode [112].

The most important use of the GCD test is checking the stability of SCs. Recently, Cao et al. [113] found that the C_S of capacitors could be as high as 520 F/g^{-1} at 0.5 A g^{-1}. They calculated energy and power densities as 58.5 Wh kg^{-1} and 22.5 W kg^{-1}, respectively. Moreover, the C_S decreased slowly, and 82% of the capacitance was retained after 800 field cycles at a current density of 3 A g^{-1}. Hou et al. [114] checked the performance of their SCs using GCD tests. They reported a C_s and energy density as high as 286 F/g^{-1} and 39.7 Wh kg^{-1}, respectively, at 0.5 A g^{-1}, and they found that 88.6% of the initial capacitance was retained after 3000 cycles. Although GCD is an appropriate technique to evaluate electrical properties, it shows the same triangular shape between cell voltage and time for all double layer capacitive materials.

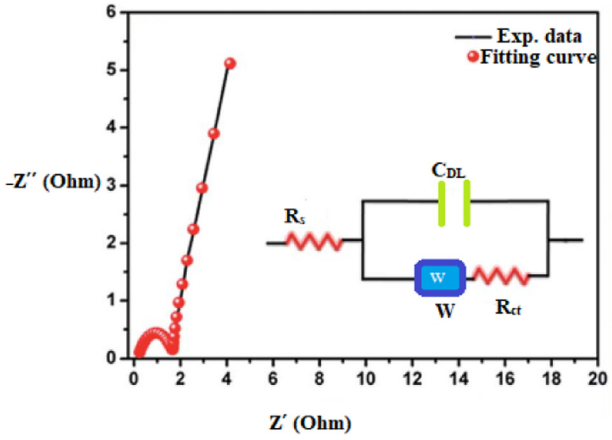

Fig. 9. Nyquist plot of AC electrode materials and the corresponding equivalent circuit (inset) in 20% KOH solution [116].

4.3. Electrochemical impedance spectroscopy

Electrochemical impedance spectroscopy (EIS) is an important technique for assessing the capacitive performance of a material and determining the contribution of the electrodes and electrolytic processes that participate in the electrical performance of an energy storage device. In general, for EIS measurements, the impedance data are collected at the open circuit potential by applying alternating potential at a small amplitude (*e.g.,* ± 5 to ± 10 mV) over a wide range of frequencies (e.g., from 0.01 to 100 kHZ) [89]. The capacitance can be calculated from EIS as $C = 1/(2\pi f|Z|)$ (using a linear portion of a log |Z| vs. log f curve: Bode plot) where |Z| is the imaginary part of impedance, and f is the frequency [115]. From the Bode plot, it is clear that capacitance decreases as frequency increases. At higher frequencies, SCs become pure resistance, showing that the electrolyte ions cannot penetrate the micropores at high frequencies.

The Nyquist diagram (Fig. 9) is another expression for describing EIS; it graphically represents the imaginary part of impedance, Z(*f*)", vs. the real part of impedance, Z(*f*)' [116]. From the Nyquist diagram, the charge transfer resistance can easily be calculated as the semicircle diameter on this expression. The pseudo-charge transfer resistance (associated with the porous structure of the electrodes) is observed in high to low frequencies (10^4 to 1 Hz). In contrast, at very low frequencies (< 1 Hz), pure capacitive behavior is a key feature of the impedance plot. Theoretically, a pure capacitor parallels the Nyquist plot's imaginary axis [117]. However, in normal cases, there is an inclined angle (45 and 90°) between the plot line and the real axis that corresponds (via the ion diffusion mechanisms) to Warburg and ideal capacitive ionic diffusion. In conclusion, EIS experiments can be conducted over a wide range of frequencies, from 10 mHz to 100 kHz. The use of alternating potential with very small amplitude, such as 5–10 mV, is the main drawback of this technique.

5. Material for supercapacitor electrodes

As discussed, the charge storage and capacitance of an SC depend heavily on the electrode materials. Thus, the use of newly designed materials with high capacitance and upgraded performance relative to conventional materials is the utmost goal for SC devices. The capacitance of an SC depends on the effective area for its particular electrode materials. It is also worth noting that not all the effective area is fully accessible to the interaction of the electrolyte and electrode material, which signifies that the capacitance for different materials isn't linearly proportional to the effective surface area [118]. Thus, the electrochemically accessible area can be called the electrochemical active surface area [119].

The electrochemical active surface area depends on the pore size of the conducting materials, which can be tuned easily by introducing nanostructures. Largeot et al. [120] proposed that the pore size of the electrode materials in a double-layer capacitor should resemble the ionic size of the electrolyte, with larger and smaller pores resulting a big reduction in capacitance. The results presented in Fig. 10, demonstrate the effect of pore size. A decrease in pore size from 1.1 to 0.7 nm ultimately increased the normalized capacitance; the maximum was achieved at ~ 0.7 nm, with a large decrease observed below 0.7 nm. In fact, increasing the pore size increases the available space (d) between the pore walls and therefore the center of the associated ions, which indicates that the capacitance will be weakened as the pore size increases. Obviously, the porosity of a material greatly influences its capacitance; therefore, pore sizes and pore size distributions cannot be ignored. The exact relationship between porosity and high capacitance is not particularly straightforward, comprising the pore size and pore size distribution for each available specific area ($m^2\ g^{-1}$). Fig. 11, shows the specific capacitance of EDLCs and PC systems using various active materials (carbon, metal oxides, conducting polymers, and carbon-based materials) [49,121–123].

5.1. Carbon-based electrode materials

Electrode materials derived from carbon are attractive for energy storage devices because of their low cost, high chemical/thermal stability, and excellent conductivity [124]. Carbon materials are used in EDLCs [125]. The high surface area of those materials is ultimately responsible for their excellent capacitance; therefore, the use of carbon-based materials as the electrode material for EDLCs has provided a breakthrough in energy storage (high capacitance).

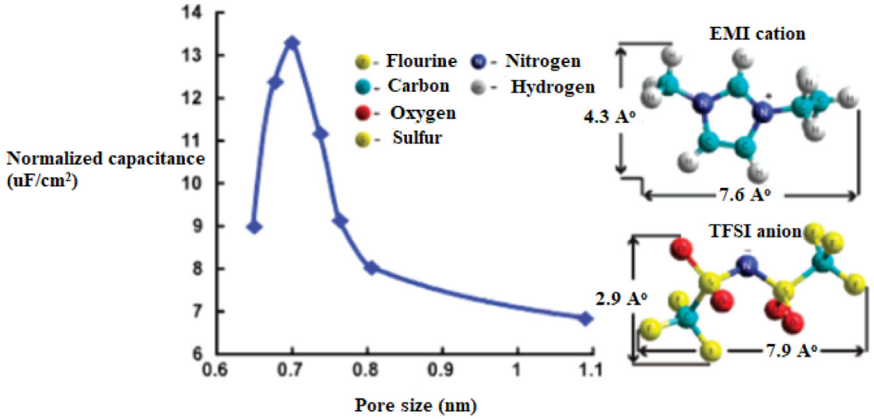

Fig. 10. Normalized capacitance change vs. pore size [120].

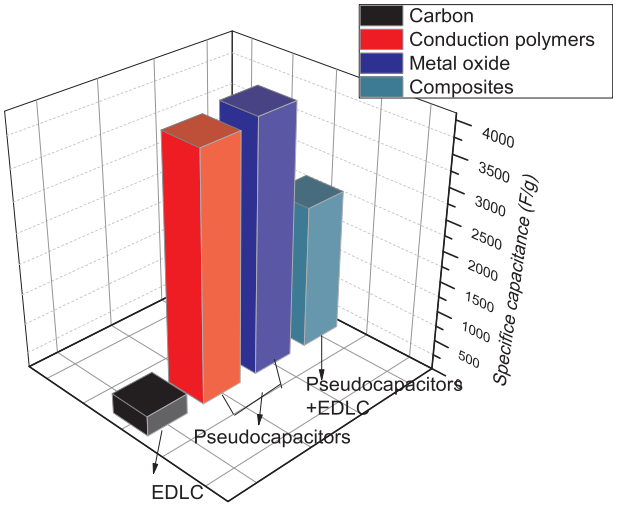

Fig. 11. Comparison of various novel materials for SC applications [121].

5.1.1. Activated carbons

A promising material for SCs is activated carbon (AC), which exhibits a large surface area, good electrical performance, and affordable cost. ACs are usually made from various carbonaceous materials (*i.e.* waste, coal, nutshells, and wood) via physical (thermal) or chemical steps. Physical activation describes thermal treatment of carbon precursors at high temperatures (700–1200 °C) with the help of reducing and oxidizing agents (*i.e.,* air, CO_2, and steam). Chemical treatment is conducted in lower temperature conditions (400–700 °C) using chemical agents such as oxyacid, potash, hydroxide, or metal chloride, depending on the activation method and the precursors used in fabrication. Considerable technical advances have been achieved to enhance the surface area of ACs up to 3000 $m^2\ g^{-1}$ and improve their electrochemical properties (total capacitance, real time constant, gravimetric capacitance, energy density, and electrical conductivity) [69,126–129].

The porous structure of ACs created through the activation process can be classified as micro-, meso-, and macropores. There are many discrepancies between specific surface area and capacitance for AC (e.g., in the case of graphene, sheets agglomerate during the reduction process of GO resulting in low surface area and an uncontrollable pore size distribution that ultimately lowers capacitance) [70,130,131]. Even under the condition of a highly available surface area (3000 $m^2\ g^{-1}$), an insignificant specific capacitance of < 10 mF cm^{-2} was achieved, which is inferior to the EDLC theoretical capacitance (15–25 mF cm^{-2}).

Although the EDLC performance relies on the available surface area, other parameters such as the pore size distribution, structure, and shape; surface functionality; and conductivity all have a large influence on EDLC electrical properties. Ba et al. [132] recently developed bio-derived and cost-effective porous carbon architectures for SC electrodes using chemical activation of fig waste. This newly fabricated porous material exhibited excellent surface area (2000 $m^2\ g^{-1}$) and high porosity, with well-organized micro-, meso-, and macropores. This material displayed improved specific capacitances of 340 and 217 F/g at current densities of 0.5 and 20 A g^{-1}, respectively, as well as higher energy and power densities than previously reported, commercially available SCs [84]. Moreover, the material showed exceptionally high stability, with more than 99% capacitive retention after 10,000 cycles. The high capacitance value can be credited to three facts: (i) the combination of a high specific surface area, > 2000 $m^2\ g^{-1}$ [133] and nano-platelet microstructures such as graphene that can deliver a high ionic diffusion during charging/discharging; (ii) hierarchical porosity, which imparts a high capacitance and high rate performance [134]; and (iii) the excellent electrical conductivity of the electrode material [135]. The obtained results make clear that the electrical performance of ACs is greater than that of various pure or other carbon-based nanostructures, *i.e.,* graphene and carbon nanotubes (CNTs), including ACs from waste such as sugar cane bagasse, cellulose, sawdust, cherry stone, and corn grains.

It is pertinent that excessive activation will lead to higher pore volumes, which ultimately reduces the material density and conductivity and thereby lowers power capability. Furthermore, the higher specific area of ACs will ultimately increase their active surface area, which could intensify the electrolyte decomposition risk at the dangling bond (immobilized free radical) positions, particularly in organic medium. Thus, it is highly recommended that the porosity and active surface functionality be optimized to maximize performance [129]. Also, the acidic functionalities and moisture content of ACs contribute to aging in organic electrolytes [136]. Many researchers have used different electrolytes and higher specific capacitance to establish correlations between capacitance performance and the nanoporous structure of ACs. For instance, the capacitance in aqueous electrolytes (100–300 F/g^{-1}) is higher than in organic electrolytes (< 150 F/g^{-1}) because organic electrolyte ions are larger than those in water-based electrolytes [64]. Organic electrolytes thus increase the quantity of pores that are smaller than the ions, which results in an increase in the number of pores that do not take part in the charge storage mechanisms. The wettability of the carbon surface by the organic solution determines the chemical affinity between them and is thus an important factor. The surface functionalities can affect the wettability of the electrode surface, which can also provide extra capacitance [56,137].

5.1.2. Carbon nanotubes

Since their discovery in 1991, Carbon nanotubes (CNTs) have received much attention as promising materials for diverse applications, *e.g.*, pollution control, separation, and energy storage, due to their structural, electrical, and mechanical properties [138]. Generally, CNTs can be categorized into two types. A single graphite sheet curled into cylindrical form forms a single-walled CNT (SWCNT), and multi-walled CNTs (MWCNTs) contain many concentric SWCNTs with different diameters [139,140]. Due to their fascinating electrochemical properties, such as high specific capacitance, stability under high current loads, and low internal resistance [141–144], CNTs make excellent polarizable electrodes, and therefore many studies have discussed both SWCNTs and MWCNTs as electrochemical SC electrodes [145–151]. Also, combinations of nano-tubular structures could open new avenues for SCs for three basic reasons: (1) active particle surfaces with nanotubes are more proficient than those of carbon-based materials such as ACs; (2) the mesoporous matrix created by the nanotubes accelerates the diffusion of ions to the active surfaces of the composites; and (3) cyclic performance can be improved dramatically because nano-tubular materials are characterized by their resilience and easy storage mechanisms for volumetric changes during charging and discharging [152–155].

CNTs are a prominent SC electrode material because of their light weight, intrinsic flexibility, high surface area (1600 $m^2\ g^{-1}$), and electrical conductivity (105 S cm^{-1}) [156]. However, their performance is highly affected by micropores and internal resistance, which can reduce the actual capacitance from the theoretically predicted one. Therefore, researchers are now trying to develop flexible carbon fiber (CF) hybrid electrodes (CF-CNT) to take advantage of their synergistic effects. To fabricate a flexible electrode material for energy storage that maintains its electrochemical performance characteristics under diverse conditions, it is highly desirable to develop a 3D composite architecture with a combination of CF, CNT, and graphene. Xiong et al. [157] worked on reduced graphene oxide (rGO)-CNTs grown on CF using electrophoretic deposition and chemical vapor deposition. The reported composite showed a specific capacitance of 203 F/g^{-1}, which is 4 times greater than that of pure CF. This hybrid also exhibited high electrochemical stability at various bending angles and could be directly used as a binder-free and flexible electrode material with excellent SC

performance. Therefore, we conclude that 3D hybrid architectures are promising candidates for flexible SC applications.

5.1.3. Graphene

Graphene is a structural arrangement of sp^2-bonded carbon atoms in a honeycombed single layer. Although it contains only carbon, arranging the atoms in different ways tunes its properties within broad ranges [158–161]. For example, graphene has potential in energy storage devices because of its high cyclic life and excellent chemical and thermal properties [162]. Parameters such as wide potential windows, high availability of functional groups with a large surface area, and excellent thermochemical stability, processability, and electrical performance have been widely studied and make graphene advantageous for energy devices [163–166].

In particular, the high specific area ($2630\ m^2\ g^{-1}$) [167] of graphene sheets has attracted much interest for energy storage devices such as SCs and batteries. This available surface area is much higher than that of black carbon ($< 900\ m^2\ g^{-1}$) [168] and CNTs ($50–1315\ m^2\ g^{-1}$) [169] but similar to ACs. The emergence of graphene has undoubtedly changed the status of SC technology through its extraordinary electrochemical characteristics and other distinctive properties. Current developments in fabricating graphene–polymer composites reveal the promising features of those materials for SC applications. Composites of graphene and CPs can provide a high mechanical support that ultimately increases both the cycling performance and specific capacitance.

Graphene-based SCs using ionic liquid electrolytes, aqueous electrolytes, and organic electrolytes were found to have specific capacitances of 75 [170], 135, and 99 F/g^{-1}[171], respectively. Reduced graphene, with a lower agglomeration, attained a maximum specific capacitance of 205 F/g^{-1} in an aqueous electrolyte, with an energy density of $28.5\ W\,h\,kg^{-1}$ [172]. Navarro-Suárez et al. [173] followed the Li-Wallace method, which uses hydrazine hydrate to create rGO, which showed a high gravimetric capacitance (251 F/g^{-1} at $2\ mV\,s^{-1}$). Li et al. [174] introduced stretchable supercapacitors using reduced graphene oxide 3D interdigital electrodes to achieve adjustable volumetric capacitance. As such, it is favorable to fabricate ultra-high performance supercapacitors to meet energy demands in sensitive devices.

A freestanding MXene/rGO-5 wt% electrode was recently prepared by Yan et al. [175] using a novel electrostatic self-assembly technique for modified rGO, poly(diallyldimethylammonium chloride), and titanium carbide. This electrode displayed the high volumetric capacitance of 1040 F/cm^{-3} at a scan rate of $2\ mV\,s^{-1}$, with 61% capacitive retention and maximum cycle life. Moreover, this electrode had a high energy density (volumetric) of $32.6\ Wh\,L^{-1}$, making it one of the best materials reported for carbon and MXene in aqueous media. A novel quasi state Li-ion capacitor was proposed by employing TiO_2 hollow microspheres with graphene nanosheets [176]. They obtained well defined TiO_2 nanocrystals embedded with graphene nanosheets. This combination provided ultrahigh energy density ($72\ Wh\,kg^{-1}$) along with long cycle life (1000 cycles). Further, they extended this concept to prepare another Li-ion capacitor by using Li_3VO_4/CNF and electrochemically exfoliated graphene sheets as the anode in a polymeric gel electrolyte. Accordingly, they were able to achieve an energy density of $110\ Wh\,kg^{-1}$ with good cycling performance [177]. This quasi solid state concept can alleviate many problems associated with the electrolyte leakage with the potential to reduce the gap between conventional Li-batteries and future supercapaciotrs.

5.2. Conducting polymers

Conducting polymers (CPs) are organic polymers that conduct electricity through a conjugated bond matrix. In the past two decades, CPs have been extensively studied for use in diverse SC applications due to their higher energy density than metal oxides, low cost, and reversible Faradaic redox capabilities [178–180]. Among the CPs, polyaniline (PANI), polypyrrole (PPy), and polythiophene derivatives have particularly been studied as SC electrode materials for their high conductivity and low cost [181–187]. Optimizing the morphology of CPs is an important factor for the electrochemical performance of the resulting SCs. In previous studies, CPs in various forms (e.g., nanorods, nanosheets, and nanowalls) have been developed and applied effectively as energy storage options [188]. CPs with nano architectures possess high surface area and high porosity that ultimately results in good performances because of their intrinsic conduction, high surface to volume ratio, and surface interactions at the nanoscale. Recent developments in CPs have demonstrated that as one-dimensional nanostructures, these materials could achieve much better PC than their bulk counterparts [189].

5.2.1. Polyaniline

PANI (polyaniline) is an electricity-conducting polymer that has found promising applications in energy storage devices due to its easy synthesis, low cost, good electrical activity, and good stability [126,190]. However, for energy storage devices, bulk PANI is ineffective due to its low available surface area. Therefore, PANI with nanostructures that provide a large surface-area has gained much interest as a promising material for SC electrodes. Many PANI hierarchical nanocomposites have been investigated for SC electrodes and produced promising electrochemical performances [191–194]. Luo and co-workers used a simple polymerization route to synthesize a hierarchical graphene@polyaniline nanocomposite with excellent specific capacitance (488 F/g^{-1})[195]. Miao et al. [196] used sacrificial templates to fabricate hollow PANI nanostructures for SC electrodes that had excellent specific capacitance ($601\ F\,g^{-1}$). Those electrodes were synthesized by polymerizing a monomer of aniline on poly(amic acid) (PAA) nanofibers and then selectively removing the poly PAA nanofiber template. However, potential structural degradation during the template removal process limits this approach to fabricating PANI nanostructures. Therefore, other techniques should be used to fabricate PANI nanostructures with good electrical performance.

Although many routes are available for the fabrication for PANI nanostructures, many challenges remain in synthesizing these nanostructures and assembling them into an electrode. For example, hybrid electrodes with a low-capacitance substrate require additional time, cost, and resources for multistep fabrication. In general, SC electrodes are being prepared by mixing PANI nanostructures with binders such as polyvinylidene fluoride and some conductive additives. This fabrication process can distort the PANI nanostructures and introduce inert materials through binder deposition on the electrode surface. Therefore, a single and straightforward synthesis process to fabricate self-supporting PANI nanostructures is needed.

Electrospinning is a technique with a simple setup and methodology for fabricating electrospun nanofiber morphologies [197]. However, PANI is not a good candidate for electrospinning because the aromaticity in the PANI backbone makes individual PANI chains highly rigid [198], which prevents the chain entanglements within the PANI solution needed to attain the viscosity required for successful electrospinning. Additionally, the limited solubility and dispersion of PANI in organic solvents adds to the difficulty in achieving sufficient viscosity (2000–3000 cP) by simply adding more polymer concentration. A suitable polymer blend can be used to overcome those issues, but the need for a substantial amount of carrier polymer prevents the formation of smooth and continuous nanofibers at high PANI concentrations. Typically, the carrier polymer shows electrically insulating properties; thus, adding carrier polymer in high concentrations reduces the electrical properties of the electrospun PANI nanofibers. Chaudhari et al. [199] fabricated SC electrodes (specific capacitance of 267 F/g^{-1} at a current density of $0.35\ A\ g^{-1}$) with an equivalent mass ratio of PANI/PEO electrospun nanofibers. That novel work opens new avenues for using electrospinning to fabricate PANI nanofibers.

A freestanding, binder-free approach to fabricating an SC electrode

with high-purity PANI nanofibers through a single electrospinning step was reported by Simotwo et al. [200]. They successfully electrospun PANI nanofibers at a 93 wt% concentration by mixing poly(ethylene oxide) (PEO), which has an ultrahigh molecular weight, with the PANI solution to provide adequate chain entanglements. They also used a low concentration of CNTs (12 wt%) to improve the stability and conductivity of the SC electrode made from the PANI/PEO composite solution. The morphology characterization of the synthesized nanofibers was done by scanning electron microscopy (SEM) and BET porosimetry. CV, GCD, and EIS were used to characterize the electroactivity of the pure PANI and PANI-CNT nanofiber electrodes. The PANI and PANI-CNT electrodes showed specific capacitances of 308 and 385 Fg^{-1} with capacitive retention of 70% and 81.4%, respectively, at a current density of 0.5 Ag^{-1}, and they were stable for up to 1000 cycles. The consistent nanofiber architecture enabled excellent electronic conductivity, and the inter- and intra-fiber porosity allowed effective penetration of the electrolyte in the polymer matrix, expediting ionic transportation to the active sites. Thus, Simotwo et al. [200] found a facile approach to fabricating PANI and PANI-CNT nanofiber electrodes without any binder. The combination of low electrochemical impedance and good inter- and intra-fiber porosity provided excellent electrochemical properties for the newly synthesized electrode. The need for an electrochemically inert or insulating electrode was removed by the free-standing approach and resulting 3D porous structure that remained stable throughout the capacitor life. The SEM image in Fig. 12(a), shows that electrospinning PANI93 solution produces a continuous and nonwoven nanofiber structure with precise inter-fiber porosity. Adding CNTs did not impart any negative effect on the electrospinning: smooth PANI-CNT fiber mats were produced, as shown in Fig. 12(b). Li et al. [190] prepared a PANI nanofiber–coated graphite electrode with excellent reversible capacity of 2136 F/g^{-1} at a current density of 1 A g^{-1}, with excellent rate capability (Fig. 13) in 6 M H_2SO_4 and 91% capacitive retention for up to 1000 cycles.

5.2.2. Polypyrrole

The unique features of polypyrrole (PPy), such as high conductivity, high thermal stability, quick charging/discharging, low cost, and high energy density, make it most promising for Faradaic PC applications [201]. PPy is one of the most flourishing CPs because its monomer can be easily oxidized [202]. In addition, this monomer is water soluble and commercially available. The major advantages arising from the diverse applications of PPy as an electrode material are its high energy density, reversible electrochemical doping/dedoping, and easy electrochemical processability.

The appropriate use of dopants (i.e., aromatic anions) in the electropolymerization of PPy can enhance the properties of charge storage and cycling performance, conferring high specific capacitance and maximum thermal stability [203]. However, anionic dopants can disturb the stability of PPy during charging/discharging [204].

Composites of PPy and graphene have received much interest in the field of energy storage applications. One group of researchers [202] recently developed hybrid materials that combined the advantages of EDLC and PC. They prepared rGO/PPy/Cu_2O-$Cu(OH)_2$ ternary nanocomposites as an electrode material for SCs. In three electrode systems, rGO/PPy/Cu_2O-$Cu(OH)_2$ showed an excellent gravimetric specific capacitance (997 F g^{-1} at a current density of 10 A g^{-1}). The EDLC of graphene, together with the PC behavior of PPy and Cu_2O-$Cu(OH)_2$, resulted in energy and power densities of 20 Wh kg^{-1} and 8000 W kg^{-1}, respectively. For the rGO/PPy/Cu_2O-$Cu(OH)_2$ SCs, the maximum power density was 19998.5 W kg^{-1} at an energy density of 5.8 Wh kg^{-1}, with a capacitance retention of 90% after 2000 cycles.

An asymmetric SC composed of PPy-CNT electrodes achieved good specific capacitance, stability, and energy density [204]. Many researchers have reported that PPy-CNT composite-based asymmetric SCs showed excellent specific capacitance values. Lin et al. [205] even reported an exceptionally high value of 890 F/g^{-1}. Dubal et al. [206] explored organic-inorganic hybrid materials based on open-ended, porous, one dimensional PPy nano-pipes (PPy-NPipes) and heteropolyoxometalate (phosphotungstate ($[PW_{12}O_{40}]^{3-}$ (PW_{12}) or phosphomolybdate $[PMo_{12}O_{40}]^{3-}$(PMo_{12})). Those hybrid materials showed excellent areal capacitances that were 1.5–2-fold higher than that of pristine PPy-NPipes (Fig. 14). However, on the practical and research forefronts, new and improved methods for synthesizing PPy are needed to improve the interfacial compatibility between it and other materials and achieve high theoretical and practical specific capacitance values.

5.3. Metals oxides

Many oxides from the transition metal family, such as nickel oxides (NiO), cobalt oxide (Co_3O_4), ruthenium oxide (RuO_2), and manganese dioxide (MnO_2), and have been intensively studied as SC electrode materials due to their mesoporous structures [207,208], which makes them promising materials due to their high specific surface areas and even pore size distributions. Effective interactions between electrodes and electrolytes favor a fast transportation rate for ionic species in the bulk electrode and at the electrode/electrolyte interface, which gives these materials high specific capacitances. In addition to metal oxides, the composites of metal oxides with other materials such MnO_2 – graphene have also been studied widely for supercapacitor applications [209].

The metal oxide most commonly used in energy devices is RuO_2, which has a specific capacitance of 905 F/g^{-1}; however, its high cost restricts RuO_2 in commercial markets [210]. To circumvent that problem, earth-abundant and non-noble, metal-based materials have gained great attention. In particular, cobalt sulfide materials, such as Co_3S_4, CoS_2, Co_9S_8, $Co_{1-x}S$, and Co_xS_y, have gained attention for their wide stoichiometric composition and good stability. However, the development of those materials remains at a rudimentary stage. Thus, there is considerable demand for economical materials that can be easily used for energy devices and ecofriendly electrolytes. To date, many

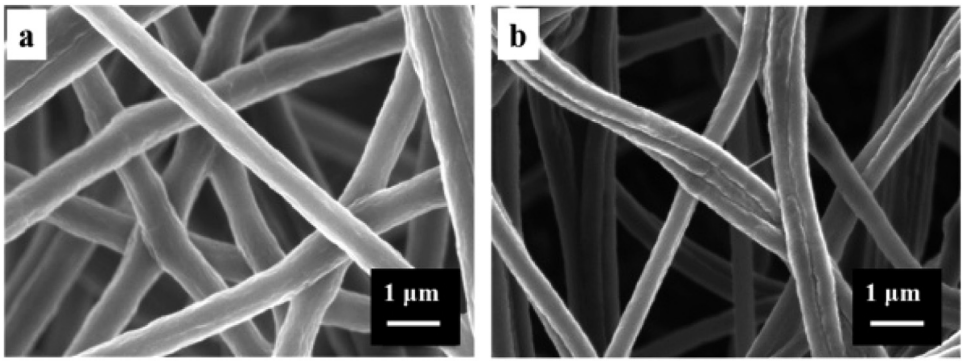

Fig. 12. SEM images of **(a)** PANI and **(b)** PANI-CNT [197].

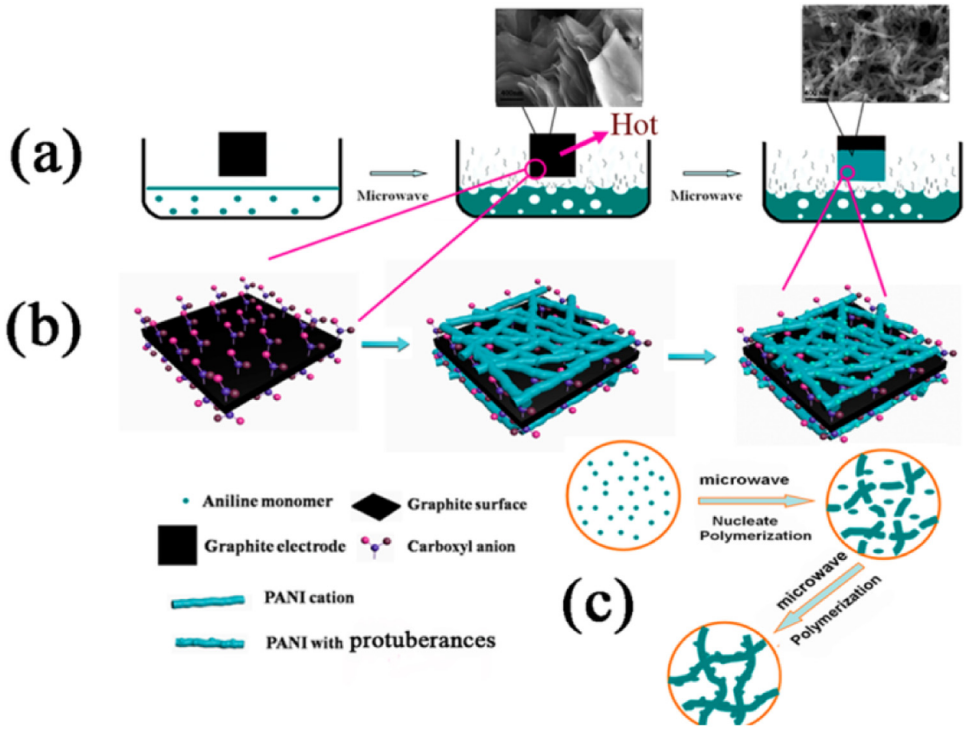

Fig. 13. Schematic of the possible formation process for a PANI-coated graphite electrode under microwave radiation [190].

materials have been investigated and used as metallic oxide electrodes in neutral electrolytic solutions, including iron oxide (Fe_2O_3), vanadium oxide (V_2O_5), indium oxide (In_2O_3), tin oxide (SnO_2), and manganese oxide (MnO_2).

5.4. Composites

Carbon-based materials (graphene and CNTs) are widely used as electrode materials, even though their specific capacitance is quite low [211,212]. On the other hand, metal oxides and CPs were seen to offer good PC that can produce maximum energy storage capability [213]. However, they have low cyclic stability during the charge/discharge process to restrict their growth in practical SC applications. These challenges can be minimized by using composite materials as electrodes with high energy and power densities. This combination could improve the performance of SCs to meet energy storage demand in a sustainable way. Likewise, Au/Ni12P5 core/shell nanocrystals were fabricated by using bimetallic hetrostructures. The shell of the fabricated

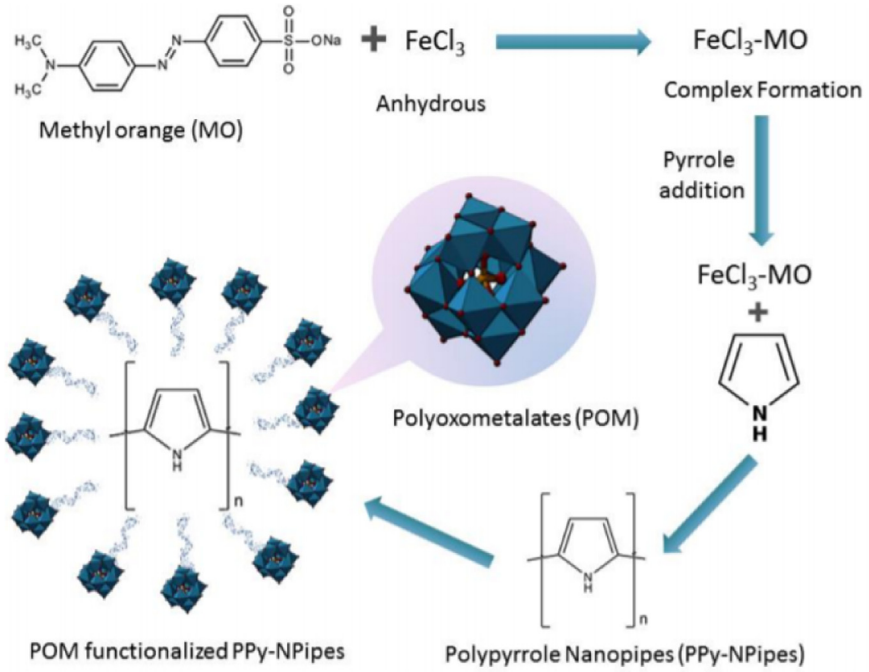

Fig. 14. Schematic of the steps involved in the synthesis of a polypyrrole nanopipe (PPy Npipe) and polyoxometalate (POM, PMo_{12} or PW_{12}) hybrid material using a simple chemical method [206].

nanostructures was controlled to 5 nm. The electrochemical analysis of this concept showed specific capacitance of 806.1 F/g (91.1% retention) up to 500 charge-discharge cycles [214]. These authors claimed that the noble metal phosphide modification will open new avenues for energy storage materials such as advanced supercapacitor and battery technology.

A novel direct ink writing technique was proposed and developed to fabricate planer SC electrodes by Wang et al. [215]. A composite of PANI/GO ink was used to make different architectures such as 3D honeycomb, column lattice, and hollow thin-wall column. A planar SC reported in this study showed remarkable electrical performance with 1329 $mFcm^{-2}$. Furthermore, these results suggest that 3D printing could facilitate the scale-up process for composite structures on SC electrodes. Pandey et al. [216] reported the synthesis of a nanocomposite (NiS/G) for SC electrodes, which they claimed offered high storage capacity with minimum impedance, a cycle life of more than 1000 cycles, and a maximum observed specific capacitance of 187.53 Fg^{-1}. In another study, Mao and Rasheed describe a porous composite of Mn_2TiO_4/TiO_2 as a high performance electrode for SCs. This composite exhibited maximum surface area and reaction sites for electrochemical reactions. The synthesized composite showed excellent electrochemical performance, with a specific capacitance of 98.2Fg-1 at a current density of 0.5 Ag^{-1} and stability up to 10,000 cycles [217]. As shown by these excellent performance reports, composite materials are currently the best choices for SC electrodes. Furthermore, graphene composite electrodes are also used in SCs. Graphene composites are usually multiphase materials in which graphene is mixed into a ceramic, polymeric, or metallic matrix by physical processing techniques such as shear mixing or ball milling [218,219]. Table 3 lists some of the recent literature on different electrode materials for SC applications.

6. Electrolytes

The electrolyte, meaning salt + solvent, is an important element of ESs, giving ionic conductivity and resulting charge compensation on both electrodes in a cell [220]. Within an ES, the electrolyte not only plays a fundamental role in the creation of the double layer (EDLCs) and reversible redox reactions (PC) for electric charge storage, it also predicts an SC's performance. Most existing commercial ESs use organic electrolytes with a cell electric potential range from 2.5to 2.8 V, mostly acetonitrile (ACN), though some use propylene carbonate.

The important factors in choosing an electrolyte are (a) the ionic size and type, (b) the electrode materials, (c) the ion and solvent concentration, (d) the ion and solvent interaction, and (e) the potential window. Electrolytes can affect the capacitance and PC of an EDL, the cycle-life of the ES, and the energy/power densities. For example, the electrochemical stable potential window (ESPW) directly measures the operation cell voltage of an ES, which influences both the power densities and energy [220].

Many electrolytes for energy storage devices have been reported in the literature. As shown in Fig. 15, these electrolytes are mainly categorized as liquid (aqueous, organic, and ionic liquid (IL)) and solid/quasi-solid-state (organic and inorganic) electrolytes [221–223]. No perfect electrolyte has yet been developed; both types of electrolyte have technical merits and demerits. For example, aqueous electrolytes can provide high capacitance and conductivity, but their working voltage is narrow due to constricted decomposition voltage. ILs and organic electrolytes can function at higher voltages, but they suffer from inferior ionic conductivity. Solid-state electrolytes evade the risk of leakage, a common problem for liquid electrolytes, but they offer lower conductivity than liquids. Many efforts have been made to find new electrolyte materials that can maximize the performance of energy storage devices, and those efforts have produced many technical advances, including (a) the development of new materials with: (1) a wider operational voltage window, (2) higher ionic conductivity, (3) a wider range of working temperature, and (4) thermal stability [221,224,225]; (b) the evaluation of the positive characteristics of specific electrolytes on SC properties, including (1) capacitance, (2) power and energy densities, and (3) the charging/discharging process; and (c) creating a better understanding of the electrolyte's role in the performance of an ES by progressive modeling of experimental results using simulation methods.

6.1. Aqueous electrolytes

Generally, aqueous electrolytes show good conductivity (*e.g.*, 0.8 S cm^{-2} for 1 M H_2SO_4 at 25 °C), at least one order of magnitude higher than that of ILs and organic electrolytes. This is advantageous for decreasing the ESR, which enhances the power delivery of ESs. Aqueous electrolytes are usually selected by the size of their hydrated cations and the mobility of their anions. These factors affect both ionic conductivity and specific capacitance. An electrolyte's corrosive power and ESPW should also be considered. However, aqueous electrolytes are not a suitable choice for commercial electrochemical SCs because of their small electric potential windows, which is one key reason that commercial ESs generally use organic electrolytes rather than aqueous ones. Usually, aqueous electrolytes are grouped into alkaline, acid, and neutral solutions, of which Na_2SO_4, H_2SO_4, and KOH are the most commonly used representatives. Qu et al. [226] investigated the performance of MnO_2 nanorods using neutral aqueous electrolytes (*e.g.* Li_2SO_4, K_2SO_4, and Na_2SO_4). The newly fabricated AC supercapacitor showed excellent cycling behavior with large energy density (17 Wh kg^{-1}) and power density (2 kW kg^{-1}). This investigation opened new doors for low cost and environmental friendly electrolytic solutions for energy storage technology. In another study, the combination of $NaMnO_2$ and activated carbon was tested using aqueous solution of Na_2SO_4 electrolyte [227]. This system delivers maximum energy density (19.5 Wh kg^{-1}) and higher power density (130 Wh kg^{-1}) with excellent cycling behavior (less than 3% capacitance loss). This combination was helpful to further extend applications of environmental friendly aqueous electrolytes [227]. In the industrialization of SCs, many researchers have worked to replace conventional electrolytes and achieve better electrical performance.

In SC technology, the main objectives for electrolytes are easy handling, no leakage, and high capacitance. In this regard, aqueous electrolytes can be modified slightly by adding different gels to create a stable electrolytic system. Wang et al. [228] made a novel gel by immersing polyacrylamide gel (PAM-G) into an aqueous solution of 6 M KOH for about 60 h. The resulting electrolytic system provided excellent cycling stability, rate capability, and high specific capacitance (196 Fg^{-1} at GCD 1 Ag^{-1}), which the researchers attributed to the homogeneous three-dimensional microporous structure of the PAM-G, which facilitated the permeability of ionic transportation.

Recently, solid-state electrolytes for energy storage devices have received much attention because they eliminate the decay of ionic conductivity during long-term electrical performance. A novel solid-state matrix electrolyte was reported by Pan et al. [229]. They prepared an electrospun matrix of PVA and GO and achieved excellent performance after filtering it with an aqueous electrolyte. This novel matrix showed much less ionic conductivity decay (38.4%) than pure PVA (84.0%) after 1 month of testing in a humid (RH:45%) atmosphere. These results clearly show that a solid state matrix made from aqueous electrolytes can provide stable electrical performance for electronic devices.

6.2. Organic electrolytes

ESs that use organic electrolytes currently lead the commercial market because of their high operating electric potential window, mostly in the range of 2.5–2.8 V [220]. Organic electrolytes also allow the use of inexpensive materials as current collectors and packages.

Table 3
Types of electrode materials recently applied for supercapacitor applications.

Order	Material used	Measurement protocol	Electrolyte	Electrode configuration	Maximum specific capacitance	Reference
[a] Graphene						
1	Poly tris[4-(2-thienyl)phenyl]amine	GCD (2.5 $mAcm^{-2}$)	1 M $TEAFB_4$/ACN	3-electrode	278 F/g	[197]
2	Graphene/polyaniline nanocomposites	CV (20 $mV\,s^{-1}$)	1 M H_2SO_4	3-electrode	267.2 F/cm^3	[349]
3	$V_2O_5$0.0.5H_2O/rGO hybrid	CV (5 $mV\,s^{-1}$)	2 M KCl	3-electrode	649 F/g	[350]
4	Graphene/polyaniline/Co_3O_4 ternary composites		6 M KOH.	3-electrode	789.7 F/g	[351]
5	S-rGO/CNTs/PANI	GCD (1 A g^{-1})	1 M H_2SO_4	3-electrode	812 F/g	[191]
6	Hierarchical macro/mesoporous graphene foam (fRGO-F/PANI)	GCD (1 Ag^{-1})	1 M H_2SO_4	2-electrode	939 F/g	[352]
7	PANI-PORGO	GCD (1A g^{-1})	1 M H_2SO_4	3-electrode	369 F/g	[341]
8	3D RGO-CNT- PANI hybrid	CV (10 $mV\,s^{-1}$)	1.5 M Li_2SO_4 solution	2-electrode	741 F/g	[353]
9	RGO/PANI composite	GCD (1 A g^{-1})	3 M NaOH	3-electrode	596 F/g	[354]
10	PANI-rGO	GCD (1 A g^{-1})	1 M H_2SO_4 + 1 mM catechol	3-electrode	1967 F/g	[355]
11	3D graphene foam/PANI nanorods	CV (10 $mV\,s^{-1}$)	1 M Na_2SO_4	2- electrode	352 F/g	[356]
12	RGO/MnOx@carbon HCN nanohybrids	GCD (1 A g^{-1})	6 M KOH	3-electrode	355 F/g	[357]
13	RGOMnOx@carbon HCNs nanohybrids	GCD (1 A g^{-1})	6 M KOH	2-electrode	270 F/g	[357]
14	PANI-NFs/GO nanocomposites	GCD (0.2Ag^{-1})	1.0 M Na_2SO_4	2-electrode	79.5 F/g	[358]
15	Porous graphene-polyaniline nanoarrays composite	GCD (1 Ag^{-1})	1 M H_2SO_4	3-electrode	752 F/g	[359]
16	Reduced graphene oxide/carbon nanotube composite fibers	GCD (1 Acm^{-3})	1 M H_2SO_4	3-electrode	193.1 F /cm	[360]
17	THAQ/graphene composite	GCD (1Ag^{-1}	1 M H_2SO_4	3-electrode	259 F/ g	[361]
18	Graphene/polyaniline composites	GCD (6 $mAcm^{-2}$)	H_2SO_4/PVA gel	2-electrode	1506.6 mF/cm	[362]
19	(RGO/CNTs)@PANI composite	GCD (0.2 A cm^{-3})	poly(vinyl alcohol)/H_2O_4 gel polyelectrolyte	2-electrode	36.7 F/ cm	[360]
20	$CoMoO_4$ –3D Graphene hybrid	GCD (1.43 Ag^{-1})	2 M KOH	3-electrode	2741 F/g	[363]
21	Fe3O4 nanoparticles grown on graphene	GCD (0.5 Ag^{-1})	1 M KOH	3-electrode	220 F/g	[364]
22	Fe2O3 nanoparticles on nitrogen doped Graphene	GCD (0.5 Ag^{-1})	1 M KOH	3-electrode	267 F/g	[365]
23	3D graphene/MoS2 composites	GCD (1 Ag^{-1})	1.0 M Na_2SO_4	3-electrode	410 F/g	[366]
[b] Polyaniline						
24	Polyaniline-functionalized carbon cloth	GCD (1.4 Ag^{-1})	PVA-in-H_2SO_4 (1.0 M) gel electrolyte, containing NQ and 30% acetic acid	2-electrode	4007 F/g	[49]
25	PANI/NFs/PET-5.4	CV (1 $mV\,s^{-1}$)	NaCl/HCl aqueous solution	3-electrode	503 F/g	[367]
26	PANI-CuCo2O4 composite	GCD (0.4 Ag^{-1})	1 M of KOH	3-electrode	403 F/g	[368]
27	PPy/PANI double layer nanotubes	GCD (1 Ag^{-1})	0.5 mL aniline in 100 mL of 0.01 M H_2SO_4	3-electrode	542 F/g	[369]
28	MSNS/GO/PANI	GCD (1 Ag^{-1})	1 M H_2SO_4	3-electrode	412 F/g	[370]
29	Polyaniline with gold particles incorporation	GCD (2 Ag^{-1})	1 M H_2SO_4	3-electrode	485 F/g	[371]
30	Ni-CeO2@PANI	GCD (1 Ag^{-1})	1 M Na_2SO_4	2&3-electrode	866 F/g	[372]
31	Co3O4/PANI hollow nanocages Co3O4 NCs	GCD (1 Ag^{-1}) –	6 M KOH	3-electrode –	1301 F/g 865 F/g	[373]
32	Polyaniline/UiO-66 composites	GCD (1 Ag^{-1})	1 M H_2SO_4	3-electrode	1015 F/g	[374]
[c] Zeolites						
33	Zeolitic imidazolate framework-derived nitrogen-doped porous carbons	GCD (0.1 Ag^{-1})	6 M KOH	3-electrode	285.8 F/g	[375]
34	ZIF-8 derived nitrogen-doped porous carbon/carbon nanotube composite	GCD (0.5 Ag^{-1})	6 M KOH	3-electrode	324 F/g	[376]
35	ZIF-8@MWCNT-derived carbon composite	GCD (1 Ag^{-1})	1 M H_2SO_4	3-electrode	326 F/g	[377]
36	N-doped carbon derived from ZIF-8 nanocomposites	GCD (0.5 Ag^{-1})	6 M KOH	3-electrode	225 F/g	[378]
37	Nitrogen-doped zeolite-templated carbon	CV (2 $mV\,s^{-1}$)	1 M H_2SO_4	3-electrode	High energy density (6.7W.h/Kg)	[379]
38	Zeolitic imidazolate framework-7	GCD (1 Ag^{-1})	6 M KOH	2-electrode	202 F/g	[380]
39	3D- ZIF-8 derived carbon/LDH core-shell composite	GCD (1 Ag^{-1})	–	3-electrode	1370 F/g	[381]
[d] Nickel						
40	3D-Yolk-shell NiGa2S4 nanosheets	GCD (10 Ag^{-1})	6 M KOH	2-electrode	> 2300 F/g	[382]
41	Honeycomb-like interconnected network of nickel phosphide hetero-nanoparticles	GCD (1 Ag^{-1})	3 M KOH	3-electrode	2638 F/g	[383]
42	$CuCo_2S_4$@NiMn-layered double hydroxide core-shell	GCD (2 Ag^{-1})	6 M KOH	3-electrode	2520 F/g	[384]
43	3D NiCo2O4@$MnMoO_4$ core-shell	GCD (2.5 $mAcm^{-2}$)	3 M KOH	3-electrode	1169 F/g	[385]
44	Yolk-shelled $NiCo_2O_4$ spheres	GCD (0.5 Ag^{-1})	6 M KOH	3-electrode	835.7 F/g	[386]
45	Porous Co_3O_4-CeO_2 hollow polyhedrons	GCD (2.5 Ag^{-1})	3 M KOH	3-electrode	1288.3 F/g	[387]
46	Nickel cobalt sulfide nanoflakes on CoO nanosheets	–	6 M KOH	3-electrode	4.97 F/cm^2	[388]

(*continued on next page*)

Table 3 (*continued*)

Order	Material used	Measurement protocol	Electrolyte	Electrode configuration	Maximum specific capacitance	Reference
47	Petal-like NiAl layered double oxide/sulfide composites	GCD (1 Ag^{-1})	6 M KOH	3-electrode	2250.5F/g	[389]
48	$CoMoO_4/Co_{1-x}S$ hybrid on Ni foam	GCD (1 Ag^{-1})	3 M KOH	3-electrode	2250F/g	[390]
49	Flaky NiO, MOF derived	GCD (1 Ag^{-1})	3 M KOH	3-electrode	485F/g	[391]
50	Ni-Al double hydroxide hollow microspheres	GCD (1 Ag^{-1})	6 M KOH	2-electrode	1578 F/g	[392]
51	$Ni(OH)_2$/CNs	GCD (1 Ag^{-1})	6 M KOH	3-electrode	2218 F/g	[393]
52	$Co_{0.5}Ni_{0.5}Fe_2O_4$	CV (5 mV s^{-1})	1 M KOH	3-electrode	113 F/g	[394]
[e] MoS_2						
53	Pizza like MoS_2/polypyrrole/polyaniline ternary architecture	GCD (0.5 Ag^{-1})	0.5 M H_2SO_4	3-electrode	1273 F/g	[395]
	Metallic 1T phase MoS2 nanosheets	GCD (2 Ag^{-1})	0.5 M H_2SO_4, $Li2SO_4$, Na_2SO_4, and K_2SO_4 together with KCl and KBr	3-electrode	400–650 F/cm^3	[396]
54	MoS_2-PANI nanocomposite	GCD (1 Ag^{-1})	3.0 M KCL	3-electrode	510.12 F/g	[397]
55	MoS_2/mesoporous carbon spheres	GCD (1 Ag^{-1})	1 M Na_2SO_4	3-electrode	411 F/g	[398]
56	3D semispherical MoS_2 thin films	CV (5 mVs^{-1})	1 M Na_2SO_4	3-electrode	180 F/g	[399]
57	MoS_2-intercalated rGO membranes on Ti mesh	CV (10 mV s^{-1})	PVA gel with 1 M NaCl	2-electrode	17.6 mF/cm^2	[400]
58	MoS_2/RCF	GCD (0.5 Ag^{-1})	Na2SO4	3-electrode	225 F/g	[401]
59	MoS_2 nanowires/$NiCo_2O_4$	GCD (1.5 Ag^{-1})	3 M KOH	3-electrode	51.7 F/g	[402]
60	MoS_2/Ni_3S_4 composite	GCD (20 Ag^{-1})	2 M KOH		640 F/g	[403]
61	MnS/MoS_2/C	GCD (0.5 Ag^{-1})	2 M KOH	3-electrode	1162 F/g	[404]
		GCD (10 Ag^{-1})	2 M KOH	3-electrode	880 F/g	
62	CoS_2@MoS_2 nanocomposite	GCD (0.5 Ag^{-1})	2 M KOH	3-electrode	1038 F/g	[405]
63	$NiCo_2S_4$-C-MoS_2 composite	GCD (0.5 Ag^{-1})	6 M KOH	3-electrode	1601 F/g	[406]
[f] Polypyrrole						
64	β-MnO_2/polypyrrole nanorod composites	GCD (1 Ag^{-1})	1 M Na_2SO_4	3-electrode	294 F/g	[407]
65	PPy shell@3D-Ni	GCD (1 Ag^{-1})	1 M Na_2SO_4	3-electrode	726 F/g	[408]
66	Highly porous MnO_2/PPy	GCD (0.5 Ag^{-1})	1 M Na_2SO_4	3-electrode	320 F/g	[409]
67	NW-PPy/NFs/PET	CV(1.0 mV s^{-1})	2 M NaCl	3-electrode	680 F/g	[410]
68	COF/PPy	CV(−0.8 to 0.1 V	1 M KOH	3-electrode	244.7 F/ cm^2	[411]
[g] Carbon						
69	3D carbon nanotubes/poly(3,4-ethylenedioxythiophene) sponge electrodes	GCD (0.5 Ag^{-1})	1 M $LiClO_4$	3-electrode	147 F/g	[412]
70	$NiMoO_4$ nanosheets supported on carbon fibers	CV (10 mV s^{-1})	6 M KOH	3-electrode	1215 F/g	[413]
71	PANI/VA-CNTs	GCD (1 Ag^{-1})	1 M $HClO_4$	3-electrode	403.3 F/g	[414]
72	PCNTs with sulfur	GCD (1 Ag^{-1})	6 M KOH	3-electrode	331 F/g	[415]
73	$ZnFe_2O_4$ anchored on multiwall CNTs	CV (5 mVs^{-1})	1 M NaOH	3-electrode	217 mAh/g	[416]
74	Pristine CNTs	GCD (4 Ag^{-1})	2 M H_2SO_4	2-electrode	148.1 F/g	[417]
	Unzipped MWCNTs	–	–	–	217.1 F/g	
75	Cross-linked carbon nanofibers	GCD (0.5–50 Ag^{-1})	6 M KOH	3-electrode	222.92 F/g	[418]
[h] MOFs						
76	Zinc-organic frameworks and dual doped carbon materials	GCD (1 Ag^{-1})	3 M KOH	3-electrode	182.8 F/g	[419]
77	MOF-derived carbon polyhedrons and nanotubes	CV (10 mV s^{-1})	6 M KOH	3-electrode	343 F/g	[420]
78	MOF (HKUST−1, MOF-5 and Al-PCP) derived porous carbon	GCD (100 mAg^{-1})	30 wt% KOH	3-electrode	232.8 F/g	[421]
79	3D porous carbon from MOF- 5	GCD (0.05 Ag^{-1})	6 M KOH	2-electrode	212.8 F/g	[422]
80	MOF-5 derived mesoporous carbon nanospheres	GCD (1.5 Ag^{-1})	6 M KOH	3-electrode	300 F/g	[423]
81	MOF-derived Ni nanorods	GCD (1 Ag^{-1})	6 M KOH	3-electrode	1698 F/g	[424]
82	Ni-MOFs	GCD (1 Ag^{-1})	2 M KOH	2,3-electrode	726 F/g	[425]
		GCD (5 Ag^{-1})			313.8 F/g	
83	Zn-MOF/polyaniline composites	GCD (1 Ag^{-1})	1 M H_2SO_4	3-electrode	477 F/g	[426]
84	Ni based pillared MOF	GCD (1 Ag^{-1})	2 M KOH	3-electrode	552 F/g	[427]
		GCD (20 Ag^{-1})			438 F/g	
85	MOF-derived MxSy@C composites	GCD (1 Ag^{-1})	2 M KOH	3-electrode	833 F/g	[428]
86	Ni-MOF	GCD (1 Ag^{-1})	2 M KOH	3-electrode	804 F/g	[429]
		GCD (10 Ag^{-1})			534 F/g	
87	HKUST-1@polyaniline	GCD (1 Ag^{-1})	6 M KOH	3-electrode	270 F/g	[430]
88	HKUST-1@CC800	GCD (0.2–20(mA/Cm^2)	6 M KOH	3-electrode	480 mF/Cm^2	[431]
	HKUST-1@TS-800				1812 mF/Cm^2	

Generally, the organic electrolytes used for EDLCs are the conductive salts [230], such as tetraethylammonium tetrafluoroborate ($TEABF_4$) dissolved in propylene carbonate or ACN. Nonetheless, organic electrolytes have issues that should be addressed: they generally have low conductivity, a small specific capacitance, high cost, and are volatile, toxic, and flammable [231]. Moreover, organic electrolytes require complex assembly and purification procedures under particular environments to eliminate impurities (*i.e.*, moisture) that could cause serious self-discharge and performance degradation issues. Hashemi et al. [49] developed high-performance SCs using the redox additive–assisted regenerative electrocatalytic method for the electrode materials. They proceeded from the trial and error method to a preplanned scheme for designing all three important supercapacitor parts (the active material, electrolyte, and substrate) to work together synergistically and gain the best possible electrical performance. They added 1,4-napthoquinone (NQ) to the electrolyte as a redox additive, resulting in direct redox reactions on the electrode surface and faradic capacitance. It also provided the basis for procedures to regenerate the

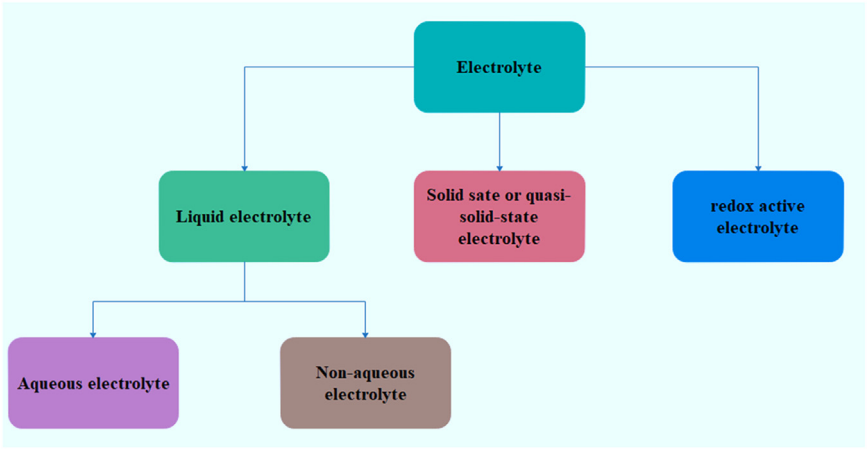

Fig. 15. Classification of electrolytes for SCs applications [220].

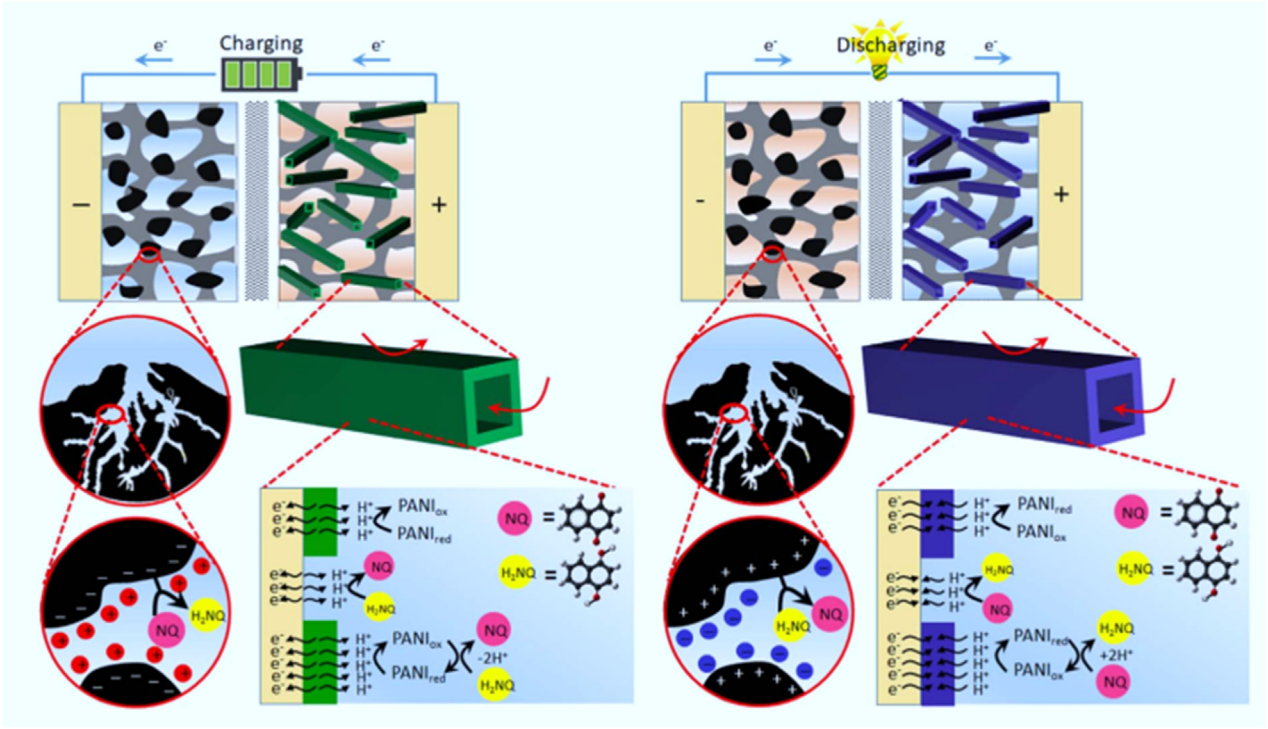

Fig. 16. Charge storage mechanisms of asymmetric activated carbon on a functionalized carbon cloth polyaniline-FCC device [49].

electrode materials for long-term use (Fig. 16). Combining this electrode with AC in an asymmetric setup created an SC with excellent specific capacitance (4007 F/g^{-1}) and 84% capacitive retention across 7000 cycles at 35 A g^{-1} [49].

6.3. Ionic liquid electrolytes

Among the important parts of an SC device, a wise choice of electrolyte is vital to retaining the stability of the electrode materials at elevated temperatures [232]. The organic electrolytes used in SCs at the commercial level are not suitable for temperatures above 70 °C because of their low ignition and detonation temperatures, and aqueous electrolytes are limited by the boiling temperature of water and cannot be used effectively above 80 °C. ILs are potential candidates for use at even very high temperatures because of their high chemical and thermal stabilities, with wide operating voltage ranges, negligible vapor pressure, and nonflammability.

Haque et al. [232] published a detailed report on the thermal effects of using an IL containing 1-ethyl-3-methylimidazolium acetate (EMIM Ac) as the electrolyte and AC as the electrode material. The temperature-dependent (21–150 °C) performance showed a high specific capacitance of 142 F/g^{-1} at 150 °C at a current density of 2 A g^{-1}, with capacitive retention of 87% at 15 A g^{-1}. At 150 °C, the equivalent series resistance value was only 0.37 Ω cm^2, probably because the ionic conductivity of the electrolyte improved at higher temperatures. The equivalent series resistance value of 2.5 Ω cm^2 at room temperature show good compatibility between the AC and EMIM Ac. Also, this system maintained a retention of more than 95% after 1000 cycles up to 120 °C, which decreased to 85% at 150 °C.

Zarrougui et al. [233] prepared six novel, low-viscosity ILs as electrolytes for SCs: one planar anion (DCA-) and five anions (PF_6^-, BF_4^-,$TFSI^-$,TFA^- and OTf^-) with non-polar architectures. The electrochemical system based on those electrolytes showed excellent performance, such as high specific capacitance (135–228 Fg^{-1}), reasonable energy density (41–115 Wh g^{-1}),

and cycling stability up to 1000 cycles. Osti et al. [234] claimed improved electrolytic dynamics in an SC using mixed ILs (1-ethyl-3methylimidazolium tetrafluoroborate (EmimBF4) + 1-ethyl-3methylimidazolium bis(trifluoromethylsulfonyl)imide (EmimTFSI)) as the electrolyte. The computational result suggested that the optimal mixture of 4:1 EmimTFSI: EmimBF4 would provide the maximum absorption of cations near the electrode surface. The DFT findings from that study can provide basic guidance for designing an optimal electrolyte system that could ultimately enhance the electrochemical properties of SCs.

7. Biomass and waste-derived hybrid materials for supercapacitors

Solid waste, including biomass and organic waste, derive primarily from five industries: forest resources, agriculture resources, wastewater (sludge), urban solid waste, and livestock excrement. It not only causes environmental pollution and health risks, but also costs a lot of money for disposal. Many people are trying to find ways use biomass and organic waste in useful, renewable products, such as fertilizer materials [235], fodder [236], construction materials [237], catalysts [238], contaminant sorbent materials [239], energy storage (power plants, methane, ethanol, hydrogen, SCs) [240–243], and other applications in environmental protection [244,245]. A summary of organic waste applications is presented in Fig. 17.

Biomass and organic waste has been highlighted as an alternative material for high performance electrodes because of its low cost, abundance, and renewability. Many waste materials, such as fruit skins, lignocellulosic powder, and animal feathers have been used to prepare porous carbons [246], composites [247–249], and graphitic carbon/reduced graphitic carbons [250] for electrodes. Using waste materials to fabricate electrodes is attractive because it not only offers a solution for waste disposal, but also provides a way to increase the economic viability of SC technology.

7.1. Porous carbon composites

Porous carbons are mostly produced from carbonaceous and polymer materials such as coal, oil, asphalt, polyene, ACN, phenolic resin, and carbon fiber [251–254] or from biomass-derived material such as peanut shells, corn, rice husks, sugarcane, tea leaves, mushrooms, wood, bamboo, and filter paper [246,255]. However, carbonaceous oils are limited and nonrenewable, and thus biomass-derived porous carbon applications have increased notably over time. In 2008, Rufford et al. [256] first used waste biomass — waste coffee beans — to produce activated carbon for SCs. The material displayed a good capacitance of 368 F/g^{-1} and was stable across 10,000 cycles at a cell potential of 1.2 V and current load of 5 Ag^{-1}.

Much attention [257–259] has been paid to carbonizing biomass wastes to prepare porous carbon SC electrodes. Guo et al. [260] prepared a microporous carbon electrode of PSC-1 & PSC-2 derived from peanut shells and used it for SCs that showed high stability and retainability (94.5%) with capacitances of 233 and 378 F/g^{-1}, respectively, at a current density of 0.1 Ag^{-1}. Mitlin et al. [261] obtained 3D macroporous carbon film by carbonizing waste chicken eggshell membranes, achieving high capacitances of 297 F/g^{-1} with 97% capacitive retention after 1000 operating cycles at a current density of 4 Ag^{-1}. Wang et al. [262] synthesized porous carbon SCs from celtuce leaves and achieved a specific capacitance as high as 421 F/g^{-1} in a three-electrode system. Farma et al. [263] used fibers from the empty fruit bunches of waste oil palm for SCs and obtained a high specific capacitance of 150 F/g^{-1}. Huang et al. [264] prepared carbon-enriched SCs from lignocellulosic waste and showed a capacitance of 165 F/g^{-1} and stable cycling performance, with a retention ratio of 99% after 20,000 cycles.

Researchers have formed porous carbon into different structures from various biomass resources. Li and Wu [265] prepared microporous carbon materials from water bamboo, and the resulting SCs exhibited a maximum capacitance of 268 F/g^{-1} at a current density of 1 Ag^{-1} in 6 M KOH electrolyte, with capacity retention as high as 97.28% after 5000 cycles at a current density of 10 Ag^{-1}. They attributed that performance to the high specific surface area, pore volume, proper pore size distribution, and functionalized oxygens. In addition, dragon fruit skin (specific area: 911.2 $m^2\ g^{-1}$, capacitance: 286.9 F/g^{-1}), *Momordica grosvenori* skin (specific area: 597.5 $m^2\ g^{-1}$, capacitance: 238.7 F/g^{-1}) and *Firmiana* catkins (specific area: 286.7 $m^2\ g^{-1}$, capacitance: 226.6 F/g^{-1}) [266], and sunflower seed shells [267] have been fabricated into electrodes. Teng et al. [268] prepared an SC with a three-dimensional network structure by carbonizing three different varieties of wood and showed a maximum energy density of ~ 45.6 W h kg^{-1}, with a power density of 2000 W kg^{-1} and 99.7% capacitance retained after 2000 cycles. Jiang et al. [269] achieved a hierarchical porous texture and ultrahigh carbon (specific area: 400 $m^2\ g^{-1}$) content for their electrode by using red cedar wood, which showed high performance (capacitance: 115F g^{-1}) in SCs. Furthermore, the use of lignocellulosic biomass such as hemp [270], sugar cane bagasse [271], and tree-bark biomass waste [272] has also been reported. Wang et al. [273] produced carbon from pigskin, which showed a specific capacitance of 278 F/g^{-1} at 10 Ag^{-1}. Other researchers used chicken feathers [266] as the carbon source for SCs, and they demonstrated a high capacitance of 351 Fg^{-1} at 0.1 Ag^{-1} and very low costs. Even food waste can be used as an electrode material; Zhan et al. [274] used flour food waste to prepare porous carbon–based SC electrodes that showed a high specific capacitance even at the ultra-high current density of 100 A g^{-1}. Chen et al. [275] prepared 3D activated carbon by carbonization and

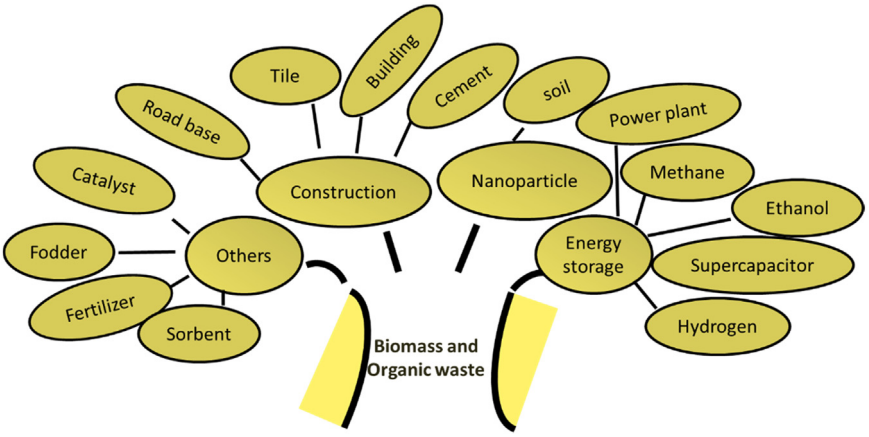

Fig. 17. Diagram of possible applications of biomass and organic wastes.

KOH chemical activation of rotten potatoes and achieved a relatively high capacitance of 260 F/g^{-1}.

Most recently, Qiu et al. [276] derived an optimized carbon material from straw biochar waste for high performance SCs, achieving a maximum capacitance of 327 F/g^{-1} and excellent cycle stability for 120,000 cycles at 5 A g^{-1}. Elmouwahidi et al. [277] transformed agricultural waste from the olive oil industry into AC and added it to SCs, obtaining a high capacitance of 325 F/g^{-1} at 0.125 A g^{-1} in 1 M H_2SO_4, with great retention at the high current density of 30 A g^{-1}. Cai et al. [278] derived nitrogen-doped porous carbon for SCs from waste cabbages, achieving a pretty high capacitance of 291 F/g^{-1} and high retention of 96.76% after 10,000 cycles in 6 M KOH. Sun et al. [279] carbonized pomelo peels as an SC material and showed high performances in a commercial organic electrolyte. Su et al. [280] used loofah sponge–derived carbon as an SC material and obtained a capacitance of 309.6 F/g^{-1} at 1 A g^{-1} in 6 M KOH. Waste medicine, an aconitum sinomontanum Nakai extraction and poly-acrylonitrile, was also transformed into carbon nanofibers for use as SCs and showed a capacitance of 295 F/g^{-1} at 1 A g^{-1} in 6 M KOH, with 98.5% retention after 1000 cycles at 2 A g^{-1} [281]. Those achievements suggest that carbon derived from biochar could be used widely in the future for SCs with good energy and power density performance.

7.2. Graphene/graphene oxide

Researchers have begun to prepare graphene and GO from organic waste for use in SCs. However, only a few papers have been published on this subject, which is still in the initial research stage. First, Sun et al. [282] synthesized porous graphene-like nanosheets from coconut shell and achieved a high capacitance of 268 Fg^{-1}, excellent cycle durability, and coulombic efficiency over 99.5% after 5000 cycles in KOH. Gong et al. [250] prepared 3D porous graphitic biomass carbon from bamboo char, and it exhibited a high capacitance of 222.0 Fg^{-1} at 0.5 Ag^{-1}. Tiwari et al. [283] intercalated sodium dodecyl benzenesulfonate surfactant into graphitic layers derived from a discharged battery electrode to obtain few-layered graphene with 4.5 V of DC (direct current). Zhang et al. [284] used willow catkins as a template and precursor in preparing porous graphene microtubes processed by activation-graphitization by $K_4Fe(CN)_6$ (Fig. 18). The composite SCs showed a specific capacitance 550.8 Fg^{-1} at a current density of 2 Ag^{-1}. Senthilkumar et al. [285] successfully used waste writing paper to synthesize highly porous graphene, which they combined with Na-ion-based hybrid capacitors to obtain a maximum specific capacitance of 1893 Fg^{-1} at 2 Ag^{-1}. Sun et al. [286] obtained 3D, vertically aligned, graphene nanosheet arrays from biomass wastes such as spruce bark and applied it in SCs, achieving a high capacitance of 398 Fg^{-1} at 0.5 Ag^{-1}, with a retention of 96.3% after 10,000 cycles in 6 M KOH. Those results indicate that graphene and GO derived from biomass are promising in the industrialization of SCs. Performance data for electrode materials made using different waste products are summarized in Table 4.

7.3. Other composites

Another wide application for waste materials is composite electrodes for SCs. Basri et al. [287] prepared symmetrical SCs from CNTs and self-adhesive carbon grains derived from the fibers of three biomass waste resources (oil palm tree, *Heliotropium dasycarpum* and *Guaiacum officinale*). The SCs showed specific capacitances of 124, 104, and 49 F/g^{-1} at 111, 87, and 31 A g^{-1}, respectively. Liu et al. [288] obtained nanofibers/mesoporous carbon composites from sawdust and produced an SC with good EDL capacitance and retention capability. The next year, Liu et al. [247] processed poplar wood into wood sawdust and then used carbonization and KOH activation to obtain a PANI-coated, boron-doped, wood-derived porous carbon composite (PANI-BAWDC), as shown in Fig. 19. The SC performance improved significantly compared to pure PANI and pure BAWDC, achieving 421 F/g^{-1} at 10 mV s^{-1} and an energy density of 45.2 Wh kg^{-1}. Ma et al. [248] used chestnut shell as an activated carbon material, which they combined with PANI to achieve a good electrochemical performance, with a specific capacitance of 597 Fg^{-1} and 80% retention of capacitance after 1000 cycles at a current density of 1 Ag^{-1} in 1 M H_2SO_4. Li et al. [249] synthesized crosslinked carbon nanosheets from willow catkins (Fig. 20), which displayed a high energy density of 23.6 Wh kg^{-1} at a power density of 188.8 W kg^{-1} within a wide voltage range of 0–1.9 V and only 1.4% capacitance loss after 10,000 cycles at 1 A g^{-1}. Sun et al. [289] used orange peel–based carbon nanosheets supported on MnO_2 nanorods and obtained a high capacitance of 656 Fg^{-1} at a current density of 1 Ag^{-1}, with a retention of capacitance above 80% after 5000 cycles. Moreover, a composite of AC and a rare-earth metal oxide (Eu_2O_3) in a PPy matrix [290], a carbonaceous aerogel and CoNiAl-LDH@CA nanocomposites [291], and 1D@2D structured Ni-Co_2O_4@Co_3O_4 and a high surface-area porous carbon composite [292] were all synthesized using carbon derived from biomass wastes, demonstrating the great potential for biomass recycling in SC manufacture.

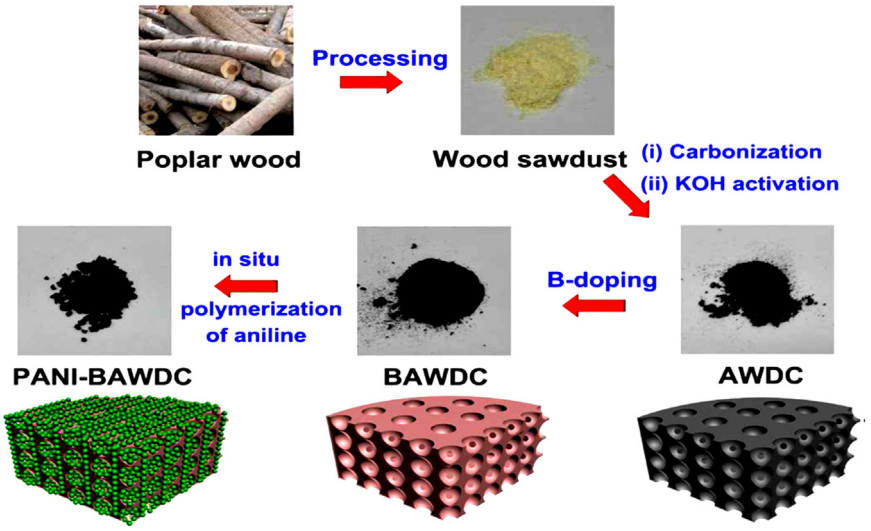

Fig. 18. Structural schematic of a PANI-BAWDC composite and their synthesis routes [247].

Table 4
Material synthesis from waste to supercapacitor electrodes.

Order	Material	Waste resource	Waste material technique	Electrolyte	Measurement protocol	Electrode configuration	Max. capacitance	Reference
1	Activated carbon	Sugar cane bagasse	$ZnCl_2$-activation and carbonization at 750 °C	1 M H_2SO_4	CV = 5–50 mV s^{-1} GCD = 0.05–50 A g^{-1}	Two- electrode	300 Fg^{-1}	[271]
2	Porous activated carbon	Chicken feathers	KOH-activation and carbonization at 600–800 °C	6 M KOH	GCD = 0.1–30 A g^{-1}	Three- electrode	350 Fg^{-1}	[432]
3	Oxygen-rich activated carbon compounds	Dragon fruit skin, *Momordica grosvenori* skin and *Firmiana* catkins	KOH, H_3PO_4, $ZnCl_2$, etc.-activation and carbonization at 400–900 °C	2.0 M KOH	GCD = 0.5 A g^{-1}	Three- electrode	286 Fg^{-1}	[266]
4	Nanoporous carbons	Sunflower seed shells	KOH-activation and carbonization at 800 °C	30 wt% KOH	GCD = 0.25 A g^{-1}	Two-electrode	311 Fg^{-1}	[267]
5	Microporous carbon	Water bamboo	KOH-activation and carbonization at 800 °C under N_2 atmosphere	6 M KOH	GCD = 1 A g^{-1}	Three-electrode	268 Fg^{-1}	[265]
6	Hierarchical porous carbon	Red cedar wood	Carbonization at 750 °C	0.5 M H_2SO_4	–	Two- electrode	115 Fg^{-1}	[269]
7	Nitrogen- and oxygen-doped carbon sheets	Pigskin	KOH-activation and carbonization at 600–900 °C	6 M KOH	GCD = 0.1 A g^{-1}	Three- electrode	547 Fg^{-1}	[273]
8	Porous carbon sphere	Hemp stems	KOH-activation and carbonization at 800 °C	6 M KOH	GCD = 0.1 A g^{-1}	Three- electrode	318 Fg^{-1}	[270]
9	Nitrogen-doped porous carbon	Wheat straw	Mixed salts (KCl and $ZnCl_2$,)	6 M KOH	CV = -1–0 V	Three- electrode	223.9 Fg^{-1}	[433]
10	Porous carbonaceous materials	Corn gluten waste	KOH-activation and carbonization at 600–900 °C	6 M KOH	GCD = 0.5 A g^{-1}	Three-electrode	488 Fg^{-1}	[434]
11	Activated carbon	Flour food waste	KOH-activation and carbonization	6 M KOH	GCD = 100 A g^{-1}	Two- electrode	278 Fg^{-1}	[274]
12	3D activated carbon	Rotten potatoes	KOH-activation and carbonization	6 M KOH	GCD = 1 A g^{-1}	Three-electrode	269 Fg^{-1}	[275]
13	Microporous carbon	Silkworm biological waste	KOH-activation and carbonization at 750 °C	6 M KOH	GCD = 1 A g^{-1}	Two and three electrode	235 Fg^{-1} 304 Fg^{-1}	[435]
14	Activated carbon nanostructures	Tree-bark biomass waste	KOH-activation and carbonization at 700 °C	PVA/KOH/ carbon black	GCD = 0.1 A g^{-1}	Two- electrode	227 Fg^{-1}	[272]
15	Graphitic biomass carbon	Bamboo	K_2FeO_4, KOH, $FeCl_3$, and carbonization	KOH/PVA	GCD = 0.5 A g^{-1}	Two-electrode	222. Fg^{-1}	[250]
16	Composite of boron doped activated carbon/ polyaniline particles	Poplar wood	KOH-activation and carbonization at 600–900 °C	1 M H_2SO_4	CV = 10mvs^{-1}	Two- electrode	421 Fg^{-1}	[247]
17	Composite of activated carbon/ polyaniline	Chestnut shells	KOH-activation and carbonization at 800 °C	1 M H_2SO_4	GCD = 1 A g^{-1}	Three-electrode	597 Fg^{-1}	[248]
18	Composite of MnO_2 nanoplates loaded on cross-linked carbon nanosheets	Willow catkins	Carbonization at 850 °C under argon atmosphere	1 M Na_2SO_4	GCD = 1 A g^{-1}	Three-electrode	262 Fg^{-1}	[249]
19	Composite of carbon nanosheets supported by MnO_2 nanorods	Orange peel	Carbonization at 800 °C	6 M KOH	GCD = 1 A g^{-1}	Three-electrode	656 Fg^{-1}	[289]
20	Composite of AC and rare-earth metal oxide (Eu_2O_3) into a PPY matrix	Coconut shells	Carbonization	1 M H_2SO_4	GCD = 1 A g^{-1}	Two- electrode	670 Fg^{-1}	[290]
21	Composite of carbon fiber/ MnO_2	Disposable bamboo chopsticks	KOH-activation and carbonization at 800 °C	0.34 M H_2SO_4	GCD = 1 A g^{-1}	Two-electrode	375 Fg^{-1}	[436]
22	Carbonaceous aerogel and CoNiAl-LDH@CA	Pomelo peel	Autoclave for 6.5 h at 180 °C followed by freeze-drying for 2d at − 42 °C	0.2 M KOH	GCD = 10 A g^{-1}	Three-electrode	1134 Fg^{-1}	[291]
23	Composite of 1D@ 2D structured $NiCo_2O_4$ @Co_3O_4 and high surface-area porous carbon	Jackfruit	KOH-activation and carbonization at 900 °C	2 M KOH	GCD = 1 A g^{-1}	Three-electrode	375 Fg^{-1}	[292]
24	Activated carbon/polyaniline composite	Waste tea	H_3PO_4-activation and carbonization at 450 °C under N_2 atmosphere	–	–	–	–	[437]
25	Core-shell composite/ MnO_2	Wood waste of agriculture and industry	Pyrolysis at 1000 °C	1 M Na_2SO_4	GCD = 0.05 A g^{-1}	Three-electrode	101 Fg^{-1}	[438]
26	Few layered graphene	Discharged battery electrodes	Intercalating sodium dodecyl benzenesulfonate surfactant into graphene layers	Aq. H_2SO_4	CV = 0–0.8 V	–	151 Fg^{-1}	[283]
27	Porous graphene microtubes / MnO_2	Willow catkins	Activation–graphitization of $K_4Fe(CN)_6$.	0.05 M $Mn(CH_3COO)_2$ and 0.1 M Na_2SO_4	GCD = 2 A g^{-1}	Three-electrode	550.8 Fg^{-1}	[284]
28	Highly porous graphene /$Ni_2P_2O_7$ hybrid device	Waste writing paper	KOH activation and carbonization	Aq. NaOH	GCD = 2 A g^{-1}	–	1893 Fg^{-1}	[285]

(*continued on next page*)

Table 4 (*continued*)

Order	Material	Waste resource	Waste material technique	Electrolyte	Measurement protocol	Electrode configuration	Max. capacitance	Reference
29	Nanoporous carbon/MnO_x composite	Waste polyvinyl chloride	Carbonization at 700 °C under Ar flow	6 M KOH	GCD = 1 Ag^{-1}	Three-electrode	751.5 Fg^{-1}	[439]
30	Nitrogen, oxygen and phosphorus decorated carbon	Shrimp shells	H_3PO_4 activation and carbonization at 400–600 °C in Ar	6 M KOH	GCD = 0.1 Ag^{-1}	Three-electrode	206 Fg^{-1}	[440]
31	Eggshell membrane/ carbon nanotube/ $NiCo_2O_4$ composite	Eggshells	Carbonization at 800 °C in N_2	6 M KOH	GCD = 10 Ag^{-1}	Three-electrode	675 Fg^{-1}	[441]
32	Composite of carbon/graphene	Oil palm empty fruit bunches	KOH activation and pyrolyzed at 500 °C	6 M KOH	CV = 5mVs^{-1}	Three-electrode	267 Fg^{-1}	[442]
33	Nitrogen-doped porous carbon-polyaniline composites	Poplar wood sawdust	KOH activation and carbonization at 750 °C in N_2	1 M H_2SO_4	GCD = 2 Ag^{-1}	Three-electrode	347 Fg^{-1}	[443]
34	Polypyrrole and graphene/ polypyrrole composite	Cellulose fibers from waste papers	Dissolved in NaOH followed by acid hydrolysis soak	1 M KCl	CV = 10mVs^{-1}	Three-electrode	243 Fg^{-1}	[444]
35	Carbon polymer composite paper	Waste tires	Pyrolysis at 400–1100 °C	1 M H_2SO_4	CV = 1mVs^{-1}	Three-electrode	480 Fg^{-1}	[445]
36	Activated carbon	Up-cycled industrial mill scale waste	Vacuum chuck hot plate at 90 °C	0.5 M Na_2SO_4	CV = 5mVs^{-1}	Three-electrode	92 Fg^{-1}	[446]
37	Activated carbon	Durian fruits	KOH activation and carbonization at 700 °C in N_2	1.5 M Na_2SO_4	CV = 50mVs^{-1}	Three-electrode	82.5 Fg^{-1}	[447]
38	P, N co-doped carbon	Spent coffee grounds	Microwave above 1000 °C	1 M H_2SO_4	CV = 5–100mVs^{-1}	Three-electrode	286 Fg^{-1}	[448]
39	Porous carbon	Corncob residue	KOH activation and carbonization at 815–900 °C	6 M KOH	CV = 5mVs^{-1}	Three-electrode	314 Fg^{-1}	[449]
40	Graphene nanosheets	Spruce bark	KOH activation	6 M KOH	GCD = 0.5 Ag^{-1}	Three-electrode	398 Fg^{-1}	[286]
41	Graphene-like nanosheets	Coconut shells	$FeCl_3$ precursor and $ZnCl_2$ activation	KOH	GCD = 1 Ag^{-1}	Three-electrode	268 Fg^{-1}	[282]
42	Porous carbon	Corn straw	KOH activation	Na_2SO_4	GCD = 100 Ag^{-1}	Two-electrode	327 Fg^{-1}	[276]
43	Activated carbon	Agricultural waste from olive oil industry	–	1 M H_2SO_4	GCD = 0.125 Ag^{-1}	–	325 Fg^{-1}	[277]
44	Nitrogen-doped porous carbon	Waste cabbage	–	6 M KOH	–	–	291 Fg^{-1}	[278]
45	3D porous activated carbon	Loofah sponge	KOH activation	Na_2SO_4	GCD = 1 Ag^{-1}	Three-electrode	309.6 Fg^{-1}	[280]
46	Carbon nanofibers	Waste medicine, aconitum sinomontanum Nakai extraction and poly-acrylonitrile	–	6 M KOH	GCD = 1 Ag^{-1}	–	295 Fg^{-1}	[281]

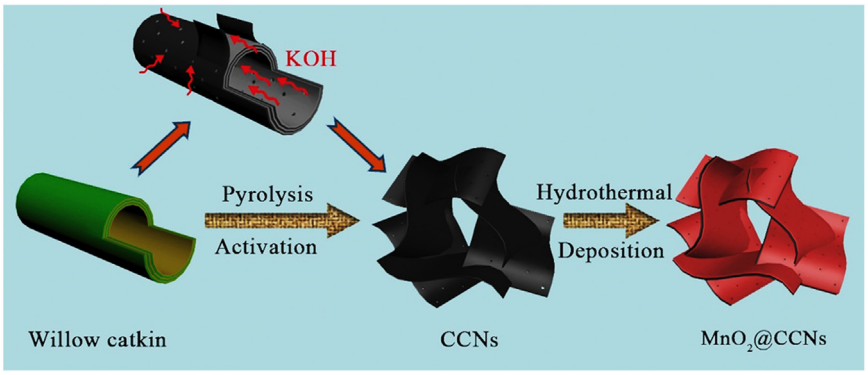

Fig. 19. Schematic of the preparation routes of MnO_2 @CCN composite [249].

7.4. Potential challenges

For the industrialization of SCs to proceed, cost reductions are essential, and biomass waste could play a key role. According to Andrew Burke's investigation, in carbon/carbon SCs, the carbon is responsible for about 60% of the total materials cost, with the total electrode material cost around 0.1cent/F, whereas biochar-derived electrode material costs only around 0.001cent/F [269,293,294]. Therefore, the use of biochar has the potential to create big profits as carbon materials cost reductions enlarge SC applications. Compared with the performance of conventional SCs (Table 3), SCs derived from waste (Table 4) showed almost the same capacitance. However, the present activation methods depend on chemical agents such as KOH, NaOH, Na_2Cl, Na_2SO_4, $ZnCl_2$, H_3PO_4, and H_2SO_4, which are expensive and directly affect the final properties of the electrode, limiting the current use of biomass waste. We expect that researchers will find lower-cost replacements for them. Moreover, hydrothermal pretreatment steps could improve the efficiency of activation. At the same time, the different capacitances of the SCs in Table 4 correspond with different carbon structures. Thus, it is worth considering multiple designs for carbon materials derived from biomass waste, which are likely to be an economical option for energy conservation in the future.

8. Latest trends in supercapacitor technology

Many portable, wearable, and implantable devices have already been integrated into daily life [295–297]. There has long been a strong drive to develop ultra-compact devices into miniaturized energy-autonomous systems (MEASs) that contain processing units, wireless transceivers, signal sensing, energy harvesters, and energy storage components [298–301]. In the past few years, significant efforts have been dedicated to manufacturing more suitable, efficient, and compact energy harvesters and energy storage components. Technologies have been advanced to harvest energy from ambient sources (solar, vibration, thermal, and radio frequencies) and the human body (such as through blood flow and body heat) for electric power input to MEASs [302,303]. An electrochemical capacitor is the main candidate for energy storage component. For use in MEASs, electrochemical capacitors need to maintain their performance under mechanical deformation such as twisting, stretching, bending, and folding while reducing their area to fit into ultra-compact devices. In this section, we provide a critical discussion of some of the latest trends in electrochemical SC technology, such as 3D porous SCs, fiber-like SCs, and paper-like SCs.

8.1. 3D porous supercapacitors

It is important to have a huge number of electrochemically available active sites on the electrode surface for electron transfer redox reactions in PC systems or electrostatic charge absorption in EDLCs. However, not all of the electrode surface in SCs is available, only the places where the active materials and electrolyte contact each other [47]. Thus, to enhance the electrode capacity for SCs, 3D architectures for electrodes have been devisednowadays, which can provide maximum number of active sites. These electrodes can help support: (i) effective contact between the active materials and electrolyte ions for chemical reactions, (ii) easy electron transportation between the current collector and the active materials, and (iii) effective accessibility on the current collector to enhance electrochemical activity [304,305]. A $Ni(OH)_2$-based electrode has been used widely in supercapacitors because of its flexibility in forming 3D structures and very high theoretical capacitance of 3750 Fg^{-1} [306]. However, due to the limited number of active sites and poor conductivity, the theoretical value cannot be achieved in actuality. To achieve those theoretical capacitances, new types of materials with higher conductivity and a larger number of accessible active sites are needed. For example, a thin layer of nickel hydroxide could be placed on a carbon-coated 3D-Cu-based structure.

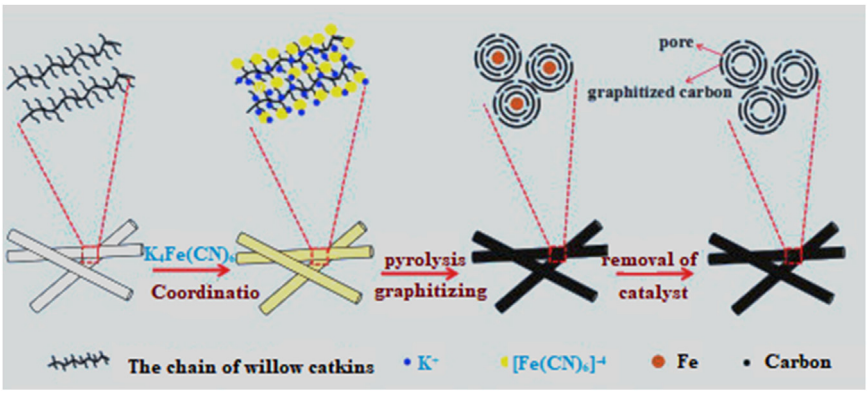

Fig. 20. Schematic of preparation procedures for PGCMT materials [284].

Table 5
Summary of some advanced architectures employed or proposed in supercapacitor technology.

Order	Material	Architecture	Electrolyte	Measurement protocol	Electrode configuration	Max. capacitance	Reference
1	Mn_3O_4 NSs/rGO NSs	Paper-like	6 M KOH	GCD = 0.5 A g−1	Three electrode	409 F/g	[312]
2	Vertically aligned CNF/BDD	Battery-like	1.0 M H_2SO_4	CV = 10 mV s^{-1}	Three electrode	116.3 mF c/m^2	[96]
3	CNF-PEDOT	Paper-like	0.1 M $HClO_4$ in water]/ acetonitrile (9/1)	–	Three electrode	230 F/g	[450]
4	NG-MnO2	Flower-like	1 M Na_2SO_4	GCD = 0.5 A g−1	Three electrode	220 F/g	[451]
5	BPC/MnO_2	Anchored MnO_2 on biomass	1 M Na_2SO_4	GCD = 0.5 A g−1	Three electrode	384.9 F/g	[452]
6	BPC/Fe_2O_3	Decorated porous carbon with Fe_2O_3	3 M KOH	GCD = 1 A g−1	Three electrode	987.9 F/g	[453]
7	3D Ni-Co LDH/NiNw	3D cotton-like	6 M KOH	GCD = 0.125 A g−1	Three electrode	466.6 F/g	[454]
8	Ni–Co hydroxide/NF	Flower-like	2 M KOH	GCD = 10 mA cm^{-2}	Three electrode	1441.5μA h/ cm^2	[455]
9	MnO2/CNT-web paper	Ultra-thin and stackable	0.5 M $LiClO_4$	CV 5 mV s^{-1}	Three electrode	135 mF/cm^2	[456]
10	HC/RGO	Belt-like	3 M KOH	GCD = 1 A g−1	Three electrode	1662 F/g	[457]
11	Nitrogen-doped graphene	Bubble-like	2 M KOH	GCD = 1 A g−1	Three electrode	481 F/g	[458]
12	$CoMoO_4$@$Co_{1.5}Ni_{1.5}S_4$	Rambutan-like	3 M KOH	GCD = 1 A g−1	Three electrode	1405 F/g	[459]
13	NiCo-LDH@NiOOH	Battery-like	6 M KOH	GCD = 1 A g−1	Three electrode	2622 F/g	[460]
14	NiCo-S	Highly open nanosheet	2 M KOH	GCD = 0.5 A g−1	Two & three electrode	2553.9 F/g	[461]
15	N-doped hierarchal carbon	Fiber web, mulberry-like	1 M H_2SO_4	GCD = 1 A g−1	Three electrode	298.6 F/g	[462]
16	$Ni_{0.4}Co_{0.6}(OH)_{2@\ CFC}$	Peony-like	2 M KOH	GCD = 1 A g−1	Three electrode	1816 F/g	[463]
17	3DPGLS	3D porous	1 M $TEMABF_4$/PC)	GCD = 0.2 A g−1	Two electrode	91.15 F/g	[464]

Such porous 3D structures can provide high conductivity and a large number of accessible active sites through direct contact between the active material and 3D-C/Cu. A thin layer of nickel hydroxide on a 3D structure can also help reduce the pathway electron transport. These nickel and C/Cu structures showed the very high specific capacitance of 1860 F/g^{-1} [307]. Zhang et al. [308] reported the fabrication of a 3D, hierarchical, porous quaternary zinc-nickel-aluminum-cobalt oxide (ZNACO) architecture for SCs. The ZNACO-based capacitors displayed a specific capacity as high as 839.2 C g^{-1} at 1 A g^{-1}. Moreover, they exhibited a high energy density of 72.4 Wh kg^{-1} at a power density of 533 W kg^{-1} while maintaining good cycling stability, with 90% capacitance retention after 10,000 cycles at 10 A g^{-1}. Song et al. [309] proposed a one-step method to obtain a 3D network of porous graphene electrodes through direct laser induction on a polyimide sheet at room temperature. By doping the laser-induced graphene electrodes with elemental N, the researchers increased the device performance to 790 μF cm^{-2} at a discharge current of 50 μA cm^{-2}. In this case, the doping with elemental N improves the number of active sites, resulting in excellent PC behavior. Liu et al. [310] reported the design of a self-assembled, 3D, porous $Ni(OH)_2$ for high performance energy storage SCs through a solvothermal-precipitation method. The $Ni(OH)_2$ obtained at 520 K exhibited a high specific capacitance of 2110 F/g at 1.0 A g^{-1} and modest cycling stability, with 53% of the high capacitance retained over 2000 cycles at 5.0 A g^{-1}. Moreover, when the $Ni(OH)_2$ was combined with porous carbon as the negative electrode material, the hybrid chemical capacitors delivered capacitance as high as 115 F/g^{-1} with a maximum energy density of 40.9 W h kg^{-1} at a power density of 405 W kg^{-1}. In conclusion, the best way to increase the capacitance of an SC is to increase the number of active sites, and 3D porous structures are an attractive way to do that.

8.2. Paper-like supercapacitors

Another new architecture is paper-like SCs, which can easily be manipulated into other modified structures according to the specific requirements of individual applications. These capacitors can also be used in wearable health monitors, electronic textiles, and electronic skins. Customized SC architectures (such as pyramid structures, honeycomb-like structures, and living-hinge structures) are highly desirable because they provide tunable stretching abilities in any random direction. For instance, an SC with a honeycomb-like structure showed a specific capacitance of 227.2 mF cm^{-2} while being stretchable up to 500% without ruining the electrochemical properties [311]. Moreover, this structure was reported to maintain 98% of its capacitance over 10^4 cycles. Recently, Wang et al. [312] synthesized flexible Mn_3O_4 nanosheets (Mn_3O_4 NSs) and rGO nanosheets (rGO NSs) into a paper-like composite using a simple ultrasonication, filtration, and hydrolysis method. The integration of rGO NSs into Mn_3O_4 NSs provided a large specific surface area, rich pores, and many electroactive sites for ion and electron access. Furthermore, the distinctive interconnection between the two nano architectures reduced the self-agglomeration of the rGO NSs. This paper-like composite exhibited the excellent specific capacitance of 409 F/g^{-1} and high cycling stability (92% of capacitance retained after 3000 charge–discharge cycles). Cai et al. [313] reported a unique design for symmetric SCs based on ultrathin, boron-doped, graphene, paper-like electrodes and boron-enriched gel polymer electrolytes. Specifically, these paper-like electrodes with B-containing electrolyte not only presented many active sites for the absorption/desorption of electrolyte ions, but also enabled electrolyte diffusion during the charging and discharging processes. The SCs could reach a specific capacitance as high as 47.15 F/g^{-1} at room temperature, and they retained 90% of their specific capacitance after 3000 charging and discharging cycles. Their maximum energy density was 39.31 W h kg^{-1}, with a power density of 1.44 kW kg^{-1}. Zhao et al. [314] reported excellent electrical properties from graphene films shaped in paper-like form by the adsorption of hydrolyzed polyimide (HPI) molecules. Various mass-loading ranges (0.5–4.8 mg cm^{-2}) were used to fabricate this new type of electrode, and the researchers suggested that functionalizing the HPI molecules could increase the capacitance. Also, given their highly flexible structure, the as-fabricated SC devices showed excellent mechanical and temperature stability. Table 5 shows some of the new architectures in SC technology.

8.3. Fiber-like supercapacitors

The future of electronic devices is expected to include wearable electronics with stretchable circuitries, implantable sensors, and smart skins. For example, a smart skin could offer on-body sensing to monitor healthcare data and physiological signals in human bodies to support people in various activities and situations. As aforementioned, SCs are energy storage devices for such systems. For wearable devices, fiber-like capacitors are particularly suitable. The purpose of evolving fiber-like supercapacitors is to fabricate an energy storage system in the form of a flexible and ultrathin fiber while maintaining outstanding

electrochemical performance.

Substantial efforts have thus been made toward developing fiber-like active materials for electrodes and designing new device configurations and structures for such applications. There are two general types of fiber-like electrode: 1) carbon-based fiber-like electrodes such as graphene and CNT fibers and 2) metal-coated plastic wire and metal wire electrodes [315,316]. The carbon-based fiber electrodes are highly porous and offer a significant amount of EDL capacitance. They also have robust mechanical properties.

With respect to the device configuration of fiber-like electrochemical capacitors, two types are available: coaxial fiber-like SCs and two-ply fiber-like SCs. The former is fabricated by assembling capacitor components (such as a core fiber electrode, gel polymer electrolyte, and outer coating electrode) layer by layer [315,317]. The latter has been invented by twining two fiber-like electrodes together with a separator or gel polymer electrolyte [316]. Recently, Ren et al. [318] proposed a superficial preparation technique to synthesize composite elastic cord/CNT/PANI fibers with a core-sheath-structure. The fibers had excellent electrical, mechanical, and stretching properties and exhibited a large capacitance of 394 F/g^{-1} and great rate capability. Stretching the fibers from their original state produced no noticeable effect on the capacitance, and the capacitive retention was 98% after 100 stretch–release cycles. Gu et al. [319] reported a flexible fiber-like electrochemical SC made using single-step hydrothermal synthesis and $CuCo_2O_4$ nanostructures on nickel wires as fibrous electrodes. The specific capacitance of the fiber-like supercapacitor reached 11.09 F/g^{-1}, and it had good cycling stability, with about 93.5% retention after 4000 charging/discharging cycles. Moreover, their SC showed no deceptive degradation in the bending test.

9. Characteristic comparison of selective supercapacitors

An SC is a proficient energy storage system with attractive properties such as high energy and power densities, long lifetime, high reliability, excellent rate behavior, and environmental friendliness. Each type of SC (EDLCs, pseudo-capacitors, and hybrid capacitors) has different characteristics. Although the energy storage density in EDLCs is relatively small, the power density is higher than that of pseudo-capacitors. Cycle life is another important factor in evaluating SCs. Generally, tests for stability involve charging and discharging capacitors for a certain number of cycles and then comparing the capacitances before and after the field cycling stress. Most EDLCs use carbon-based electrodes, which have a long lifetime and can be cycled at a high rate, 10^5–10^6, with the very small degradation in performance [320,321]. As shown in Table 6, EDLCs show good field cycling stability, with 10–20% degradation in capacitance after field cycling stress tests [320–324]. Pseudo-capacitors are profoundly different from EDLCs. They store energy through reversible faradic reactions, with capacitance 10–100 times larger than available with EDLCs, as shown in Table 5 [325]. But repeated reduction and oxidation processes can change the structure of PC electrodes, resulting in decreased field cycling stability. Moreover, the power density of pseudo-capacitors is smaller than that of EDLCs because faradic processes are slower than electrostatic processes. For example, the capacitance of a $Co(OH)_2$-based capacitor decreased ~40% after field cycling [326]. Both EDL and PC SCs use two electrodes made from the same type of material.

To increase the operating voltage window and the power and energy density, hybrid capacitors have been developed. For example, EDLC/redox-type hybrid capacitors integrate the advantages of EDCLs and pseudo-capacitors by coupling both types of materials. As shown in Table 6, MnO_2–NPG/PPy-NPG capacitors have high energy and power densities and show good field cycling stability [327]. New developments are making portable devices and electronics thinner and more power demanding, opening new commercial opportunities for SCs, which are lighter and more powerful than batteries. Because of all their exciting properties and probable usage in an increasing number of applications, the SC market is expected to top $11 billion by 2024. Nonetheless, SCs are not yet in extensive use. According to the developers, manufacturers, and suppliers of SCs, this lack of commercial success is due to their present low energy density and high cost-to-performance ratio. Therefore, the development of materials and configurations to increase the energy density and reduce the costs of processing and preparation methods is necessary, and multiple ambitious research activities are currently being conducted.

10. Conclusion and future prospects

SCs are an essential element of diverse applications (i.e., hybrid vehicles, military warheads, communication devices, uninterruptible power supplies, mobile phones, laser technology, and solar cell energy storage). SCs flourish because of their many technical advantages, such as high power densities, quick charging and discharging processes, and

Table 6
Comparison of the key performance metrics between diverse supercapacitors.

Order	Supercapacitor, electrode	S_A ($m^2 g^{-1}$)	C_{SP} ($F g^{-1}$)	E_D ($Wh kg^{-1}$)	P_D ($kW kg^{-1}$)	Cycling stability	Measurement done at	Electrolyte	Reference
a	**EDLC**								
1	CNS	791.0	560	78	2.8	97%(1000)	10mVs^{-1}	1 M HCL	[322]
2	PCNC	1779.3	161	30.2	20.3625	85.4%(5000)	1 Ag^{-1}	1 M $TEABF_4$/AN	[323]
3	CMCNC	1198	194	56.1	61.25	90.6%(100k)	1 Ag^{-1}	ionic liquid	[320]
4	CNDHS	2091	183	28.875	37.125	91.1%(100K)	1 Ag^{-1}	1 M $TEABF_4$/AN	[321]
5	AC	2731	311	8.3	18.75	96.4% (5000)	0.5 Ag^{-1}	6 M KOH	[324]
6	AC	2731	178	39	6.7	87.5%	0.5 Ag^{-1}	1 M $TEABF_4$/AN	[324]
b	**Pseudo**								
7	Ni-based MOF	–	705	29.6	0.46	92.1% (5000)	1 Ag^{-1}	6 M KOH	[107]
8	$Co(OH)_2$	–	1287.2	–	–	59.2%	2 Ag^{-1}	1 M KOH	[326]
9	$Co(OH)_2$ on Ni	–	2646	–	–	96.1% (300)	8 Ag^{-1}	2 M KOH	[465]
10	$Ni(OH)_2$	–	2188	–	–	97% (1000)	1mVs^{-1}	1 M KOH	[325]
c	**Hybrid**								
11	$Ni(OH)_2$/graphite	–	153	35.7	0.490	97% (5000)	5mVs^{-1}	1 M KOH	[325]
12	MnO_2–NPG/ PPy-NPG	–	193	86	25	85% (2000)	1.8V	1 M $LiClO_4$	[327]
13	MnO_2/ NiNTAs@PPy	–	141.9	50.5	–	81.3% (1000)	1.6V	PVA-LiCl	[466]
14	Ni–Co LDH/ PPy films	–	261	61.3	0.65	91% (5000)	1.3V	1 M KOH	[467]
15	VO_x. YH_2 O/ WO_3. ZH_2 O	–		10.4	2.23	–	1.9V	12 M LiCl	[468]

exceptional cycle stability. However, the low energy density (10 Wh kg^{-1}) and high cost of SCs currently used at the commercial level prevent them from replacing batteries [173,328].

Those two main challenges for SCs, high cost and low energy density, must be overcome without losing their high cycle life and exceptional rate performance. The wide potential window in which SCs can operate efficiently is implemented because of the V^2 term (square of potential window) in the stored energy, which results in high energy density and can improve the power performance proportional to V^2. Recently, many efforts have been devoted to solving the technical problems associated with low energy density by developing nanostructured electrode materials with enhanced specific capacitances and increased operating voltages. Generally, two approaches have been explored for high-voltage SC designs [173,329]: replacing aqueous electrolytes with ILs or organic electrolytes with large operating potential windows and introducing hybrid, asymmetric SCs that use both a capacitive electrode as a source of power, and a Faradaic electrode as source of energy. Recently, a new class of electrolytes have been introduced which is a combination of both aqueous and non-aqueous electrolytes [330]. However, as this combination is yet applied to Li-ion batteries, it needs further exploration for supercapacitor applications. The development of asymmetric SCs is an active way to increase the cell potential window of aqueous electrolytes beyond the thermodynamic limit of ~1.2 V, which could significantly enhance the energy density. In search of high power densities, another option in supercapacitor technology is to develop flexible solid state supercapacitors. The clear demonstration of these supercapacitors has been reported elsewhere [331]. Briefly, solid state supercapacitors are promising candidates for energy storage devices because of their flexibility, safety, high power density, and easy integration with other energy storage systems [332]. Another approach to fabricate supercapacitors having higher energy densities with safe and environmental friendly electrolytes is to expand the concept of quasi solid state by employing metallic ions (e.g., quasi solid state Na ion supercapacitors) [333,334]. Wang et al. [335] employed quasi solid state concept to fabricate sodium ion capacitor with nanoporous carbon. They achieved energy density of 168 Wh kg^{-1} with stable cycling stability. Thus, optimization in quasi solid state concept can bring new advances in metallic ion solid state supercapacitors for energy storage applications. As such, many researchers are attempting to introduce this concept for commercial supercapacitor technology.

Reductions in operating cost can be attained by applying higher operating voltages. As the operating potential window increases, the energy density increases also, requiring less material, separator, and electrolyte to store the same amount of energy. A high cell voltage implies that fewer cells are required in series to build a specific-voltage system, which ultimately reduces the load of external voltage-balance circuits now frequently used. Last but not least, the electrode materials for SCs have been a great point of interest in recent years for making energy storage devices that are cost effective and well performing. For this purpose, waste materials are highly economical options to fabricate supercapacitors electrodes although such options need many improvements (fabrication methods, choice of electrolyte, etc.) to practically produce a raw electrode material in the commercial market.

Acknowledgement

KHK acknowledges support from National Research Foundation of Korea (NRF) funded by the Ministry of Science, ICT & Future Planning (No. 2016R1E1A1A01940995). This research was also supported partially by the R&D Center for Green Patrol Technologies through the R&D for Global Top Environmental Technologies funded by the Ministry of Environment (MOE), Republic of Korea and "Cooperative Research Program for Agriculture Science and Technology Development (Grant no. PJ012521032018)" Rural Development Administration, Republic of Korea. Sandeep Kumar thanks DST-PURSE, sanctioned to GJUS&T, Hisar under the PURSE program (No. SR/PURSE Phase 2/40(G)). Waseem thanks Science Foundation of China and the Scholarship Council.

References

[1] R.J. Kuhns, G.H. Shaw, Coal and natural gas, in: Navigating the Energy Maze, Springer, 2018, pp. 65–69.
[2] S. Chu, Y. Cui, N. Liu, The path towards sustainable energy, Nat. Mater. 16 (2017) 16.
[3] S. Singh, S. Jain, V. Ps, A.K. Tiwari, M.R. Nouni, J.K. Pandey, et al., Hydrogen: a sustainable fuel for future of the transport sector, Renew. Sustain. Energy Rev. 51 (2015) 623–633.
[4] H. Yousefi, M. Hamlehdar, S. Tabasi, Y. Noorollahi Economic and thermodynamic evaluations of using geothermal heat pumps in different climate zone (Case Study: Iran), in: Proceedings Geothermal Reservoir Engineering, 2017.
[5] P. Dhepe, K. Tomishige, K.C.W. Wu, Catalytic conversion of biomass, ChemCatChem 9 (2017) 2613–2614.
[6] A. Dunn, M. Calais, G. ,T. Pryor, The impact of energy security and environment concerns on the fuel mix for light passenger vehicles in Australia during the near future: findings from a 2015 Murdoch University Survey, in: Transition Towards 100%Renewable Energy, Springer, 2018, pp. 115–123.
[7] D. Nyberg, C. Wright, J. Kirk Fracking the future: temporality, framing and the politics of unconventional fossil fuels, Academy of Management Proceedings: Academy of Management, 2017, p. 10744.
[8] S. Piao, J. Fang, P. Ciais, P. Peylin, Y. Huang, S. Sitch, et al., The carbon balance of terrestrial ecosystems in China, Nature 458 (2009) 1009.
[9] S. Gunster, This Changes Everything: Capitalism vs the Climate, Taylor & Francis, Milton Park, Abingdon, UK, 2017.
[10] H. Gonenc, B. Scholtens, Environmental and financial performance of fossil fuel firms: a closer inspection of their interaction, Ecol. Econ. 132 (2017) 307–328.
[11] T.R. Karl, K.E. Trenberth, Modern globalclimate change, science 302 (2003) 1719–1723.
[12] N. Stern, What is the economics of climate change? World Econ.-Henley Thames 7 (2006) 1.
[13] N. Oreskes, The scientific consensus on climate change: how do we know we're not wrong?, in: Climate Modelling, Springer, 2018, pp. 31–64.
[14] R. Trancoso, J.R. Larsen, T.R. McVicar, S.R. Phinn, C.A. McAlpine, CO_2-vegetation feedbacks and other climate changes implicated in reducing base flow, Geophys. Res. Lett. 44 (2017) 2310–2318.
[15] Actions on Climate Change Will Define Global Legacy Left for Future Generations, Says Secretary-general, as High-level Event Convenes, High-Level Event on Climate Change: UN, 2007.
[16] J. Milano, H.C. Ong, H. Masjuki, W. Chong, M.K. Lam, P.K. Loh, et al., Microalgae biofuels as an alternative to fossil fuel for power generation, Renew. Sustain. Energy Rev. 58 (2016) 180–197.
[17] M. Dresselhaus, I. Thomas, Alternative energy technologies, Nature 414 (2001) 332.
[18] N. Abas, A. Kalair, N. Khan, Review of fossil fuels and future energy technologies, Futures 69 (2015) 31–49.
[19] N. Yilmaz, A. Atmanli, Sustainable alternative fuels in aviation, Energy 140 (2017) 1378–1386.
[20] C. Bae, J. Kim, Alternative fuels for internal combustion engines, Proc. Combust. Inst. 36 (2017) 3389–3413.
[21] A. Dunn, M. Calais, G. Lee, T. Pryor, Why EVs? A Comparison of Alternative Fuels to Help Australia Regain Energy Security. Transition Towards 100% Renewable Energy, Springer, 2018, pp. 103–114.
[22] J.-C. Sabonnadiere, Renewable Energy Technologies, John Wiley & Sons, Hoboken, NJ, USA, 2010.
[23] C. Weigelt, E. Shittu, Competition, regulatory policy, and firms' resource investments: the case of renewable energy technologies, Acad. Manag. J. 59 (2016) 678–704.
[24] A. Baldock, R. Rankin, A. Jones, I. Wilson, H. Bower, T.W. Baker, et al., Support structure for tidal energy converter system, US Patent App. 15/318,657, 2017.
[25] C. Azcárate, F. Mallor, P. Mateo, Tactical and operational management of wind energy systems with storage using a probabilistic forecast of the energy resource, Renew. Energy 102 (2017) 445–456.
[26] O. Kolditz, L.C. Gutiérrez-Negrín, E. Huenges, L. Jakobs, T. Kohl, I. Moeck, The new Geothermal Energy: Science, Society, and Technology, Springer, New York, USA, 2017.
[27] I.A. Gondal, S.A. Masood, M. Amjad, Review of geothermal energy development efforts in Pakistan and way forward, Renew. Sustain. Energy Rev. 71 (2017) 687–696.
[28] S. Wagh, P. Walke, Review on wind-solar hybrid power system, Int. J. Res. Sci. Eng. (2017) 3.
[29] J.R. McKone, F.J. DiSalvo, H.D. Abruña, Solar energy conversion, storage, and release using an integrated solar-driven redox flow battery, J. Mater. Chem. A 5 (2017) 5362–5372.
[30] B. Sütterlin, M. Siegrist, Public acceptance of renewable energy technologies from an abstract versus concrete perspective and the positive imagery of solar power, Energy Policy 106 (2017) 356–366.
[31] D. Fytili, A. Zabaniotou, Social acceptance of bioenergy in the context of climate change and sustainability–a review, Curr. Opin. Green. Sustain. Chem. 8 (2017) 5–9.
[32] A.F. Hollenkamp, P.C. Howlett, D.R. MacFarlane, S.A. Forsyth, M. Forsyth, Energy

storage devices, Google Patents, 2009.
[33] W. Tasnin, L. Saikia, Performance comparison of several energy storage devices in Ddregulated AGC of a multi area system incorporating geothermal power plant, IET Renew. Power Gener. (2018).
[34] CADEX, How Does a Supercapacitor Work?
[35] Z. Song, J. Hou, H. Hofmann, J. Li, M. Ouyang, Sliding-mode and Lyapunov function-based control for battery/supercapacitor hybrid energy storage system used in electric vehicles, Energy 122 (2017) 601–612.
[36] M.G. Carignano, R. Costa-Castelló, V. Roda, N.M. Nigro, S. Junco, D. Feroldi, Energy management strategy for fuel cell-supercapacitor hybrid vehicles based on prediction of energy demand, J. Power Sources 360 (2017) 419–433.
[37] J. Kerns, What's the difference between batteries and capacitors? Mach. Des. (2015).
[38] R. Kötz, M. Carlen, Principles and applications of electrochemical capacitors, Electrochim. Acta 45 (2000) 2483–2498.
[39] R. Kötz, M. Carlen, Principles and applications of electrochemical capacitors, Electrochim. Acta 45 (2000) 2483–2498.
[40] B.K. Deka, A. Hazarika, J. Kim, Y.B. Park, H.W. Park, Recent development and challenges of multifunctional structural supercapacitors for automotive industries, Int. J. Energy Res. 41 (2017) 1397–1411.
[41] B. Hartmann, L. Prikler, I. Varjasi, Revealing technological possibilities of recovering braking energy of electric traction vehicles. PowerTech, 2017 IEEE Manch.: IEEE (2017) 1–6.
[42] Y. Lu, Y. Zhao, X. Zhao, G. Li, C. Zhang Status analysis of regenerative braking energy utilization equipments in urban rail transit, Transportation Electrification Asia-Pacific (ITEC Asia-Pacific) IEEE Conference and Exp: IEEE, 2017, pp. 1–6.
[43] G. Wang, L. Zhang, J. Zhang, A review of electrode materials for electrochemical supercapacitors, Chem. Soc. Rev. 41 (2012) 797–828.
[44] P. Simon, Y. Gogotsi, Materials for electrochemical capacitors, Nat. Mater. 7 (2008) 845.
[45] S. Zhang, N. Pan, Supercapacitors performance evaluation, Adv. Energy Mater. (2015) 5.
[46] F. Wang, X. Wu, X. Yuan, Z. Liu, Y. Zhang, L. Fu, et al., Latest advances in supercapacitors: from new electrode materials to novel device designs, Chem. Soc. Rev. 46 (2017) 6816–6854.
[47] Q. Ke, J. Wang, Graphene-based materials for supercapacitor electrodes – a review, J. Mater. 2 (2016) 37–54.
[48] J. Huang, B.G. Sumpter, V. Meunier, A universal model for nanoporous carbon supercapacitors applicable to diverse pore regimes, carbon materials, and electrolytes, Chem. Eur. J. 14 (2008) 6614–6626.
[49] M. Hashemi, M.S. Rahmanifar, M.F. El-Kady, A. Noori, M.F. Mousavi, R.B. Kaner, The use of an electrocatalytic redox electrolyte for pushing the energy density boundary of a flexible polyaniline electrode to a new limit, Nano Energy 44 (2018) 489–498.
[50] A. González, E. Goikolea, J.A. Barrena, R. Mysyk, Review on supercapacitors: technologies and materials, Renew. Sustain. Energy Rev. 58 (2016) 1189–1206.
[51] A. Divyashree, G. Hegde, Activated carbon nanospheres derived from bio-waste materials for supercapacitor applications–a review, RSC Adv. 5 (2015) 88339–88352.
[52] F. Ali, X. Liu, D. Zhou, X. Yang, J. Xu, T. Schenk, et al., Silicon-doped hafnium oxide anti-ferroelectric thin films for energy storage, J. Appl. Phys. 122 (2017) 144105.
[53] G. Xiong, A. Kundu, T.S. Fisher, Thermal management in electrochemical energy storage systems, in: Thermal Effects in Supercapacitors, Springer, 2015, pp.1–10.
[54] K. Hung, C. Masarapu, T. Ko, B. Wei, Wide-temperature range operation supercapacitors from nanostructured activated carbon fabric, J. Power Sources 193 (2009) 944–949.
[55] N.A. Kumar, J.-B. Baek, Electrochemical supercapacitors from conducting polyaniline–graphene platforms, Chem. Commun. 50 (2014) 6298–6308.
[56] Q. Cheng, J. Tang, N. Shinya, L.-C. Qin, Co (OH) 2 nanosheet-decorated graphene–CNT composite for supercapacitors of high energy density, Sci. Technol. Adv. Mater. 15 (2014) 014206.
[57] B. You, N. Li, H. Zhu, X. Zhu, J. Yang, Graphene oxide-dispersed pristine CNTs support for MnO2 nanorods as high performance supercapacitor electrodes, ChemSusChem 6 (2013) 474–480.
[58] M. Armand, J.-M. Tarascon, Building better batteries, nature 451 (2008) 652.
[59] I. Shakir, High energy density based flexible electrochemical supercapacitors from layer-by-layer assembled multiwall carbon nanotubes and graphene, Electrochim. Acta 129 (2014) 396–400.
[60] H. Wang, C.M. Holt, Z. Li, X. Tan, B.S. Amirkhiz, Z. Xu, et al., Graphene-nickel cobaltite nanocomposite asymmetrical supercapacitor with commercial level mass loading, Nano Res. 5 (2012) 605–617.
[61] A.A. Yadav, Influence of electrode mass-loading on the properties of spray deposited Mn3O4 thin films for electrochemical supercapacitors, Thin Solid Films. 608 (2016) 88–96.
[62] A. Sumboja, C.Y. Foo, X. Wang, P.S. Lee, Large areal mass, flexible and free--standing reduced graphene oxide/manganese dioxide paper for asymmetric supercapacitor device, Adv. Mater. 25 (2013) 2809–2815.
[63] X. Fan, B.D. Phebus, L. Li, S. Chen, Graphene-based composites for supercapacitor electrodes, Sci. Adv. Mater. 7 (2015) 1916–1944.
[64] L.L. Zhang, X. Zhao, Carbon-based materials as supercapacitor electrodes, Chem. Soc. Rev. 38 (2009) 2520–2531.
[65] D.L. Chapman, LI. A contribution to the theory of electrocapillarity, Lond. Dublin Philos. Mag. J. Sci. 25 (1913) 475–481.
[66] M. Gouy, Sur la constitution de la charge électrique à la surface d'un électrolyte, J. Phys. Theor. Appl. 9 (1910) 457–468.
[67] E. Frackowiak, Carbon materials for supercapacitor application, Phys. Chem. Chem. Phys. 9 (2007) 1774–1785.
[68] M. Endo, T. Maeda, T. Takeda, Y. Kim, K. Koshiba, H. Hara, et al., Capacitance and pore-size distribution in aqueous and nonaqueous electrolytes using various activated carbon electrodes, J. Electrochem. Soc. 148 (2001) A910–A914.
[69] D. Qu, H. Shi, Studies of activated carbons used in double-layer capacitors, J. Power Sources 74 (1998) 99–107.
[70] E. Raymundo-Pinero, K. Kierzek, J. Machnikowski, F. Béguin, Relationship between the nanoporous texture of activated carbons and their capacitance properties in different electrolytes, Carbon 44 (2006) 2498–2507.
[71] T. Lin, I.-W. Chen, F. Liu, C. Yang, H. Bi, F. Xu, et al., Nitrogen-doped mesoporous carbon of extraordinary capacitance for electrochemical energy storage, Science 350 (2015) 1508–1513.
[72] P. Kleszyk, P. Ratajczak, P. Skowron, J. Jagiello, Q. Abbas, E. Frąckowiak, et al., Carbons with narrow pore size distribution prepared by simultaneous carbonization and self-activation of tobacco stems and their application to supercapacitors, Carbon 81 (2015) 148–157.
[73] X. Ma, L. Gan, M. Liu, P.K. Tripathi, Y. Zhao, Z. Xu, et al., Mesoporous size controllable carbon microspheres and their electrochemical performances for supercapacitor electrodes, J. Mater. Chem. A 2 (2014) 8407–8415.
[74] T. Yang, R. Zhou, D.-W. Wang, S.P. Jiang, Y. Yamauchi, S.Z. Qiao, et al., Hierarchical mesoporous yolk–shell structured carbonaceous nanospheres for high performance electrochemical capacitive energy storage, Chem. Commun. 51 (2015) 2518–2521.
[75] Y.J. Kim, Y. Horie, S. Ozaki, Y. Matsuzawa, H. Suezaki, C. Kim, et al., Correlation between the pore and solvated ion size on capacitance uptake of PVDC-based carbons, Carbon 42 (2004) 1491–1500.
[76] L. Peng, Y. Liang, H. Dong, H. Hu, X. Zhao, Y. Cai, et al., Super-hierarchical porous carbons derived from mixed biomass wastes by a stepwise removal strategy for high-performance supercapacitors, J. Power Sources 377 (2018) 151–160.
[77] J. Chmiola, G. Yushin, R. Dash, Y. Gogotsi, Effect of pore size and surface area of carbide derived carbons on specific capacitance, J. Power Sources 158 (2006) 765–772.
[78] Z. Yu, L. Tetard, L. Zhai, J. Thomas, Supercapacitor electrode materials: nanostructures from 0 to 3 dimensions, Energy Environ. Sci. 8 (2015) 702–730.
[79] E.J. Ra, E. Raymundo-Piñero, Y.H. Lee, F. Béguin, High power supercapacitors using polyacrylonitrile-based carbon nanofiber paper, Carbon 47 (2009) 2984–2992.
[80] E. Raymundo-Piñero, K. Kierzek, J. Machnikowski, F. Béguin, Relationship between the nanoporous texture of activated carbons and their capacitance properties in different electrolytes, Carbon 44 (2006) 2498–2507.
[81] N. Yoshida, Y. Yamada, S.-I. Nishimura, Y. Oba, M. Ohnuma, A. Yamada, Unveiling the origin of unusual pseudocapacitance of RuO2·n H2O from Its hierarchical nanostructure by small-angle X-ray Scattering, J. Phys. Chem. C 117 (2013) 12003–12009.
[82] J.W. Kim, V. Augustyn, B. Dunn, The effect of crystallinity on the rapid pseudocapacitive response of Nb2O5, Adv. Energy Mater. 2 (2012) 141–148.
[83] V. Augustyn, P. Simon, B. Dunn, Pseudocapacitive oxide materials for high-rate electrochemical energy storage, Energy Environ. Sci. 7 (2014) 1597–1614.
[84] J.R. Miller, P. Simon, Electrochemical capacitors for energy management, Sci. Mag. 321 (2008) 651–652.
[85] K. Naoi, P. Simon, New materials and new configurations for advanced electrochemical capacitors, J. Electrochem. Soc. (JES). 17 (2008) 34–37.
[86] Zhu Z-z, Wang G-c, Sun M-q, Li X-w, Li C-z, Fabrication and electrochemical characterization of polyaniline nanorods modified with sulfonated carbon nanotubes for supercapacitor applications, Electrochim. Acta 56 (2011) 1366–1372.
[87] A. Burke, Ultracapacitors: why, how, and where is the technology, J. Power Sources 91 (2000) 37–50.
[88] S. Wu, Y. Zhu, Highly densified carbon electrode materials towards practical supercapacitor devices, Sci. China Mater. 60 (2017) 25–38.
[89] J. Zhang, X. Zhao, On the configuration of supercapacitors for maximizing electrochemical performance, ChemSusChem 5 (2012) 818–841.
[90] H.-P. Cong, X.-C. Ren, P. Wang, S.-H. Yu, Flexible graphene–polyaniline composite paper for high-performance supercapacitor, Energy Environ. Sci. 6 (2013) 1185–1191.
[91] B. Anothumakkool, R. Soni, S.N. Bhange, S. Kurungot, Novel scalable synthesis of highly conducting and robust PEDOT paper for a high performance flexible solid supercapacitor, Energy Environ. Sci. 8 (2015) 1339–1347.
[92] G. Binitha, M. Soumya, A.A. Madhavan, P. Praveen, A. Balakrishnan, K. Subramanian, et al., Electrospun α-Fe 2 O 3 nanostructures for supercapacitor applications, J. Mater. Chem. A 1 (2013) 11698–11704.
[93] S.-L. Chou, J.-Z. Wang, H.-K. Liu, S.-X. Dou, Electrochemical deposition of porous Co (OH) 2 nanoflake films on stainless steel mesh for flexible supercapacitors, J. Electrochem. Soc. 155 (2008) A926–A929.
[94] D.P. Dubal, O. Ayyad, V. Ruiz, P. Gomez-Romero, Hybrid energy storage: the merging of battery and supercapacitor chemistries, Chem. Soc. Rev. 44 (2015) 1777–1790.
[95] S. Pay, Y. Baghzouz Effectiveness of battery-supercapacitor combination in electric vehicles, in: Power Tech Conference Proceedings IEEE Bologna: IEEE, vol. 3, 2003, p. 6.
[96] S. Yu, N. Yang, M. Vogel, S. Mandal, O.A. Williams, S. Jiang, et al., Battery-like supercapacitors from vertically aligned carbon nanofiber coated diamond: design and demonstrator, Adv. Energy Mater. (2018).
[97] M. Ates, M. El-Kady, R.B. Kaner, Three-dimensional design and fabrication of reduced graphene oxide/polyaniline composite hydrogel electrodes for high performance electrochemical supercapacitors, Nanotechnology 29 (2018) 175402.

[98] J. Xu, Y. Sun, M. Lu, L. Wang, J. Zhang, J. Qian, et al., Fabrication of hierarchical MnMoO4·H2O@ MnO2 core-shell nanosheet arrays on nickel foam as an advanced electrode for asymmetric supercapacitors, Chem. Eng. J. 334 (2018) 1466–1476.

[99] B.-J. Yang, L.-l. Jiang, Y.-J. Li, F.-G. Cai, Q.-Y. Zhang, Three-dimensional porous biocarbon wrapped by graphene and polypyrrole composite as electrode materials for supercapacitor, J. Mater. Sci.: Mater. Electron. 29 (2018) 2568–2572.

[100] L. Yao, Q. Wu, P. Zhang, J. Zhang, D. Wang, Y. Li, et al., Scalable 2D Hierarchical Porous Carbon Nanosheets for Flexible Supercapacitors with Ultrahigh Energy Density, Adv. Mater. 30 (2018) 1706054.

[101] D. Song, J. Zhu, L. Xuan, C. Zhao, L. Xie, L. Chen, Freestanding two-dimensional Ni (OH) 2 thin sheets assembled by 3D nanoflake array as basic building units for supercapacitor electrode materials, J. Colloid Interface Sci. 509 (2018) 163–170.

[102] Y. Guan, Z. Guo, H. Che, J. Mu, X. Zhang, Z. Zhang, et al., Core/shell nanorods of MnO2/carbon embedded with Ag nanoparticles as high-performance electrode materials for supercapacitors, Chem. Eng. J. 331 (2018) 23–30.

[103] D. Qi, X. Chen, Flexible supercapacitors based on two-dimensional materials, Flex. Stretchable Med. Devices (2018).

[104] R.-R. Zhang, Y.-M. Xu, D. Harrison, J. Fyson, F.-L. Qiu, D. Southee, Flexible strip supercapacitors for future energy storage, Int. J. Autom. Comput. 12 (2015) 43–49.

[105] R. Zhang, Y. Xu, D. Harrison, J. Fyson, D. Southee, A. Tanwilaisiri Fabrication and characterisation of energy storage fibres, in: Proceedings of the 2014 20th International Conference on Automation and Computing (ICAC), IEEE, 2014, pp. 228–230.

[106] A. Tanwilaisiri, Y. Xu, R. Zhang, D. Harrison, J. Fyson, M. Areir, Design and fabrication of modular supercapacitors using 3D printing, J. Energy Storage 16 (2018) 1–7.

[107] K. Wang, Z. Wang, X. Wang, X. Zhou, Y. Tao, H. Wu, Flexible long-chain-linker constructed Ni-based metal-organic frameworks with 1D helical channel and their pseudo-capacitor behavior studies, J. Power Sources 377 (2018) 44–51.

[108] Elgrishi Nm, K.J. Rountree, B.D. McCarthy, E.S. Rountree, T.T. Eisenhart, J.L. Dempsey, A practical Beginner's guide to cyclic voltammetry, J. Chem. Educ. (2017).

[109] M. Li, M. Zhou, Z.Q. Wen, Y.X. Zhang, Flower-like NiFe layered double hydroxides coated MnO2 for high-performance flexible supercapacitors, J. Energy Storage 11 (2017) 242–248.

[110] H. Yu, Q. Tang, J. Wu, Y. Lin, L. Fan, M. Huang, et al., Using eggshell membrane as a separator in supercapacitor, J. Power Sources 206 (2012) 463–468.

[111] J. Zhou, J. Lian, L. Hou, J. Zhang, H. Gou, M. Xia, et al., Ultrahigh volumetric capacitance and cyclic stability of fluorine and nitrogen co-doped carbon microspheres, Nat. Commun. 6 (2015) 8503.

[112] W. Li, L. Xin, X. Xu, Q. Liu, M. Zhang, S. Ding, et al., Facile synthesis of three-dimensional structured carbon fiber-NiCo 2 O 4-Ni (OH) 2 high-performance electrode for pseudocapacitors, Sci. Rep. 5 (2015) 9277.

[113] P. Cao, Y. Fan, J. Yu, R. Wang, P. Song, Y. Xiong, Polypyrrole nanocomposites doped with functional ionic liquids for high performance supercapacitors, New J. Chem. 42 (2018) 3909–3916.

[114] Z. Hou, H. Lu, Q. Yang, Q. Zhao, J. Liu, Micromorphology-controlled synthesis of polypyrrole films by using binary surfactant of Span80/OP10 via interfacial polymerization and their enhanced electrochemical capacitance, Electrochim. Acta 265 (2018) 601–608.

[115] D.K. Kampouris, X. Ji, E.P. Randviir, C.E. Banks, A new approach for the improved interpretation of capacitance measurements for materials utilised in energy storage, RSC Adv. 5 (2015) 12782–12791.

[116] K. Subramani, N. Sudhan, R. Divya, M. Sathish, All-solid-state asymmetric supercapacitors based on cobalt hexacyanoferrate-derived CoS and activated carbon, RSC Adv. 7 (2017) 6648–6659.

[117] J. Yan, T. Wei, B. Shao, F. Ma, Z. Fan, M. Zhang, et al., Electrochemical properties of graphene nanosheet/carbon black composites as electrodes for supercapacitors, Carbon 48 (2010) 1731–1737.

[118] B. Lobato, L. Suárez, L. Guardia, T.A. Centeno, Capacitance and surface of carbons in supercapacitors, Carbon 122 (2017) 434–445.

[119] L.-F. Cai, J. Xu, J.-Y. Huang, H.-J. Xu, et al., F. Xu, Y.-R. Liang, Structure control of powdery carbon aerogels and their use in high-voltage aqueous supercapacitors, Carbon 130 (2018) 847.

[120] C. Largeot, C. Portet, J. Chmiola, P.-L. Taberna, Y. Gogotsi, P. Simon, Relation between the ion size and pore size for an electric double-layer capacitor, J. Am. Chem. Soc. 130 (2008) 2730–2731.

[121] I. Shown, A. Ganguly, L.C. Chen, K.H. Chen, Conducting polymer-based flexible supercapacitor, Energy Sci. Eng. 3 (2015) 2–26.

[122] Y. Luo, W. Hong, Z. Xiao, H. Bai, A high-performance electrochemical supercapacitor based on a polyaniline/reduced graphene oxide electrode and a copper (ii) ion active electrolyte, Phys. Chem. Chem. Phys. 20 (2018) 131–136.

[123] W. Liu, S. Zhang, S.U. Dar, Y. Zhao, R. Akram, X. Zhang, et al., Polyphosphazene-derived heteroatoms-doped carbon materials for supercapacitor electrodes, Carbon 129 (2018) 420–427.

[124] M. Cakici, R.R. Kakarla, F. Alonso-Marroquin, Advanced electrochemical energy storage supercapacitors based on the flexible carbon fiber fabric-coated with uniform coral-like MnO 2 structured electrodes, Chem. Eng. J. 309 (2017) 151–158.

[125] S.S. Jayaseelan, S. Radhakrishnan, B. Saravanakumar, M.-K. Seo, M.-S. Khil, H.-Y. Kim, et al., Mesoporous 3D NiCo2O4/MWCNT nanocomposite aerogels prepared by a supercritical CO_2 drying method for high performance hybrid supercapacitor electrodes, Colloids Surf. A: Physicochem. Eng. Asp. 538 (2018) 451–459.

[126] O. Barbieri, M. Hahn, A. Herzog, R. Kötz, Capacitance limits of high surface area activated carbons for double layer capacitors, Carbon 43 (2005) 1303–1310.

[127] K. Kierzek, E. Frackowiak, G. Lota, G. Gryglewicz, J. Machnikowski, Electrochemical capacitors based on highly porous carbons prepared by KOH activation, Electrochim. Acta 49 (2004) 515–523.

[128] G. Salitra, A. Soffer, L. Eliad, Y. Cohen, D. Aurbach, Carbon electrodes for double-layer capacitors I. Relations between ion and pore dimensions, J. Electrochem. Soc. 147 (2000) 2486–2493.

[129] E. Raymundo-Piñero, F. Leroux, F. Béguin, A high-performance carbon for supercapacitors obtained by carbonization of a seaweed biopolymer, Adv. Mater. 18 (2006) 1877–1882.

[130] L. Wang, H. Ji, S. Wang, L. Kong, X. Jiang, G. Yang, Preparation of Fe 3 O 4 with high specific surface area and improved capacitance as a supercapacitor, Nanoscale 5 (2013) 3793–3799.

[131] Z.Y. Yang, L.J. Jin, G.Q. Lu, Q.Q. Xiao, Y.X. Zhang, L. Jing, et al., Sponge-templated preparation of high surface area graphene with ultrahigh capacitive deionization performance, Adv. Funct. Mater. 24 (2014) 3917–3925.

[132] H. Ba, W. Wang, S. Pronkin, T. Romero, W. Baaziz, L. Nguyen-Dinh, et al., Biosourced foam-like activated carbon materials as high-performance supercapacitors, Adv. Sustain. Syst. (2018).

[133] K. Xu, J. Yang, S. Li, Q. Liu, J. Hu, Facile synthesis of hierarchical mesoporous NiCo2O4 nanoflowers with large specific surface area for high-performance supercapacitors, Mater. Lett. 187 (2017) 129–132.

[134] J. Gu, X. Fan, X. Liu, S. Li, Z. Wang, S. Tang, et al., Mesoporous manganese oxide with large specific surface area for high-performance asymmetric supercapacitor with enhanced cycling stability, Chem. Eng. J. 324 (2017) 35–43.

[135] D. Su, J. Ma, M. Huang, F. Liu, T. Chen, C. Liu, et al. Manganese oxides-based composite electrodes for supercapacitors, IOP Conference Series: Materials Science and Engineering: IOP Publishing, 2017, p. 012087.

[136] P. Azaïs, L. Duclaux, P. Florian, D. Massiot, M.-A. Lillo-Rodenas, A. Linares-Solano, et al., Causes of supercapacitors ageing in organic electrolyte, J. Power Sources 171 (2007) 1046–1053.

[137] M. Seredych, D. Hulicova-Jurcakova, G.Q. Lu, T.J. Bandosz, Surface functional groups of carbons and the effects of their chemical character, density and accessibility to ions on electrochemical performance, Carbon 46 (2008) 1475–1488.

[138] S. Iijima, Helical microtubules of graphitic carbon, Nature 354 (1991) 56–58.

[139] M.S. Dresselhaus, G. Dresselhaus, P.C. Eklund, Science of Fullerenes and Carbon Nanotubes: Their Properties and Applications, Academic Press, Waltham, Massachusetts, USA, 1996.

[140] S.N. Ahmad, S. Hakeem, R.A. Alvi, K. Farooq, N. Farooq, F. Yasmin, et al. Synthesis of multi-walled carbon nanotubes and their application in resin based nanocomposites, Journal of Physics: Conference Series: IOP Publishing, 2013, p. 012009.

[141] M. Dresselhaus, G. Dresselhaus, R. Saito, C60-related tubules, Solid State Commun. 84 (1992) 201–205.

[142] J.-P. Issi, L. Langer, J. Heremans, C. Olk, Electronic properties of carbon nanotubes: experimental results, Carbon 33 (1995) 941–948.

[143] T. Ebbesen, H. Lezec, H. Hiura, J. Bennett, H. Ghaemi, T. Thio, Electrical conductivity of individual carbon nanotubes, Nature 382 (1996) 54–56.

[144] C. Meng, C. Liu, S. Fan, Flexible carbon nanotube/polyaniline paper-like films and their enhanced electrochemical properties, Electrochem. Commun. 11 (2009) 186–189.

[145] K.H. An, W.S. Kim, Y.S. Park, H.J. Jeong, Y.C. Choi, J.-.M. Moon, et al. Supercapacitors using singlewalled carbon nanotube electrodes, AIP Conference Proceedings: AIP, 2001, pp. 241–244.

[146] C. Du, N. Pan, High power density supercapacitor electrodes of carbon nanotube films by electrophoretic deposition, Nanotechnology 17 (2006) 5314.

[147] C. Niu, E.K. Sichel, R. Hoch, D. Moy, H. Tennent, High power electrochemical capacitors based on carbon nanotube electrodes, Appl. Phys. Lett. 70 (1997) 1480–1482.

[148] E. Frackowiak, K. Metenier, V. Bertagna, F. Beguin, Supercapacitor electrodes from multiwalled carbon nanotubes, Appl. Phys. Lett. 77 (2000) 2421–2423.

[149] A.L.M. Reddy, F.E. Amitha, I. Jafri, S. Ramaprabhu, Asymmetric flexible supercapacitor stack, Nanoscale Res. Lett. 3 (2008) 145.

[150] C. Liu, M. Liu, F. Li, H. Cheng, Frequency response characteristic of single-walled carbon nanotubes as supercapacitor electrode material, Appl. Phys. Lett. 92 (2008) 143108.

[151] J.N. Barisci, G.G. Wallace, D. Chattopadhyay, F. Papadimitrakopoulos, R.H. Baughman, Electrochemical properties of single-wall carbon nanotube electrodes, J. Electrochem. Soc. 150 (2003) E409–E415.

[152] L. Su, X. Zhang, C. Yuan, B. Gao, Symmetric self-hybrid supercapacitor consisting of multiwall carbon nanotubes and Co–Al layered double hydroxides, J. Electrochem. Soc. 155 (2008) A110–A114.

[153] C.Y. Lee, H.M. Tsai, H.J. Chuang, S.Y. Li, P. Lin, T.Y. Tseng, Characteristics and electrochemical performance of supercapacitors with manganese oxide-carbon nanotube nanocomposite electrodes, J. Electrochem. Soc. 152 (2005) A716–A720.

[154] G. Arabale, D. Wagh, M. Kulkarni, I. Mulla, S. Vernekar, K. Vijayamohanan, et al., Enhanced supercapacitance of multiwalled carbon nanotubes functionalized with ruthenium oxide, Chem. Phys. Lett. 376 (2003) 207–213.

[155] M. Hughes, G.Z. Chen, M.S. Shaffer, D.J. Fray, A.H. Windle, Electrochemical capacitance of a nanoporous composite of carbon nanotubes and polypyrrole, Chem. Mater. 14 (2002) 1610–1613.

[156] K. Koziol, J. Vilatela, A. Moisala, M. Motta, P. Cunniff, M. Sennett, et al., High-performance carbon nanotube fiber, Science 318 (2007) 1892–1895.

[157] C. Xiong, T. Li, T. Zhao, A. Dang, H. Li, X. Ji, et al., Reduced graphene oxide-carbon nanotube grown on carbon fiber as binder-free electrode for flexible high-performance fiber supercapacitors, Compos. Part B: Eng. 116 (2017) 7–15.

[158] Z.-S. Wu, G. Zhou, L.-C. Yin, W. Ren, F. Li, H.-M. Cheng, Graphene/metal oxide composite electrode materials for energy storage, Nano Energy 1 (2012) 107–131.
[159] K.S. Novoselov, A.K. Geim, S.V. Morozov, D. Jiang, Y. Zhang, S.V. Dubonos, et al., Electric field effect in atomically thin carbon films, Science 306 (2004) 666–669.
[160] K.S. Novoselov, A.K. Geim, S. Morozov, D. Jiang, M. Katsnelson, I. Grigorieva, et al., Two-dimensional gas of massless Dirac fermions in graphene, Nature 438 (2005) 197–200.
[161] A.K. Geim, Graphene: status and prospects, Science 324 (2009) 1530–1534.
[162] H. Zhang, M. Chhowalla, Z. Liu, 2D nanomaterials: graphene and transition metal dichalcogenides, Chem. Soc. Rev. 47 (2018) 3015–3017.
[163] M. Pumera, Graphene-based nanomaterials and their electrochemistry, Chem. Soc. Rev. 39 (2010) 4146–4157.
[164] Y. Gao, Graphene and polymer composites for supercapacitor applications: a review, Nanoscale Res. Lett. 12 (2017) 387.
[165] X. Zhang, H. Zhang, C. Li, K. Wang, X. Sun, Y. Ma, Recent advances in porous graphene materials for supercapacitor applications, RSC Adv. 4 (2014) 45862–45884.
[166] X. Yang, C. Cheng, Y. Wang, L. Qiu, D. Li, Liquid-mediated dense integration of graphene materials for compact capacitive energy storage, Science 341 (2013) 534–537.
[167] J. Xie, M. Wang, High surface area nano-structured graphene composites and capacitive devices incorporating the same, Google Patents, 2018.
[168] M. Depardieu, R. Janot, C. Sanchez, A. Bentaleb, C. Gervais, M. Birot, et al., Carbonaceous multiscale-cellular foams as novel electrodes for stable, efficient lithium–sulfur batteries, RSC Adv. 4 (2014) 23971–23976.
[169] A. Peigney, C. Laurent, E. Flahaut, R.R. Bacsa, A. Rousset, Specific surface area of carbon nanotubes and bundles of carbon nanotubes, Carbon 39 (2001) 507–514.
[170] S. Vivekchand, C.S. Rout, K. Subrahmanyam, A. Govindaraj, C. Rao, Graphene-based electrochemical supercapacitors, J. Chem. Sci. 120 (2008) 9–13.
[171] M.D. Stoller, S. Park, Y. Zhu, J. An, R.S. Ruoff, Graphene-based ultracapacitors, Nano Lett. 8 (2008) 3498–3502.
[172] Y. Wang, Z. Shi, Y. Huang, Y. Ma, C. Wang, M. Chen, et al., Supercapacitor devices based on graphene materials, J. Phys. Chem. C 113 (2009) 13103–13107.
[173] A.M. Navarro-Suárez, K.L. Van Aken, T. Mathis, T. Makaryan, J. Yan, J. Carretero-González, et al., Development of asymmetric supercapacitors with titanium carbide-reduced graphene oxide couples as electrodes, Electrochim. Acta (2017).
[174] F. Li, J. Chen, X. Wang, M. Xue, G. Chen, Stretchable supercapacitor with adjustable volumetric capacitance based on 3D interdigital electrodes, Adv. Funct. Mater. 25 (2015) 4601–4606.
[175] J. Yan, C.E. Ren, K. Maleski, C.B. Hatter, B. Anasori, P. Urbankowski, et al., Flexible MXene/graphene films for ultrafast supercapacitors with outstanding volumetric capacitance, Adv. Funct. Mater. 27 (2017).
[176] F. Wang, C. Wang, Y. Zhao, Z. Liu, Z. Chang, L. Fu, et al., A quasi-solid-state Li-ion capacitor based on porous TiO2 hollow microspheres wrapped with graphene nanosheets, Small 12 (2016) 6207–6213.
[177] F. Wang, Z. Liu, X. Yuan, J. Mo, C. Li, L. Fu, et al., A quasi-solid-state Li-ion capacitor with high energy density based on Li3VO4/carbon nanofibers and electrochemically-exfoliated graphene sheets, J. Mater. Chem. A 5 (2017) 14922–14929.
[178] K.S. Ryu, K.M. Kim, N.-G. Park, Y.J. Park, S.H. Chang, Symmetric redox supercapacitor with conducting polyaniline electrodes, J. Power Sources 103 (2002) 305–309.
[179] A. Rudge, I. Raistrick, S. Gottesfeld, J.P. Ferraris, A study of the electrochemical properties of conducting polymers for application in electrochemical capacitors, Electrochim. Acta 39 (1994) 273–287.
[180] A. Burke, R&D considerations for the performance and application of electrochemical capacitors, Electrochim. Acta 53 (2007) 1083–1091.
[181] E. Frackowiak, V. Khomenko, K. Jurewicz, K. Lota, F. Béguin, Supercapacitors based on conducting polymers/nanotubes composites, J. Power Sources 153 (2006) 413–418.
[182] K. Lota, V. Khomenko, E. Frackowiak, Capacitance properties of poly (3, 4-ethylenedioxythiophene)/carbon nanotubes composites, J. Phys. Chem. Solids 65 (2004) 295–301.
[183] T. Girija, M. Sangaranarayanan, Polyaniline-based nickel electrodes for electrochemical supercapacitors—Influence of Triton X-100, J. Power Sources 159 (2006) 1519–1526.
[184] J.-Y. Kim, K.H. Kim, K.B. Kim, Fabrication and electrochemical properties of carbon nanotube/polypyrrole composite film electrodes with controlled pore size, J. Power Sources 176 (2008) 396–402.
[185] H. Zhang, G. Cao, W. Wang, K. Yuan, B. Xu, W. Zhang, et al., Influence of microstructure on the capacitive performance of polyaniline/carbon nanotube array composite electrodes, Electrochim. Acta 54 (2009) 1153–1159.
[186] H. Zhang, G. Cao, Z. Wang, Y. Yang, Z. Shi, Z. Gu, Tube-covering-tube nanostructured polyaniline/carbon nanotube array composite electrode with high capacitance and superior rate performance as well as good cycling stability, Electrochem. Commun. 10 (2008) 1056–1059.
[187] C. Peng, S. Zhang, D. Jewell, G.Z. Chen, Carbon nanotube and conducting polymer composites for supercapacitors, Prog. Nat. Sci. 18 (2008) 777–788.
[188] Q. Meng, K. Cai, Y. Chen, L. Chen, Research progress on conducting polymer based supercapacitor electrode materials, Nano Energy 36 (2017) 268–285.
[189] K. Wang, H. Wu, Y. Meng, Z. Wei, Conducting polymer nanowire arrays for high performance supercapacitors, Small 10 (2014) 14–31.
[190] X. Li, L. Yang, Y. Lei, L. Gu, D. Xiao, Microwave-assisted chemical-vapor-induced in situ polymerization of polyaniline nanofibers on graphite electrode for high-performance supercapacitor, ACS Appl. Mater. Interfaces 6 (2014) 19978–19989.
[191] D. Liu, P. Du, W. Wei, H. Wang, Q. Wang, P. Liu, Flexible and robust sandwich-structured S-doped reduced graphene oxide/carbon nanotubes/polyaniline (S-rGO/CNTs/PANI) composite membranes: excellent candidate as free-standing electrodes for high-performance supercapacitors, Electrochim. Acta 233 (2017) 201–209.
[192] A. Eftekhari, L. Li, Y. Yang, Polyaniline supercapacitors, J. Power Sources 347 (2017) 86–107.
[193] Jose R. Misnon II, Synthesis and electrochemical evaluation of the PANI/δ-MnO 2 electrode for high performing asymmetric supercapacitors, New J. Chem. 41 (2017) 6574–6584.
[194] N. Arsalani, A.G. Tabrizi, L.S. Ghadimi, Novel PANI/MnFe2O4 nanocomposite for low-cost supercapacitors with high rate capability, J. Mater. Sci.: Mater. Electron. (2018) 1–9.
[195] Y. Luo, D. Kong, Y. Jia, J. Luo, Y. Lu, D. Zhang, et al., Self-assembled graphene@PANI nanoworm composites with enhanced supercapacitor performance, RSC Adv. 3 (2013) 5851–5859.
[196] Y.-E. Miao, W. Fan, D. Chen, T. Liu, High-performance supercapacitors based on hollow polyaniline nanofibers by electrospinning, ACS Appl. Mater. Interfaces 5 (2013) 4423–4428.
[197] D.D. Potphode, S.P. Mishra, P. Sivaraman, M. Patri, Asymmetric supercapacitor devices based on dendritic conducting polymer and activated carbon, Electrochim. Acta 230 (2017) 29–38.
[198] A. Razak, S. Izwan, I.F. Wahab, F. Fadil, F.N. Dahli, M. Khudzari, et al., A review of electrospun conductive polyaniline based nanofiber composites and blends: processing features, applications, and future directions, Adv. Mater. Sci. Eng. 2015 (2015).
[199] S. Chaudhari, Y. Sharma, P.S. Archana, R. Jose, S. Ramakrishna, S. Mhaisalkar, et al., Electrospun polyaniline nanofibers web electrodes for supercapacitors, J. Appl. Polym. Sci. 129 (2013) 1660–1668.
[200] S.K. Simotwo, C. DelRe, V. Kalra, Supercapacitor electrodes based on high-purity electrospun polyaniline and polyaniline–carbon nanotube nanofibers, ACS Appl. Mater. Interfaces 8 (2016) 21261–21269.
[201] L.-Z. Fan, J. Maier, High-performance polypyrrole electrode materials for redox supercapacitors, Electrochem. Commun. 8 (2006) 937–940.
[202] P. Asen, S. Shahrokhian, A high performance supercapacitor based on graphene/polypyrrole/Cu2O–Cu (OH) 2 ternary nanocomposite coated on nickel foam, J. Phys. Chem. C 121 (2017) 6508–6519.
[203] K. Shi, I. Zhitomirsky, Influence of current collector on capacitive behavior and cycling stability of Tiron doped polypyrrole electrodes, J. Power Sources 240 (2013) 42–49.
[204] A. Afzal, F.A. Abuilaiwi, A. Habib, M. Awais, S.B. Waje, M.A. Atieh, Polypyrrole/carbon nanotube supercapacitors: technological advances and challenges, J. Power Sources 352 (2017) 174–186.
[205] X. Lin, Y. Xu, Facile synthesis and electrochemical capacitance of composites of polypyrrole/multi-walled carbon nanotubes, Electrochim. Acta 53 (2008) 4990–4997.
[206] D.P. Dubal, B. Ballesteros, A.A. Mohite, P. Gómez-Romero, Functionalization of polypyrrole nanopipes with redox-active polyoxometalates for high energy density supercapacitors, ChemSusChem 10 (2017) 731–737.
[207] Y. Wang, J. Guo, T. Wang, J. Shao, D. Wang, Y.-W. Yang, Mesoporous transition metal oxides for supercapacitors, Nanomaterials 5 (2015) 1667–1689.
[208] M. Zhi, C. Xiang, J. Li, M. Li, N. Wu, Nanostructured carbon–metal oxide composite electrodes for supercapacitors: a review, Nanoscale 5 (2013) 72–88.
[209] S. Chen, J. Zhu, X. Wu, Q. Han, X. Wang, Graphene oxide– MnO2 nanocomposites for supercapacitors, ACS Nano 4 (2010) 2822–2830.
[210] R. Rakhi, W. Chen, M.N. Hedhili, D. Cha, H.N. Alshareef, Enhanced rate performance of mesoporous Co3O4 nanosheet supercapacitor electrodes by hydrous RuO2 nanoparticle decoration, ACS Appl. Mater. Interfaces 6 (2014) 4196–4206.
[211] S. Ratha, S.R. Marri, J. Behera, C.S. Rout, High-energy-density supercapacitors based on patronite/single-walled carbon nanotubes/reduced graphene oxide hybrids, Eur. J. Inorg. Chem. 2016 (2016) 259–265.
[212] A. Borenstein, O. Hanna, R. Attias, S. Luski, T. Brousse, D. Aurbach, Carbon-based composite materials for supercapacitor electrodes: a review, J. Mater. Chem. A 5 (2017) 12653–12672.
[213] K.M. Lee, M. Kim, E. Lee, S.H. Baeck, S.E. Shim, Nylon 6, 6/polyaniline based sheath nanofibers for high-performance supercapacitors, Electrochim. Acta 213 (2016) 124–131.
[214] S. Duan, R. Wang, Au/Ni12P5 core/shell nanocrystals from bimetallic heterostructures: in situ synthesis, evolution and supercapacitor properties, Npg Asia Mater. 6 (2014) e122.
[215] Z. Wang, Qe Zhang, S. Long, Y. Luo, P. Yu, Z. Tan, et al., Three-dimensional printing of polyaniline/reduced graphene oxide composite for high-performance planar supercapacitor, ACS Appl. Mater. Interfaces 10 (2018) 10437–10444.
[216] C.A. Pandey, S. Ravuri, R. Ramachandran, R. Santhosh, S. Ghosh, S. Sitaraman, et al., Synthesis of NiS–graphene nanocomposites and its electrochemical performance for supercapacitors, Int. J. Nanosci. 17 (2018) 1760021.
[217] H. Mao, A. Rasheed, Facile synthesis of porous Mn2TiO4/TiO2 composites for high performance supercapacitors, Mater. Lett. 215 (2018) 114–117.
[218] H. Bai, C. Li, G. Shi, Functional composite materials based on chemically converted graphene, Adv. Mater. 23 (2011) 1089–1115.
[219] Y. Xu, G. Shi, Assembly of chemically modified graphene: methods and applications, J. Mater. Chem. 21 (2011) 3311–3323.
[220] C. Zhong, Y. Deng, W. Hu, J. Qiao, L. Zhang, J. Zhang, A review of electrolyte materials and compositions for electrochemical supercapacitors, Chem. Soc. Rev. 44 (2015) 7484–7539.
[221] S.L. Guillot, M.L. Usrey, A.P. Hueso, R.J. Hamers Characterization of the intrinsic thermal and high-voltage stability of organosilicon-containing electrolytes, in:

Meeting Abstracts: The Electrochemical Society, 2018,p. 573.
[222] A. Lewandowski, A. Olejniczak, M. Galinski, I. Stepniak, Performance of carbon–carbon supercapacitors based on organic, aqueous and ionic liquid electrolytes, J. Power Sources 195 (2010) 5814–5819.
[223] Types of Electrolytes, SCRIBD.
[224] L. Demarconnay, E. Raymundo-Pinero, F. Béguin, Adjustment of electrodes potential window in an asymmetric carbon/MnO2 supercapacitor, J. Power Sources 196 (2011) 580–586.
[225] H. Li, T. Lv, N. Li, Y. Yao, K. Liu, T. Chen, Ultraflexible and tailorable all-solid-state supercapacitors using polyacrylamide-based hydrogel electrolyte with high ionic conductivity, Nanoscale 9 (2017) 18474–18481.
[226] Q. Qu, P. Zhang, B. Wang, Y. Chen, S. Tian, Y. Wu, et al., Electrochemical performance of MnO2 nanorods in neutral aqueous electrolytes as a cathode for asymmetric supercapacitors, J. Phys. Chem. C 113 (2009) 14020–14027.
[227] Q.T. Qu, Y. Shi, S. Tian, Y.H. Chen, Y.P. Wu, R. Holze, A new cheap asymmetric aqueous supercapacitor: activated carbon//NaMnO2, J. Power Sources 194 (2009) 1222–1225.
[228] D. Wang, L. Yu, B. He, L. Wang, A high-performance carbon-carbon (C/C) Quasi-Solid-State Supercapacitor with conducting gel electrolyte, Int. J. Electrochem. Sci. 13 (2018) 2530–2543.
[229] Q. Pan, N. Tong, N. He, Y. Liu, E. Shim, B. Pourdeyhimi, et al., Electrospun mat of poly (vinyl alcohol)/graphene oxide for superior electrolyte performance, ACS Appl. Mater. Interfaces 10 (2018) 7927–7934.
[230] P. Azais, J. Lejosne, M. Picot, Electrochemical supercapacitor device made from an electrolyte comprising, as a conductive salt, at least one salt made from an alkali element other than lithium, Google Patents, 2017.
[231] L. Xia, L. Yu, D. Hu, G.Z. Chen, Electrolytes for electrochemical energy storage, Mater. Chem. Front. 1 (2017) 584–618.
[232] M. Haque, Q. Li, A.D. Smith, V. Kuzmenko, E. Köhler, P. Lundgren, et al., Thermal influence on the electrochemical behavior of a supercapacitor containing an ionic liquid electrolyte, Electrochim. Acta (2018).
[233] R. Zarrougui, R. Hachicha, R. Rjab, O. Ghodbane, 1-Allyl-3-methylimidazolium-based ionic liquids employed as suitable electrolytes for high energy density supercapacitors based on graphene nanosheets electrodes, J. Mol. Liq. 249 (2018) 795–804.
[234] N.C. Osti, A. Gallegos, B. Dyatkin, J. Wu, Y. Gogotsi, E. Mamontov, Mixed ionic liquid improves electrolyte dynamics in supercapacitors, J. Phys. Chem. C (2018).
[235] C. Edwards, J. Steele, Using earthworm systems, Biocycle (1997).
[236] M. Petre, G. Zarnea, P. Adrian, E. Gheorghiu, Biodegradation and bioconversion of cellulose wastes using bacterial and fungal cells immobilized in radiopolymerized hydrogels, Resour. Conserv. Recycl. 27 (1999) 309–332.
[237] J. Roselló, L. Soriano, M.P. Santamarina, J.L. Akasaki, J. Monzó, J. Payá, Rice straw ash: a potential pozzolanic supplementary material for cementing systems, Ind. Crops Prod. 103 (2017) 39–50.
[238] P. Azadi, R. Farnood, Review of heterogeneous catalysts for sub-and supercritical water gasification of biomass and wastes, Int. J. Hydrog. Energy 36 (2011) 9529–9541.
[239] M. Ahmad, A.U. Rajapaksha, J.E. Lim, M. Zhang, N. Bolan, D. Mohan, et al., Biochar as a sorbent for contaminant management in soil and water: a review, Chemosphere 99 (2014) 19–33.
[240] Z. Al-Hamamre, M. Saidan, M. Hararah, K. Rawajfeh, H.E. Alkhasawneh, M. Al-Shannag, Wastes and biomass materials as sustainable-renewable energy resources for Jordan, Renew. Sustain. Energy Rev. 67 (2017) 295–314.
[241] F. Mushtaq, R. Mat, F.N. Ani, A review on microwave assisted pyrolysis of coal and biomass for fuel production, Renew. Sustain. Energy Rev. 39 (2014) 555–574.
[242] Y. Li, S.Y. Park, J. Zhu, Solid-state anaerobic digestion for methane production from organic waste, Renew. Sustain. Energy Rev. 15 (2011) 821–826.
[243] Tan X-f, Liu S-b, Liu Y-g, Gu Y-l, Zeng G-m, X.-J. Hu, et al., Biochar as potential sustainable precursors for activated carbon production: multiple applications in environmental protection and energy storage, Bioresour. Technol. 227 (2017) 359–372.
[244] K. Srirangan, L. Akawi, M. Moo-Young, C.P. Chou, Towards sustainable production of clean energy carriers from biomass resources, Appl. Energy 100 (2012) 172–186.
[245] G. Yang, J. Wang, Pretreatment of grass waste using combined ionizing radiation-acid treatment for enhancing fermentative hydrogen production, Bioresour. Technol. 255 (2018) 7–15.
[246] A. Jain, R. Balasubramanian, M. Srinivasan, Hydrothermal conversion of biomass waste to activated carbon with high porosity: a review, Chem. Eng. J. 283 (2016) 789–805.
[247] D. Liu, S. Yu, Y. Shen, H. Chen, Z. Shen, S. Zhao, et al., Polyaniline coated boron doped biomass derived porous carbon composites for supercapacitor electrode materials, Ind. Eng. Chem. Res. 54 (2015) 12570–12579.
[248] G. Ma, H. Wang, K. Sun, H. Peng, Y. Wu, Z. Lei, A multi-level structure bio-carbon composite with polyaniline for high performance supercapacitors, RSC Adv. 5 (2015) 12230–12236.
[249] Y. Li, N. Yu, P. Yan, Y. Li, X. Zhou, S. Chen, et al., Fabrication of manganese dioxide nanoplates anchoring on biomass-derived cross-linked carbon nanosheets for high-performance asymmetric supercapacitors, J. Power Sources 300 (2015) 309–317.
[250] Y. Gong, D. Li, C. Luo, Q. Fu, C. Pan, Highly porous graphitic biomass carbon as advanced electrode materials for supercapacitors, Green Chem. 19 (2017) 4132–4140.
[251] S. Mohammadi, N. Mirghaffari, A preliminary study of the preparation of porous carbon from oil sludge for water treatment by simple pyrolysis or KOH activation, New Carbon Mater. 30 (2015) 310–318.
[252] S.I. Tsyganova, Thermal treatment of sawdust and coal-tar pitch mixture to produce porous carbon materials by chemical activation, Wood Sci. Technol. 47 (2013) 77–82.
[253] Y. Liu, P. Li, Y. Wang, J. Liu, Y. Wang, J. Zhang, et al., A green and template recyclable approach to prepare Fe3O4/porous carbon from petroleum asphalt for lithium-ion batteries, J. Alloy. Compd. 695 (2017) 2612–2618.
[254] J.-H. Lin, T.-H. Ko, Y.-H. Lin, C.-K. Pan, Various treated conditions to prepare porous activated carbon fiber for application in supercapacitor electrodes, Energy Fuels 23 (2009) 4668–4677.
[255] R.J. White, V. Budarin, R. Luque, J.H. Clark, D.J. Macquarrie, Tuneable porous carbonaceous materials from renewable resources, Chem. Soc. Rev. 38 (2009) 3401–3418.
[256] T.E. Rufford, D. Hulicova-Jurcakova, Z. Zhu, G.Q. Lu, Nanoporous carbon electrode from waste coffee beans for high performance supercapacitors, Electrochem. Commun. 10 (2008) 1594–1597.
[257] B.-H. Cheng, R.J. Zeng, H. Jiang, Recent developments of post-modification of biochar for electrochemical energy storage, Bioresour. Technol. (2017).
[258] J. Deng, M. Li, Y. Wang, Biomass-derived carbon: synthesis and applications in energy storage and conversion, Green Chem. 18 (2016) 4824–4854.
[259] S. Lei, L. Chen, W. Zhou, P. Deng, Y. Liu, L. Fei, et al., Tetra-heteroatom self-doped carbon nanosheets derived from silkworm excrement for high-performance supercapacitors, J. Power Sources 379 (2018) 74–83.
[260] P.-Z. Guo, Q.-Q. Ji, L.-L. Zhang, S.-Y. Zhao, X.-S. Zhao, Preparation and characterization of peanut shell-based microporous carbons as electrode materials for supercapacitors, Acta Phys.-Chim. Sin. 27 (2011) 2836–2840.
[261] D. Mitlin, Z. Li Carbonized chicken eggshell membranes with 3D architectures as flexible high-performance electrode materials for supercapacitors, in: Meeting Abstracts: The Electrochemical Society, 2013, p. 555.
[262] R. Wang, P. Wang, X. Yan, J. Lang, C. Peng, Q. Xue, Promising porous carbon derived from celtuce leaves with outstanding supercapacitance and CO_2 capture performance, ACS Appl. Mater. Interfaces 4 (2012) 5800–5806.
[263] R. Farma, M. Deraman, A. Awitdrus, I. Talib, E. Taer, N. Basri, et al., Preparation of highly porous binderless activated carbon electrodes from fibres of oil palm empty fruit bunches for application in supercapacitors, Bioresour. Technol. 132 (2013) 254–261.
[264] C. Huang, A.M. Puziy, T. Sun, O.I. Poddubnaya, F. Suárez-García, J.M. Tascón, et al., Capacitive behaviours of phosphorus-rich carbons derived from lignocelluloses, Electrochim. Acta 137 (2014) 219–227.
[265] J. Li, Q. Wu, Water bamboo-derived porous carbons as electrode materials for supercapacitors, New J. Chem. 39 (2015) 3859–3864.
[266] W. Feng, P. He, S. Ding, G. Zhang, M. He, F. Dong, et al., Oxygen-doped activated carbons derived from three kinds of biomass: preparation, characterization and performance as electrode materials for supercapacitors, RSC Adv. 6 (2016) 5949–5956.
[267] X. Li, W. Xing, S. Zhuo, J. Zhou, F. Li, S.-Z. Qiao, et al., Preparation of capacitor's electrode from sunflower seed shell, Bioresour. Technol. 102 (2011) 1118–1123.
[268] S. Teng, G. Siegel, W. Wang, A. Tiwari, Carbonized wood for supercapacitor electrodes, ECS Solid State Lett. 3 (2014) M25–M28.
[269] J. Jiang, L. Zhang, X. Wang, N. Holm, K. Rajagopalan, F. Chen, et al., Highly ordered macroporous woody biochar with ultra-high carbon content as supercapacitor electrodes, Electrochim. Acta 113 (2013) 481–489.
[270] Y. Wang, R. Yang, M. Li, Z. Zhao, Hydrothermal preparation of highly porous carbon spheres from hemp (Cannabis sativa L.) stem hemicellulose for use in energy-related applications, Ind. Crops Prod. 65 (2015) 216–226.
[271] T.E. Rufford, D. Hulicova-Jurcakova, K. Khosla, Z. Zhu, G.Q. Lu, Microstructure and electrochemical double-layer capacitance of carbon electrodes prepared by zinc chloride activation of sugar cane bagasse, J. Power Sources 195 (2010) 912–918.
[272] D. Momodu, A. Bello, K. Oyedotun, F. Ochai-Ejeh, J. Dangbegnon, M. Madito, et al., Enhanced electrochemical response of activated carbon nanostructures from tree-bark biomass waste in polymer-gel active electrolytes, RSC Adv. 7 (2017) 37286–37295.
[273] Y. Wang, R. Yang, Y. Wei, Z. Zhao, M. Li, Preparation of novel pigskin-derived carbon sheets and their low-temperature activation-induced high capacitive performance, RSC Adv. 4 (2014) 45318–45324.
[274] C. Zhan, X. Yu, Q. Liang, W. Liu, Y. Wang, R. Lv, et al., Flour food waste derived activated carbon for high-performance supercapacitors, RSC Adv. 6 (2016) 89391–89396.
[275] X. Chen, K. Wu, B. Gao, Q. Xiao, J. Kong, Q. Xiong, et al., Three-dimensional activated carbon recycled from rotten potatoes for high-performance supercapacitors, Waste Biomass-. Valoriz. 7 (2016) 551–557.
[276] Z. Qiu, Y. Wang, X. Bi, T. Zhou, J. Zhou, J. Zhao, et al., Biochar-based carbons with hierarchical micro-meso-macro porosity for high rate and long cycle life supercapacitors, J. Power Sources 376 (2018) 82–90.
[277] A. Elmouwahidi, J. Castelo-Quibén, J.F. Vivo-Vilches, A.F. Pérez-Cadenas, F.J. Maldonado-Hódar, F. Carrasco-Marín, Activated carbons from agricultural waste solvothermally doped with sulphur as electrodes for supercapacitors, Chem. Eng. J. 334 (2018) 1835–1841.
[278] T. Cai, H. Wang, C. Jin, Q. Sun, Y. Nie, Fabrication of nitrogen-doped porous electrically conductive carbon aerogel from waste cabbage for supercapacitors and oil/water separation, J. Mater. Sci.: Mater. Electron. 29 (2018) 4334–4344.
[279] F. Sun, L. Wang, Y. Peng, J. Gao, X. Pi, Z. Qu, et al., Converting biomass waste into microporous carbon with simultaneously high surface area and carbon purity as advanced electrochemical energy storage materials, Appl. Surf. Sci. 436 (2018) 486–494.
[280] X.-L. Su, J.-R. Chen, G.-P. Zheng, J.-H. Yang, X.-X. Guan, P. Liu, et al., Three-

dimensional porous activated carbon derived from loofah sponge biomass for supercapacitor applications, Appl. Surf. Sci. 436 (2018) 327–336.
[281] Y.-Q. Zhang, G.-F. Shi, B. Chen, G.-Y. Wang, T.-C. Guo, Biomass-based carbon nanofibers prepared by electrospinning for supercapacitor, J. Nanosci. Nanotechnol. 18 (2018) 5731–5737.
[282] L. Sun, C. Tian, M. Li, X. Meng, L. Wang, R. Wang, et al., From coconut shell to porous graphene-like nanosheets for high-power supercapacitors, J. Mater. Chem. A. 1 (2013) 6462–6470.
[283] S.K. Tiwari, A. Huczko, R. Oraon, A. De Adhikari, G. Nayak, Facile electrochemical synthesis of few layered graphene from discharged battery electrode and its application for energy storage, Arab. J. Chem. 10 (2017) 556–565.
[284] X. Zhang, K. Zhang, H. Li, Q. Cao, Jin Le, P. Li, Porous graphitic carbon microtubes derived from willow catkins as a substrate of MnO2 for supercapacitors, J. Power Sources 344 (2017) 176–184.
[285] B. Senthilkumar, Z. Khan, S. Park, K. Kim, H. Ko, Y. Kim, Highly porous graphitic carbon and Ni 2 P 2 O 7 for a high performance aqueous hybrid supercapacitor, J. Mater. Chem. A 3 (2015) 21553–21561.
[286] Z. Sun, M. Zheng, H. Hu, H. Dong, Y. Liang, Y. Xiao, et al., From biomass wastes to vertically aligned graphene nanosheet arrays: a catalyst-free synthetic strategy towards high-quality graphene for electrochemical energy storage, Chem. Eng. J. 336 (2018) 550–561.
[287] N.H. Basri, M. Deraman, S. Kanwal, I. Talib, J. Manjunatha, A. Aziz, et al., Supercapacitors using binderless composite monolith electrodes from carbon nanotubes and pre-carbonized biomass residues, Biomass. Bioenergy 59 (2013) 370–379.
[288] W.-J. Liu, K. Tian, Y.-R. He, H. Jiang, H.-Q. Yu, High-yield harvest of nanofibers/mesoporous carbon composite by pyrolysis of waste biomass and its application for high durability electrochemical energy storage, Environ. Sci. Technol. 48 (2014) 13951–13959.
[289] K. Sun, H. Wang, H. Peng, Y. Wu, G. Ma, Z. Lei, Manganese oxide nanorods supported on orange peel-based carbon nanosheets for high performance supercapacitors, Int. J. Electrochem Sci. 10 (2015) 2000–2013.
[290] A.K. Thakur, R.B. Choudhary, M. Majumder, G. Gupta, In-situ integration of waste coconut shell derived activated carbon/polypyrrole/rare earth metal oxide (Eu2O3): a novel step towards ultrahigh volumetric capacitance, Electrochim. Acta 251 (2017) 532–545.
[291] S. Zhang, J. Liu, P. Huang, H. Wang, C. Cao, W. Song, Carbonaceous aerogel and CoNiAl-LDH@ CA nanocomposites derived from biomass for high performance pseudo-supercapacitor, Sci. Bull. 62 (2017) 841–845.
[292] P. Sennu, V. Aravindan, Y.-S. Lee, High energy asymmetric supercapacitor with 1D@ 2D structured NiCo2O4@ Co3O4 and jackfruit derived high surface area porous carbon, J. Power Sources 306 (2016) 248–257.
[293] J. Yoder, S. Galinato, D. Granatstein, M. Garcia-Perez, Economic tradeoff between biochar and bio-oil production via pyrolysis, Biomass. Bioenergy 35 (2011) 1851–1862.
[294] S.P. Galinato, J.K. Yoder, D. Granatstein, The economic value of biochar in crop production and carbon sequestration, Energy Policy 39 (2011) 6344–6350.
[295] D.P. Hickey, R.C. Reid, R.D. Milton, S.D. Minteer, A self-powered amperometric lactate biosensor based on lactate oxidase immobilized in dimethylferrocene-modified LPEI, Biosens. Bioelectron. 77 (2016) 26–31.
[296] F.R. Fan, W. Tang, Z.L. Wang, Flexible nanogenerators for energy harvesting and self-powered electronics, Adv. Mater. 28 (2016) 4283–4305.
[297] Q. Zhou, J.G. Park, K.N. Kim, A.K. Thokchom, J. Bae, J.M. Baik, et al., Transparent-flexible-multimodal triboelectric nanogenerators for mechanical energy harvesting and self-powered sensor applications, Nano Energy (2018).
[298] H. Hu, Z. Pei, H. Fan, C. Ye, 3D interdigital Au/MnO2/Au stacked hybrid electrodes for on-chip microsupercapacitors, Small 12 (2016) 3059–3069.
[299] X. Pu, W. Hu, Z.L. Wang, Toward wearable self-charging power systems: the integration of energy-harvesting and storage devices, Small 14 (2018) 1702817.
[300] B. Swain, D.P. Kar, P.P. Nayak, S. Bhuyan, Thermal energy based Resonant inductively coupled wireless energization method for implantable biomedical sensor, Prog. Electromagn. Res. 67 (2018) 129–136.
[301] X. Lai, J.E. Halpert, D. Wang, Recent advances in micro-/nano-structured hollow spheres for energy applications: from simple to complex systems, Energy Environ. Sci. 5 (2012) 5604–5618.
[302] Z.L. Wang, Self-powered nanosensors and nanosystems, Adv. Mater. 24 (2012) 280–285.
[303] Y. Yuan, H. Zhang, J. Wang, Y. Xie, S.A. Khan, L. Jin, et al., Hybrid nanogenerators for low frequency vibration energy harvesting and self-powered wireless locating, Mater. Res. Express (2018).
[304] M.F. El-Kady, et al., M. Ihns, M. Li, J.Y. Hwang, M.F. Mousavi, L. Chaney, Engineering three-dimensional hybrid supercapacitors and microsupercapacitors for high-performance integrated energy storage, Proc. Natl. Acad. Sci. USA 112 (2015) 4233–4238.
[305] S.-I. Kim, J.-H. Kang, S.-W. Kim, J.-H. Jang, A new approach to high-performance flexible supercapacitors: mesoporous three-dimensional Ni-electrodes, Nano Energy 39 (2017) 639–646.
[306] S.-I. Kim, S.-W. Kim, K. Jung, J.-B. Kim, J.-H. Jang, Ideal nanoporous gold based supercapacitors with theoretical capacitance and high energy/power density, Nano Energy 24 (2016) 17–24.
[307] K.-N. Kang, I.-H. Kim, A. Ramadoss, S.-I. Kim, J.-C. Yoon, J.-H. Jang, Ultrathin nickel hydroxide on carbon coated 3D-porous copper structures for high performance supercapacitors, Phys. Chem. Chem. Phys. 20 (2018) 719–727.
[308] Q. Zhang, B. Zhao, J. Wang, C. Qu, H. Sun, K. Zhang, et al., High-performance hybrid supercapacitors based on self-supported 3D ultrathin porous quaternary Zn-Ni-Al-Co oxide nanosheets, Nano Energy 28 (2016) 475–485.
[309] W. Song, J. Zhu, B. Gan, S. Zhao, H. Wang, C. Li, et al., Flexible, stretchable, and transparent planar microsupercapacitors based on 3D porous laser-induced graphene, Small 14 (2018) 1702249.
[310] F. Liu, X. Chu, H. Zhang, B. Zhang, H. Su, L. Jin, et al., Synthesis of self-assembly 3D porous Ni(OH)2 with high capacitance for hybrid supercapacitors, Electrochim. Acta 269 (2018) 102–110.
[311] Z. Lv, Y. Luo, Y. Tang, J. Wei, Z. Zhu, X. Zhou, et al., Editable supercapacitors with customizable stretchability based on mechanically strengthened ultralong MnO2 nanowire composite, Adv. Mater. (2018) 30.
[312] W. Wang, Y. Zhang, L. Zhang, Y. Shi, L. Jia, Q. Zhang, et al., Flexible Mn3O4 nanosheet/reduced graphene oxide nanosheet paper-like electrodes for electrochemical energy storage and three-dimensional multilayers printing, Mater. Lett. 213 (2018) 100–103.
[313] C. Cai, P. Yuan, J. Tang, Y. Guo, X. Ma, Ultrathin paper-like boron-doped carbon nanosheet electrodes combined with boron-enriched gel polymer electrolytes for high-performance energy storage, J. Mater. Chem. A 4 (2016) 15589–15596.
[314] Y. Zhao, J. Liu, D. Zheng, B. Wang, M. Hu, J. Sha, et al., Achieving high capacitance of paper-like graphene films by adsorbing molecules from hydrolyzed polyimide, Small 14 (2018) 1702809.
[315] D. Harrison, F. Qiu, J. Fyson, Y. Xu, P. Evans, D. Southee, A coaxial single fibre supercapacitor for energy storage, Phys. Chem. Chem. Phys. 15 (2013) 12215–12219.
[316] R. Lin, Z. Zhu, X. Yu, Y. Zhong, Z. Wang, S. Tan, et al., Facile synthesis of TiO 2/Mn 3 O 4 hierarchical structures for fiber-shaped flexible asymmetric supercapacitors with ultrahigh stability and tailorable performance, J. Mater. Chem. A 5 (2017) 814–821.
[317] K. Wang, Q. Meng, Y. Zhang, Z. Wei, M. Miao, High-performance two-ply yarn supercapacitors based on carbon nanotubes and polyaniline nanowire arrays, Adv. Mater. 25 (2013) 1494–1498.
[318] D. Ren, L. Dong, J. Wang, X. Ma, C. Xu, F. Kang, Facile preparation of high--performance stretchable fiber-like electrodes and supercapacitors, ChemistrySelect 3 (2018) 4179–4184.
[319] S. Gu, Z. Lou, X. Ma, G. Shen, CuCo2O4 nanowires grown on a Ni wire for high-performance, flexible fiber supercapacitors, ChemElectroChem 2 (2015) 1042–1047.
[320] D. Wang, Y. Wang, H. Liu, W. Xu, L. Xu, Unusual carbon nanomesh constructed by interconnected carbon nanocages for ionic liquid-based supercapacitor with superior rate capability, Chem. Eng. J. 342 (2018) 474–483.
[321] D. Wang, Y. Wang, W. Xu, W. Xu, Tunable synthesis of nanocarbon architectures and their application in advanced symmetric supercapacitors, Appl. Surf. Sci. 443 (2018) 291–300.
[322] S. Haladkar, P. Alegaonkar, Preparation and performance evaluation of Carbon-Nano-Sphere for electrode double layer capacitor, Appl. Surf. Sci. (2018).
[323] D. Wang, L. Xu, Y. Wang, W. Xu, Rational synthesis of porous carbon nanocages and their potential application in high rate supercapacitors, J. Electroanal. Chem. 815 (2018) 166–174.
[324] D. Wang, G. Fang, T. Xue, J. Ma, G. Geng, A melt route for the synthesis of activated carbon derived from carton box for high performance symmetric supercapacitor applications, J. Power Sources 307 (2016) 401–409.
[325] H. Li, M. Yu, F. Wang, P. Liu, Y. Liang, J. Xiao, et al., Amorphous nickel hydroxide nanospheres with ultrahigh capacitance and energy density as electrochemical pseudocapacitor materials, Nat. Commun. 4 (2013) 1894.
[326] C. Zhao, X. Wang, S. Wang, H. Wang, Y. Yang, W. Zheng, Pseudocapacitive properties of cobalt hydroxide electrodeposited on Ni-foam-supported carbon nanomaterial, Mater. Res. Bull. 48 (2013) 3189–3195.
[327] Y. Hou, L. Chen, P. Liu, J. Kang, T. Fujita, M. Chen, Nanoporous metal based flexible asymmetric pseudocapacitors, J. Mater. Chem. A 2 (2014) 10910–10916.
[328] H. Gao, F. Xiao, C.B. Ching, H. Duan, High-performance asymmetric supercapacitor based on graphene hydrogel and nanostructured MnO2, ACS Appl. Mater. Interfaces 4 (2012) 2801–2810.
[329] Y. Chen, X. Zhang, D. Zhang, P. Yu, Y. Ma, High performance supercapacitors based on reduced graphene oxide in aqueous and ionic liquid electrolytes, Carbon 49 (2011) 573–580.
[330] F. Wang, O. Borodin, M.S. Ding, M. Gobet, J. Vatamanu, X. Fan, et al., Hybrid aqueous/non-aqueous electrolyte for safe and high-energy Li-ion batteries, Joule 2 (2018) 927–937.
[331] P. Yang, W. Mai, Flexible solid-state electrochemical supercapacitors, Nano Energy 8 (2014) 274–290.
[332] X. Wu, Q. Wang, W. Zhang, Y. Wang, W. Chen, Preparation of all-solid-state supercapacitor integrated with energy level indicating functionality, Synth. Met. 220 (2016) 494–501.
[333] A.K. Tripathi, Y.L. Verma, V.K. Singh, L. Balo, H. Gupta, S.K. Singh, et al., Quasi solid-state electrolytes based on ionic liquid (IL) and ordered mesoporous matrix MCM-41 for supercapacitor application, J. Solid State Electrochem. 21 (2017) 3365–3371.
[334] D. Xu, D. Chao, H. Wang, Y. Gong, R. Wang, B. He, et al., Flexible quasi-solid-state sodium-ion capacitors developed using 2D metal–organic-framework array as reactor, Adv. Energy Mater. 8 (2018) 1702769.
[335] F. Wang, X. Wang, Z. Chang, X. Wu, X. Liu, L. Fu, et al., A quasi-solid-state sodium-ion capacitor with high energy density, Adv. Mater. 27 (2015) 6962–6968.
[336] I. Hadjipaschalis, A. Poullikkas, V. Efthimiou, Overview of current and future energy storage technologies for electric power applications, Renew. Sustain. Energy Rev. 13 (2009) 1513–1522.
[337] T.C. Mendes, F. Zhou, A.J. Barlow, M. Forsyth, P.C. Howlett, D.R. MacFarlane, An ionic liquid based sodium metal-hybrid supercapacitor-battery, Sustain. Energy Fuels (2018).

[338] A. Pandolfo, A. Hollenkamp, Carbon properties and their role in supercapacitors, J. Power Sources 157 (2006) 11–27.
[339] L. Ren, G. Zhang, J. Lei, Y. Wang, D. Hu, Novel layered polyaniline-poly (hydroquinone)/graphene film as supercapacitor electrode with enhanced rate performance and cycling stability, J. Colloid Interface Sci. 512 (2018) 300–307.
[340] L. Hou, Y. Shi, C. Wu, Y. Zhang, Y. Ma, X. Sun, et al., Monodisperse metallic NiCoSe2 hollow sub-microspheres: formation process, intrinsic charge-storage mechanism, and appealing pseudocapacitance as highly conductive electrode for electrochemical supercapacitors, Adv. Funct. Mater. (2018).
[341] Q. Zhao, J. Chen, F. Luo, L. Shen, Y. Wang, K. Wu, et al., Vertically oriented polyaniline-graphene nanocomposite based on functionalized graphene for supercapacitor electrode, J. Appl. Polym. Sci. (2017) 134.
[342] A.M. Navarro-Suárez, K.L. Van Aken, T. Mathis, T. Makaryan, J. Yan, J. Carretero-González, et al., Development of asymmetric supercapacitors with titanium carbide-reduced graphene oxide couples as electrodes, Electrochim. Acta 259 (2018) 752–761.
[343] O. Parlak, Y.K. Mishra, A. Grigoriev, M. Mecklenburg, W. Luo, S. Keene, et al., Hierarchical Aerographite nano-microtubular tetrapodal networks based electrodes as lightweight supercapacitor, Nano Energy 34 (2017) 570–577.
[344] M. Zhang, X. Yu, H. Ma, W. Du, L. Qu, C. Li, et al., Robust graphene composite films for multifunctional electrochemical capacitors with an ultrawide range of areal mass loading toward high-rate frequency response and ultrahigh specific capacitance, Energy Environ. Sci. (2018).
[345] H.-J. Lee, I.-J. Park, S.-R. Choi, J.-G. Kim, Effect of chloride on anodic dissolution of aluminum in 4 M NaOH solution for aluminum-air battery, J. Electrochem. Soc. 164 (2017) A549–A554.
[346] J. Yu, M. Wang, P. Xu, S.-H. Cho, J. Suhr, K. Gong, et al., Ultrahigh-rate wire-shaped supercapacitor based on graphene fiber, Carbon 119 (2017) 332–338.
[347] A. Oz, D. Gelman, E. Goren, N. Shomrat, S. Baltianski, Y. Tsur, A novel approach for supercapacitors degradation characterization, J. Power Sources 355 (2017) 74–82.
[348] F. Rafik, H. Gualous, R. Gallay, A. Crausaz, A. Berthon, Frequency, thermal and voltage supercapacitor characterization and modeling, J. Power Sources 165 (2007) 928–934.
[349] V.H. Souza, M.M. Oliveira, A.J. Zarbin, Bottom-up synthesis of graphene/polyaniline nanocomposites for flexible and transparent energy storage devices, J. Power Sources 348 (2017) 87–93.
[350] A. Qian, K. Zhuo, B.N. Choi, S.J. Lee, J.W. Bae, P.J. Yoo, et al., Capacitance enhancement in supercapacitors by incorporating ultra-long hydrated vanadium-oxide nanobelts into graphene, J. Alloy. Compd. 688 (2016) 814–821.
[351] H. Wang, Z. Guo, S. Yao, Z. Li, W. Zhang, Design and synthesis of ternary graphene/polyaniline/Co3O4 hierarchical nanocomposites for supercapacitors, Int. J. Electrochem Sci. 12 (2017) 3721–3731.
[352] P. Yu, X. Zhao, Y. Li, Q. Zhang, Controllable growth of polyaniline nanowire arrays on hierarchical macro/mesoporous graphene foams for high-performance flexible supercapacitors, Appl. Surf. Sci. 393 (2017) 37–45.
[353] C. Xiong, T. Li, Y. Zhu, T. Zhao, A. Dang, H. Li, et al., Two-step approach of fabrication of interconnected nanoporous 3D reduced graphene oxide-carbon nanotube-polyaniline hybrid as a binder-free supercapacitor electrode, J. Alloy. Compd. 695 (2017) 1248–1259.
[354] L. Tang, Z. Yang, F. Duan, M. Chen, Fabrication of graphene sheets/polyaniline nanofibers composite for enhanced supercapacitor properties, Colloids Surf. A: Physicochem. Eng. Asp. 520 (2017) 184–192.
[355] M.F. Mousavi, M. Hashemi, M.S. Rahmanifar, A. Noori, Synergistic effect between redox additive electrolyte and PANI-rGO nanocomposite electrode for high energy and high power supercapacitor, Electrochim. Acta 228 (2017) 290–298.
[356] T. Zhao, X. Ji, P. Bi, W. Jin, C. Xiong, A. Dang, et al., In situ synthesis of interlinked three-dimensional graphene foam/polyaniline nanorod supercapacitor, Electrochim. Acta 230 (2017) 342–349.
[357] M. Liu, M. Shi, W. Lu, D. Zhu, L. Li, L. Gan, Core–shell reduced graphene oxide/MnOx@ carbon hollow nanospheres for high performance supercapacitor electrodes, Chem. Eng. J. 313 (2017) 518–526.
[358] J. Zhu, M. Chen, H. Qu, X. Zhang, H. Wei, Z. Luo, et al., Interfacial polymerized polyaniline/graphite oxide nanocomposites toward electrochemical energy storage, Polymer 53 (2012) 5953–5964.
[359] H. Yu, G. Xin, X. Ge, C. Bulin, R. Li, R. Xing, et al., Porous graphene-polyaniline nanoarrays composite with enhanced interface bonding and electrochemical performance, Compos. Sci. Technol. 154 (2018) 76–84.
[360] D. Liu, P. Du, W. Wei, H. Wang, Q. Wang, P. Liu, Skeleton/skin structured (RGO/CNTs)@ PANI composite fiber electrodes with excellent mechanical and electrochemical performance for all-solid-state symmetric supercapacitors, J. Colloid Interface Sci. 513 (2018) 295–303.
[361] L. Xu, R. Shi, H. Li, C. Han, M. Wu, C.-P. Wong, et al., Pseudocapacitive anthraquinone modified with reduced graphene oxide for flexible symmetric all-solid-state supercapacitors, Carbon 127 (2018) 459–468.
[362] J. Yu, F. Xie, Z. Wu, T. Huang, J. Wu, D. Yan, et al., Flexible metallic fabric supercapacitor based on graphene/polyaniline composites, Electrochim. Acta 259 (2018) 968–974.
[363] X. Yu, B. Lu, Z. Xu, Super long-life supercapacitors based on the construction of nanohoneycomb-like strongly coupled CoMoO4–3D graphene hybrid electrodes, Adv. Mater. 26 (2014) 1044–1051.
[364] Q. Wang, L. Jiao, H. Du, Y. Wang, H. Yuan, Fe3O4 nanoparticles grown on graphene as advanced electrode materials for supercapacitors, J. Power Sources 245 (2014) 101–106.
[365] Z. Ma, X. Huang, S. Dou, J. Wu, S. Wang, One-pot synthesis of Fe2O3 nanoparticles on nitrogen-doped graphene as advanced supercapacitor electrode materials, J. Phys. Chem. C 118 (2014) 17231–17239.
[366] T. Sun, Z. Li, X. Liu, L. Ma, J. Wang, S. Yang, Facile construction of 3D graphene/MoS2 composites as advanced electrode materials for supercapacitors, J. Power Sources 331 (2016) 180–188.
[367] B. Wang, X. Liu, Q. Liu, J. Chen, H. Jiang, Y. Wang, et al., Three-dimensional non-woven poly(vinyl alcohol-co-ethylene) nanofiber based polyaniline flexible electrode for high performance supercapacitor, J. Alloy. Compd. 715 (2017) 137–145.
[368] F.S. Omar, A. Numan, N. Duraisamy, M.M. Ramly, K. Ramesh, S. Ramesh, Binary composite of polyaniline/copper cobaltite for high performance asymmetric supercapacitor application, Electrochim. Acta 227 (2017) 41–48.
[369] L. Zhang, W. Wang, J. Cheng, Y. Shi, Q. Zhang, P. Dou, et al., Skeleton networks of graphene wrapped double-layered polypyrrole/polyaniline nanotubes for supercapacitor applications, J. Mater. Sci. 53 (2018) 787–798.
[370] M. Javed, S.M. Abbas, M. Siddiq, D. Han, L. Niu, Mesoporous silica wrapped with graphene oxide-conducting PANI nanowires as a novel hybrid electrode for supercapacitor, J. Phys. Chem. Solids 113 (2018) 220–228.
[371] F. Ran, Y. Tan, W. Dong, Z. Liu, L. Kong, L. Kang, In situ polymerization and reduction to fabricate gold nanoparticle-incorporated polyaniline as supercapacitor electrode materials, Polym. Adv. Technol. (2018).
[372] Q. Gong, Y. Li, H. Huang, J. Zhang, T. Gao, G. Zhou, Shape-controlled synthesis of Ni-CeO 2@ PANI nanocomposites and their synergetic effects on supercapacitors, Chem. Eng. J. (2018).
[373] X. Ren, H. Fan, J. Ma, C. Wang, M. Zhang, N. Zhao, Hierarchical Co3O4/PANI hollow nanocages: synthesis and application for electrode materials of supercapacitors, Appl. Surf. Sci. 441 (2018) 194–203.
[374] L. Shao, Q. Wang, Z. Ma, Z. Ji, X. Wang, D. Song, et al., A high-capacitance flexible solid-state supercapacitor based on polyaniline and Metal-Organic Framework (UiO-66) composites, J. Power Sources 379 (2018) 350–361.
[375] S. Zhong, C. Zhan, D. Cao, Zeolitic imidazolate framework-derived nitrogen-doped porous carbons as high performance supercapacitor electrode materials, Carbon 85 (2015) 51–59.
[376] L. Wan, E. Shamsaei, C.D. Easton, D. Yu, Y. Liang, X. Chen, et al., ZIF-8 derived nitrogen-doped porous carbon/carbon nanotube composite for high-performance supercapacitor, Carbon 121 (2017) 330–336.
[377] Y. Wang, B. Chen, Y. Zhang, L. Fu, Y. Zhu, L. Zhang, et al., ZIF-8@MWCNT-derived carbon composite as electrode of high performance for supercapacitor, Electrochim. Acta 213 (2016) 260–269.
[378] M. Jiang, X. Cao, D. Zhu, Y. Duan, J. Zhang, Hierarchically porous N-doped carbon derived from ZIF-8 nanocomposites for electrochemical applications, Electrochim. Acta 196 (2016) 699–707.
[379] M.J. Mostazo-López, R. Ruiz-Rosas, A. Castro-Muñiz, H. Nishihara, T. Kyotani, E. Morallón, et al., Ultraporous nitrogen-doped zeolite-templated carbon for high power density aqueous-based supercapacitors, Carbon 129 (2018) 510–519.
[380] B. Joshi, S. Park, E. Samuel, H.S. Jo, S. An, M.-W. Kim, et al., Zeolitic imidazolate framework-7 textile-derived nanocomposite fibers as freestanding supercapacitor electrodes, J. Electroanal. Chem. (2018).
[381] B. Han, G. Cheng, E. Zhang, L. Zhang, X. Wang, Three dimensional hierarchically porous ZIF-8 derived carbon/LDH core-shell composite for high performance supercapacitors, Electrochim. Acta 263 (2018) 391–399.
[382] S. Liu, K.H. Kim, J.M. Yun, A. Kundu, K.V. Sankar, U.M. Patil, et al., 3D yolk–shell NiGa 2 S 4 microspheres confined with nanosheets for high performance supercapacitors, J. Mater. Chem. A 5 (2017) 6292–6298.
[383] S. Liu, K.V. Sankar, A. Kundu, M. Ma, J.-Y. Kwon, S.C. Jun, Honeycomb-like interconnected network of nickel phosphide heteronanoparticles with superior electrochemical performance for supercapacitors, ACS Appl. Mater. Interfaces 9 (2017) 21829–21838.
[384] J. Lin, H. Jia, H. Liang, S. Chen, Y. Cai, J. Qi, et al., Hierarchical CuCo2S4@ NiMn-layered double hydroxide core-shell hybrid arrays as electrodes for supercapacitors, Chem. Eng. J. 336 (2018) 562–569.
[385] Y. Yuan, W. Wang, J. Yang, H. Tang, Z. Ye, Y. Zeng, et al., Three-Dimensional NiCo2O4@ MnMoO4 core–shell nanoarrays for high-performance asymmetric supercapacitors, Langmuir : ACS J. Surf. Colloids 33 (2017) 10446–10454.
[386] L. Wang, X. Jiao, P. Liu, Y. Ouyang, X. Xia, W. Lei, et al., Self-template synthesis of yolk-shelled NiCo2O4 spheres for enhanced hybrid supercapacitors, Appl. Surf. Sci. 427 (2018) 174–181.
[387] C. Wei, K. Liu, J. Tao, X. Kang, H. Hou, C. Cheng, et al., Self-template synthesis of hybrid porous Co3O4–CeO2 hollow polyhedrons for high-performance Supercapacitors, Chemistry– Asian J. 13 (2018) 111–117.
[388] J. Lin, Y. Liu, Y. Wang, H. Jia, S. Chen, J. Qi, et al., Rational construction of nickel cobalt sulfide nanoflakes on CoO nanosheets with the help of carbon layer as the battery-like electrode for supercapacitors, J. Power Sources 362 (2017) 64–72.
[389] L. Li, K. San Hui, K.N. Hui, Y.-R. Cho, Ultrathin petal-like NiAl layered double oxide/sulfide composites as an advanced electrode for high-performance asymmetric supercapacitors, J. Mater. Chem. A 5 (2017) 19687–19696.
[390] J. Ge, J. Wu, L. Fan, Q. Bao, J. Dong, J. Jia, et al., Hydrothermal synthesis of CoMoO4/Co1-xS hybrid on Ni foam for high-performance supercapacitors, J. Energy Chem. 27 (2018) 478–485.
[391] S. Gao, Y. Sui, F. Wei, J. Qi, Q. Meng, Y. He, Facile synthesis of nickel metal–organic framework derived hexagonal flaky NiO for supercapacitors, J. Mater. Sci.: Mater. Electron. 29 (2018) 2477–2483.
[392] W. Wang, N. Zhang, Z. Shi, Z. Ye, Q. Gao, M. Zhi, et al., Preparation of Ni-Al layered double hydroxide hollow microspheres for supercapacitor electrode, Chem. Eng. J. 338 (2018) 55–61.
[393] M. Xie, Z. Xu, S. Duan, Z. Tian, Y. Zhang, K. Xiang, et al., Facile growth of homogeneous Ni (OH) 2 coating on carbon nanosheets for high-performance asymmetric supercapacitor applications, Nano Res. 11 (2018) 216–224.

[394] Y. Lin, J. Wang, H. Yang, L. Wang, M. Cao, Increased capacitance of porous Co 0.5 Ni 0.5 Fe 2 O 4 for supercapacitor application, Mater. Sci. Eng.: B 228 (2018) 103–108.
[395] K. Wang, L. Li, Y. Liu, C. Zhang, T. Liu, Constructing a "Pizza-Like" MoS2/Polypyrrole/Polyaniline Ternary Architecture with High Energy Density and Superior Cycling Stability for Supercapacitors, Adv. Mater. Interfaces (2016) 3.
[396] M. Acerce, D. Voiry, M. Chhowalla, Metallic 1T phase MoS 2 nanosheets as supercapacitor electrode materials, Nat. Nanotechnol. 10 (2015) 313.
[397] S.A. Ansari, H. Fouad, S.G. Ansari, M.P. Sk, M.H. Cho, Mechanically exfoliated MoS2 sheet coupled with conductive polyaniline as a superior supercapacitor electrode material, J. Colloid Interface Sci. 504 (2017) 276–282.
[398] S. Zhang, R. Hu, P. Dai, X. Yu, Z. Ding, M. Wu, et al., Synthesis of rambutan-like MoS2/mesoporous carbon spheres nanocomposites with excellent performance for supercapacitors, Appl. Surf. Sci. 396 (2017) 994–999.
[399] R.B. Pujari, A.C. Lokhande, A.R. Shelke, J.H. Kim, C.D. Lokhande, Chemically deposited nano grain composed MoS2 thin films for supercapacitor application, J. Colloid Interface Sci. 496 (2017) 1–7.
[400] A. Lamberti, Flexible supercapacitor electrodes based on MoS2-intercalated rGO membranes on Ti mesh, Mater. Sci. Semicond. Process. 73 (2018) 106–110.
[401] C. Zhao, Y. Zhou, Z. Ge, C. Zhao, X. Qian, Facile construction of MoS2/RCF electrode for high-performance supercapacitor, Carbon 127 (2018) 699–706.
[402] S. Wen, Y. Liu, F. Zhu, R. Shao, W. Xu, Hierarchical MoS2 nanowires/NiCo2O4 nanosheets supported on Ni foam for high-performance asymmetric supercapacitors, Appl. Surf. Sci. 428 (2018) 616–622.
[403] S. Qin, T. Yao, X. Guo, Q. Chen, D. Liu, Q. Liu, et al., MoS2/Ni3S4 composite nanosheets on interconnected carbon shells as an excellent supercapacitor electrode architecture for long term cycling at high current densities, Appl. Surf. Sci. 440 (2018) 741–747.
[404] Z.S. Yan, J.Y. Long, Q. Zhou, Y. Gong, J. Lin, One-step synthesis of MnS/MoS2/C through calcination and sulfurization of a bi-metal-organic framework for high-performance supercapacitor and its photocurrent investigation, Dalton Trans. (2018).
[405] F. Huang, R. Meng, Y. Sui, F. Wei, J. Qi, Q. Meng, et al., One-step hydrothermal synthesis of a CoS2@MoS2 nanocomposite for high-performance supercapacitors, J. Alloy. Compd. 742 (2018) 844–851.
[406] D. Wang, W. Zhu, Y. Yuan, G. Du, J. Zhu, X. Zhu, et al., Kelp-like structured NiCo2S4-C-MoS2 composite electrodes for high performance supercapacitor, J. Alloy. Compd. 735 (2018) 1505–1513.
[407] J. Zang, X. Li, In situ synthesis of ultrafine β-MnO 2/polypyrrole nanorod composites for high-performance supercapacitors, J. Mater. Chem. 21 (2011) 10965–10969.
[408] G.F. Chen, Y.Z. Su, P.Y. Kuang, Z.Q. Liu, D.Y. Chen, X. Wu, et al., Polypyrrole Shell@ 3D-Ni metal core structured electrodes for high-performance supercapacitors, Chem.-A Eur. J. 21 (2015) 4614–4621.
[409] N. Wang, P. Zhao, K. Liang, M. Yao, Y. Yang, W. Hu, CVD-grown polypyrrole nanofilms on highly mesoporous structure MnO2 for high performance asymmetric supercapacitors, Chem. Eng. J. 307 (2017) 105–112.
[410] Q. Liu, B. Wang, J. Chen, F. Li, K. Liu, Y. Wang, et al., Facile synthesis of three-dimensional (3D) interconnecting polypyrrole (PPy) nanowires/nanofibrous textile composite electrode for high performance supercapacitors, Compos. Part A: Appl. Sci. Manuf. 101 (2017) 30–40.
[411] D.J. Kim, J.W. Yoon, C.S. Lee, Y.-S. Bae, J.H. Kim, Covalent organic framework-derived microporous carbon nanoparticles coated with conducting polypyrrole as an electrochemical capacitor, Appl. Surf. Sci. 439 (2018) 833–838.
[412] X. He, W. Yang, X. Mao, L. Xu, Y. Zhou, Y. Chen, et al., All-solid state symmetric supercapacitors based on compressible and flexible free-standing 3D carbon nanotubes (CNTs)/poly(3,4-ethylenedioxythiophene) (PEDOT) sponge electrodes, J. Power Sources 376 (2018) 138–146.
[413] C. Zhou, W. Yang, G. Zeng, Y. Lei, L. Gu, X. Xi, et al., Three-dimensional NiMoO4 nanosheets supported on a carbon fibers@ pre-treated Ni Foam (CF@ PNF) substrate as advanced electrodes for asymmetric supercapacitors, Chemistry– Asian J. 10 (2015) 1745–1752.
[414] G. Wu, P. Tan, D. Wang, Z. Li, L. Peng, Y. Hu, et al., High-performance supercapacitors based on electrochemical-induced vertical-aligned carbon nanotubes and polyaniline nanocomposite electrodes, Sci. Rep. 7 (2017) 43676.
[415] W. Liu, Y. Tang, Z. Sun, S. Gao, J. Ma, L. Liu, A simple approach of constructing sulfur-containing porous carbon nanotubes for high-performance supercapacitors, Carbon 115 (2017) 754–762.
[416] S.S. Raut, B.R. Sankapal, M. Hossain, A. Shahriar, S. Pradhan, R.R. Salunkhe, et al., Zinc ferrite anchored multiwalled carbon nanotubes for high-performance supercapacitor applications, Eur. J. Inorg. Chem. 2018 (2018) 137–142.
[417] A.A. Silva, R.A. Pinheiro, A.C. Rodrigues, M.R. Baldan, V.J. Trava-Airoldi, E.J. Corat, Graphene sheets produced by carbon nanotubes unzipping and their performance as supercapacitor, Appl. Surf. Sci. (2018).
[418] J. Ding, X. Li, H.-P. Zhang, Y. Tang, G. Yang, Crosslinked carbon nanofiber films with hierarchical pores as flexible electrodes for high performance supercapacitors, Mater. Des. 141 (2018) 17–25.
[419] J. Qian, X. Wang, L. Chai, L. Liang, T.-T. Li, Y. Hu, et al., Robust cage-based zinc-organic frameworks derived Dual-doped carbon materials for supercapacitor, Cryst. Growth Des. (2018).
[420] T. Gao, F. Zhou, W. Ma, H. Li, Metal-organic-framework derived carbon polyhedron and carbon nanotube hybrids as electrode for electrochemical supercapacitor and capacitive deionization, Electrochim. Acta 263 (2018) 85–93.
[421] X. Yan, X. Li, Z. Yan, S. Komarneni, Porous carbons prepared by direct carbonization of MOFs for supercapacitors, Appl. Surf. Sci. 308 (2014) 306–310.
[422] M. Yu, L. Zhang, X. He, H. Yu, J. Han, M. Wu, 3D interconnected porous carbons from MOF-5 for supercapacitors, Mater. Lett. 172 (2016) 81–84.
[423] I.A. Khan, A. Badshah, I. Khan, D. Zhao, M.A. Nadeem, Soft-template carbonization approach of MOF-5 to mesoporous carbon nanospheres as excellent electrode materials for supercapacitor, Microporous Mesoporous Mater. 253 (2017) 169–176.
[424] J. Xu, C. Yang, Y. Xue, C. Wang, J. Cao, Z. Chen, Facile synthesis of novel metal-organic nickel hydroxide nanorods for high performance supercapacitor, Electrochim. Acta 211 (2016) 595–602.
[425] L. Kang, S.-X. Sun, L.-B. Kong, J.-W. Lang, Y.-C. Luo, Investigating metal-organic framework as a new pseudo-capacitive material for supercapacitors, Chin. Chem. Lett. 25 (2014) 957–961.
[426] S. Guo, Y. Zhu, Y. Yan, Y. Min, J. Fan, Q. Xu, et al., (Metal-Organic Framework)-Polyaniline sandwich structure composites as novel hybrid electrode materials for high-performance supercapacitor, J. Power Sources 316 (2016) 176–182.
[427] C. Qu, Y. Jiao, B. Zhao, D. Chen, R. Zou, K.S. Walton, et al., Nickel-based pillared MOFs for high-performance supercapacitors: design, synthesis and stability study, Nano Energy 26 (2016) 66–73.
[428] Z.-X. Li, B.-L. Yang, Y.-F. Jiang, C.-Y. Yu, L. Zhang, Metal-directed assembly of five 4-connected MOFs: one-pot syntheses of MOF-derived M x S y@ C composites for photocatalytic degradation and supercapacitors, Cryst. Growth Des. 18 (2018) 979–992.
[429] S. Gao, Y. Sui, F. Wei, J. Qi, Q. Meng, Y. He, Facile synthesis of cuboid Ni-MOF for high-performance supercapacitors, J. Mater. Sci. 53 (2018) 6807–6818.
[430] E.A. Jafari, M. Moradi, S. Borhani, H. Bigdeli, S. Hajati, Fabrication of hybrid supercapacitor based on rod-like HKUST-1@polyaniline as cathode and reduced graphene oxide as anode, Phys. E: Low.-Dimens. Syst. Nanostruct. 99 (2018) 16–23.
[431] D.-J. Li, S. Lei, Y.-Y. Wang, S. Chen, Y. Kang, Z.-G. Gu, et al., Helical carbon tubes derived from epitaxial Cu-MOF coating on textile for enhanced supercapacitor performance, Dalton Trans. (2018).
[432] Z. Zhao, Y. Wang, M. Li, R. Yang, High performance N-doped porous activated carbon based on chicken feather for supercapacitors and CO 2capture, RSC Adv. 5 (2015) 34803–34811.
[433] S. Zhang, K. Tian, B.-H. Cheng, H. Jiang, Preparation of N-doped supercapacitor materials by integrated salt Templating and silicon hard templating by pyrolysis of biomass wastes, ACS Sustain. Chem. Eng. 5 (2017) 6682–6691.
[434] B.-H. Cheng, K. Tian, R.J. Zeng, H. Jiang, Preparation of high performance supercapacitor materials by fast pyrolysis of corn gluten meal waste, Sustain. Energy Fuels 1 (2017) 891–898.
[435] C. Gong, X. Wang, D. Ma, H. Chen, S. Zhang, Z. Liao, Microporous carbon from a biological waste-stiff silkworm for capacitive energy storage, Electrochim. Acta 220 (2016) 331–339.
[436] Y. Wen, T. Qin, Z. Wang, X. Jiang, S. Peng, J. Zhang, et al., Self-supported binder-free carbon fibers/MnO2 electrodes derived from disposable bamboo chopsticks for high-performance supercapacitors, J. Alloy. Compd. 699 (2017) 126–135.
[437] The 5th IEEE International Conference on Renewable Energy Research and Applications (ICRERA 2016), Birmingham-United Kingdom: IEEE power Electronics Society, Institute of electrical and Electronics engineers, IEEE Ind. Appl. Soc. (2016).
[438] C. Wan, Y. Jiao, J. Li, Core–shell composite of wood-derived biochar supported MnO 2 nanosheets for supercapacitor applications, RSC Adv. 6 (2016) 64811–64817.
[439] L.X. Cheng, L. Zhang, X.Y. Chen, Z.J. Zhang, Efficient conversion of waste polyvinyl chloride into nanoporous carbon incorporated with MnOx exhibiting superior electrochemical performance for supercapacitor application, Electrochim. Acta 176 (2015) 197–206.
[440] J. Qu, C. Geng, S. Lv, G. Shao, S. Ma, M. Wu, Nitrogen, oxygen and phosphorus decorated porous carbons derived from shrimp shells for supercapacitors, Electrochim. Acta 176 (2015) 982–988.
[441] J. Geng, H. Wu, A.M. Al-Enizi, A.A. Elzatahry, G. Zheng, Freestanding eggshell membrane-based electrodes for high-performance supercapacitors and oxygen evolution reaction, Nanoscale 7 (2015) 14378–14384.
[442] S. Gharehkhani, S.F.S. Shirazi, S.P. Jahromi, M. Sookhakian, S. Baradaran, H. Yarmand, et al., Spongy nitrogen-doped activated carbonaceous hybrid derived from biomass material/graphene oxide for supercapacitor electrodes, RSC Adv. 5 (2015) 40505–40513.
[443] S. Yu, D. Liu, S. Zhao, B. Bao, C. Jin, W. Huang, et al., Synthesis of wood derived nitrogen-doped porous carbon–polyaniline composites for supercapacitor electrode materials, RSC Adv. 5 (2015) 30943–30949.
[444] A. De Adhikari, R. Oraon, S. Tiwari, J.H. Lee, G. Nayak, Effect of waste cellulose fibres on the charge storage capacity of polypyrrole and graphene/polypyrrole electrodes for supercapacitor application, RSC Adv. 5 (2015) 27347–27355.
[445] M. Boota, M.P. Paranthaman, A.K. Naskar, Y. Li, K. Akato, Y. Gogotsi, Waste tire derived carbon–polymer composite paper as pseudocapacitive electrode with long cycle life, ChemSusChem 8 (2015) 3576–3581.
[446] C. Fu, P.S. Grant, Toward low-cost grid scale energy storage: supercapacitors based on up-cycled industrial mill scale waste, ACS Sustain. Chem. Eng. 3 (2015) 2831–2838.
[447] J. Tey, A. Arof, M. Yarmo, M. Careem, Activated carbon from bio-wastes of durian fruits as active material for electrodes of electric double-layer capacitors, J. New Mater. Electron. Syst. 18 (2015) 1–9.
[448] S.K. Ramasahayam, A.L. Clark, Z. Hicks, T. Viswanathan, Spent coffee grounds derived P, N co-doped C as electrocatalyst for supercapacitor applications, Electrochim. Acta 168 (2015) 414–422.
[449] W.-H. Qu, Y.-Y. Xu, A.-H. Lu, X.-Q. Zhang, W.-C. Li, Converting biowaste corncob residue into high value added porous carbon for supercapacitor electrodes,

Bioresour. Technol. 189 (2015) 285–291.
[450] J. Edberg, O. Inganäs, I. Engquist, M. Berggren, Boosting the capacity of all-organic paper supercapacitors using wood derivatives, J. Mater. Chem. A. 6 (2018) 145–152.
[451] J. Dong, G. Lu, F. Wu, C. Xu, X. Kang, Z. Cheng, Facile synthesis of a nitrogen-doped graphene flower-like MnO2 nanocomposite and its application in supercapacitors, Appl. Surf. Sci. 427 (2018) 986–993.
[452] Q. Chen, J. Chen, Y. Zhou, C. Song, Q. Tian, J. Xu, et al., Enhancing pseudocapacitive kinetics of nanostructured MnO2 through anchoring onto biomass-derived porous carbon, Appl. Surf. Sci. 440 (2018) 1027–1036.
[453] K. Fang, J. Chen, X. Zhou, C. Mei, Q. Tian, J. Xu, et al., Decorating biomass-derived porous carbon with Fe2O3 ultrathin film for high-performance supercapacitors, Electrochim. Acta 261 (2018) 198–205.
[454] H. Wan, L. Li, Y. Xu, Q. Tan, X. Liu, J. Zhang, et al., Three-dimensional cotton-like nickel nanowire@ Ni–Co hydroxide nanosheet arrays as binder-free electrode for high-performance asymmetric supercapacitor, Nanotechnology 29 (2018) 194003.
[455] J. Gou, S. Xie, C. Liu, Flower-like Ni–Co hydroxides on Ni foam for high-performance supercapacitor applications, New J. Chem. 42 (2018) 4175–4181.
[456] B. Patil, S. Ahn, C. Park, H. Song, Y. Jeong, H. Ahn, Simple and novel strategy to fabricate ultra-thin, lightweight, stackable solid-state supercapacitors based on MnO2-incorporated CNT-web paper, Energy 142 (2018) 608–616.
[457] C. Xi, G. Zhu, Y. Liu, X. Shen, W. Zhu, Z. Ji, et al., Belt-like nickel hydroxide carbonate/reduced graphene oxide hybrids: synthesis and performance as supercapacitor electrodes, Colloids Surf. A: Physicochem. Eng. Asp. 538 (2018) 748–756.
[458] S. Zhang, L. Sui, H. Kang, H. Dong, L. Dong, L. Yu, High performance of N-doped graphene with bubble-like textures for supercapacitors, Small 14 (2018).
[459] C. Wang, Z. Guan, Y. Shen, S. Yu, X.-Z. Fu, R. Sun, et al., Shape-controlled synthesis of CoMoO4@Co1.5Ni1.5S4 hybrids with rambutan-like structure for high-performance all-solid-state supercapacitors, Chem. Eng. J. 346 (2018) 193–202.
[460] H. Liang, J. Lin, H. Jia, S. Chen, J. Qi, J. Cao, et al., Hierarchical NiCo-LDH@NiOOH core-shell heterostructure on carbon fiber cloth as battery-like electrode for supercapacitor, J. Power Sources 378 (2018) 248–254.
[461] D. Zha, Y. Fu, L. Zhang, J. Zhu, X. Wang, Design and fabrication of highly open nickel cobalt sulfide nanosheets on Ni foam for asymmetric supercapacitors with high energy density and long cycle-life, J. Power Sources 378 (2018) 31–39.
[462] C. Liu, J. Liu, J. Wang, J. Li, R. Luo, J. Shen, et al., Electrospun mulberry-like hierarchical carbon fiber web for high-performance supercapacitors, J. Colloid Interface Sci. 512 (2018) 713–721.
[463] X. Wu, L. Meng, Q. Wang, W. Zhang, Y. Wang, A novel and facile step-by-step hydrothermal fabrication of peony-like Ni0.4Co0.6(OH)2 supported on carbon fiber cloth as flexible electrodes for advanced electrochemical energy storage, Sol. Energy Mater. Sol. Cells 174 (2018) 325–332.
[464] J. Xia, N. Zhang, S. Chong, Y. Chen, C. Sun, Three-dimensional porous graphene-like sheets synthesized from biocarbon via low-temperature graphitization for a supercapacitor, Green. Chem. (2018).
[465] W.-J. Zhou, M.-W. Xu, D.-D. Zhao, C.-L. Xu, H.-L. Li, Electrodeposition and characterization of ordered mesoporous cobalt hydroxide films on different substrates for supercapacitors, Microporous Mesoporous Mater. 117 (2009) 55–60.
[466] G.F. Chen, X.X. Li, L.Y. Zhang, N. Li, T.Y. Ma, Z.Q. Liu, A porous perchlorate-doped polypyrrole nanocoating on nickel nanotube arrays for stable wide--potential-window supercapacitors, Adv. Mater. 28 (2016) 7680–7687.
[467] Y. Song, X. Cai, X. Xu, X.-X. Liu, Integration of nickel–cobalt double hydroxide nanosheets and polypyrrole films with functionalized partially exfoliated graphite for asymmetric supercapacitors with improved rate capability, J. Mater. Chem. A 3 (2015) 14712–14720.
[468] J. Suchodolski, J. Feder-Kubis, A. Krasowska, Antifungal activity of ionic liquids based on (−)-menthol: a mechanism study, Microbiol. Res. 197 (2017) 56–64.

Waseem raza is a doctoral candidate at Dalian university of technology in China. He received his master degree in Chemical engineering from University of Punjab Pakistan in 2016. His current research area is the energy conservation and pollution emissions reduction using advanced material techniques with an emphasis on membrane technology. He has published 10 articles as author and coauthor in peer-reviewed international journals.

Faizan Ali received his master degree in microelectronics engineering from university of Punjab in 2015. Currently, he is a doctoral candidate at Dalian university of technology. His current research focuses on energy related properties such as energy storage, energy harvesting and solid state cooling of HfO_2.

Nadeem Raza received his Ph.D. degree in Chemistry from Bahauddin Zakaryia University, Multan, Pakistan (2015). He was a postdoctoral fellow at University of Cambridge (2016–2017). From 2005, he has worked in various positions in the Higher Education Department, Govt. of Punjab, Pakistan. Currently, he is working as Associate Professor of Chemistry. His research focuses on materials synthesis, leaching kinetics, carbon sequestration, and application of various analytical techniques for method development. He has published more than 25 scientific articles as author and coauthor in well reputed international journals.

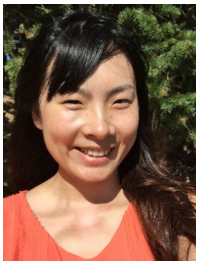

Yiwei Luo is Ph.D. Candidate in Dalian University of Technology. She also joined University of Colorado Boulder, Boulder, USA in 2014–2016 as an exchange scholar. Her current research area is the development of advanced materials for sustainable industrial operations.

Prof. Kwon completed his Ph.D. in the Department of Earth and Environmental Engineering (Interdisciplinary department between chemical and environmental engineering) at Columbia University in the City of New York, USA in 2008. Immediately following, Prof. Kwon was appointed as Associated Research Scientist at the Earth Engineering Center of the Earth Institute at Columbia University. Afterwards, Prof. Kwon returned to South Korea and worked at the Research Institute of Industrial Science and Technology (RIST) from 2010 to 2013. In 2013, Prof. Kwon joined as a faculty member in the Department of Environment and Energy at Sejong University. His research interests are focused on combustion, catalysis, fuel processing, bioenergy, and air pollution controls. To date, Prof. Kwon has published more than 160 articles in peer-reviewed international SCI journals.

Dr. Jianhua Yang received her Ph.D. degree from Hiroshima University of Science and Technology, Japan. Currently, Professor in the Department of Chemical Technology, Dalian University of Technology. Her current research area is the energy conservation and pollution emissions reduction, using advance material techniques for sustainable development of national economy.

Dr. Sandeep Kuma is working as Assistant Professor at the Department of Bio and Nano Technology, Guru Jambheshwar University of Science and Technology, Hisar, Haryana, India. Dr. Kumar did his Ph.D. from Panjab University, Chandigarh. His research interests include synthesis of nanomaterials, nanocarriers for healthcare applications, nanomaterials-based sensors, biomaterials, and nanotoxicology. He has one patent and published more than 50 research papers in many reputed international journals. Dr. Kumar runs both international and national sponsored research projects from different funding agencies. Dr. Kumar visited Hanyang University, Seoul, South Korea as a visiting Professor and also Australia, UK, Scotland, Bangkok under different supporting schemes (DST) of Govt of India.

Andleeb Mehmood received Master's degree in Physical Chemistry from Mirpur University of science and technology Mirpur Azad Kashmir Pakistan in 2014. Currently working on Ph.D at State Key Laboratory of Fine Chemicals, Technology, Dalian University of Technology, China. Her research includes Computational studies of coordination insertions in polar monomers.

Prof. Ki-Hyun Kim was at Florida State University for an M.S. (1984–1986) and at University of South Florida for a Ph.D. (1988–1992). He was a Research Associate at ORNL, USA (1992–1994). Then, he moved to Korea and joined at Sangji (1995–1998) and Sejong University (1999–2013). In 2014, he moved to Hanyang University. His research focuses on diverse interfacing fields between material and environment such as material applications for air quality management. He was awarded a National Star Faculty in 2006. He has published more than 550 articles in SCI journals including well-reputed journals like Chemical Society Reviews, Progress in Polymer Science, Progress in Materials Science, and Coordination Chemistry Reviews. He is serving as an editorial board member of journals (e.g., Sensors, Environmental Research, and Air Pollution Research).